

NEUTRONICS BENCHMARK STUDIES FOR THE TRITIUM BREEDING BLANKETS

By

SHRICHAND JAKHAR

Enrolment No: PHYS06201004001

Institute for Plasma Research, Gandhinagar

A thesis submitted to the

Board of Studies in Physical Sciences

In partial fulfillment of requirements

for the Degree of

DOCTOR OF PHILOSOPHY

of

HOMI BHABHA NATIONAL INSTITUTE



February, 2016

Homi Bhabha National Institute

Recommendations of the Viva Voce Committee

As members of the Viva Voce Committee, we certify that we have read the dissertation prepared by Shrichand Jakhar entitled "Neutronics Benchmark studies for the tritium breeding blankets" and recommend that it may be accepted as fulfilling the thesis requirement for the award of Degree of Doctor of Philosophy.



Chairman – Prof. P K Kaw

Date: 11/07/2016



Guide / Convener – Dr. M Bandyopadhyay

Date: 11/07/2016



Technology Advisor 1– Dr. C V S Rao

Date: 11/07/2016



Examiner – Prof. S L Sharma

Date: 11/07/2016



Member 1 – Dr. T K Basu

Date: 11/07/2016

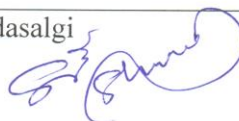
Member 2 – Dr. S Ganesan

Date: 11/07/2016



Technology Advisor 2– Mr. S Padasalgi

Date: 11/07/2016



Final approval and acceptance of this thesis is contingent upon the candidate's submission of the final copies of the thesis to HBNI.

I hereby certify that I have read this thesis prepared under my direction and recommend that it may be accepted as fulfilling the thesis requirement.

Date: 11.7.2016

Place: Gandhinagar



Guide

(Dr. M Bandyopadhyay)

STATEMENT BY AUTHOR

This dissertation has been submitted in partial fulfillment of requirements for an advanced degree at Homi Bhabha National Institute (HBNI) and is deposited in the Library to be made available to borrowers under rules of the HBNI.

Brief quotations from this dissertation are allowable without special permission, provided that accurate acknowledgement of source is made. Requests for permission for extended quotation from or reproduction of this manuscript in whole or in part may be granted by the Competent Authority of HBNI when in his or her judgment the proposed use of the material is in the interests of scholarship. In all other instances, however, permission must be obtained from the author.



(Shrichand Jakhar)

DECLARATION

I, hereby declare that the investigation presented in the thesis has been carried out by me. The work is original and has not been submitted earlier as a whole or in part for a degree / diploma at this or any other Institution / University.



(Shrichand Jakhar)

List of Publications arising from the thesis

Journal

1. “Measurement of tritium production rate distribution in natural LiAlO₂/HDPE assembly irradiated by D-T neutrons”, **Shrichand Jakhar**, M Abhangi, C V S Rao, T K Basu, Sonali P D Bhade, Priyanka J Reddy, *Fusion Eng. Des.*, **2012**, 87(2), 184-187.
2. “Tritium breeding mock-up experiments containing lithium titanate ceramic pebbles and Lead irradiated with DT neutrons”, **Shrichand Jakhar**, M Abhangi, S Tiwari, R Makwana, V Chaudhari, H L Swami, C Danani, C V S Rao, T K Basu, D Mandal, Sonali Bhade, R V Kolekar, P J Reddy, R Bhattacharyay, P Chaudhuri, *Fusion Eng. Des.*, **June 2015**, 95, 50 - 58.
3. “Neutron flux spectra investigations in breeding blanket assembly containing lithium titanate and Lead irradiated with DT neutrons”, **Shrichand Jakhar**, S Tiwari, M Abhangi, V Chaudhari, R Makwana, C V S Rao, T K Basu, D Mandal, *Fusion Eng. Des.*, **2015**, 100, 619 - 628.

Conferences

1. “Measurement of absolute neutron yield of D-T neutron generator using foil activation”, **Shrichand Jakhar**, M Abhangi, C V S Rao, T K Basu, Proceedings of 25th National Symposium on Plasma Science and Technology at IASST, Guwahati, India during 8-12 **Dec. 2010**.
2. “Experimental and Monte Carlo absolute efficiency calibration of HPGe γ -ray spectrometer for application in neutron activation analysis”, S Tiwari, **S Jakhar**, M Abhangi, R Makwana, V Chaudhari, CVS Rao, TK Basu, Proceedings of 28th National Symposium on Plasma Science and Technology at KIIT, Bhubneshwar, Odhisha, India during 3-6 **Dec 2013**.
3. “Absolute measurement of neutron yield for D-T neutron generator using water activation technique”, S Hussain, **Shrichand Jakhar**, M Abhangi, R Makwana, S Vala, C V S Rao, T K Basu, A G Krishna, International

Symposium on Accelerator and Radiation Physics, Saha Institute of Nuclear Physics, Kolkata, India; **02/2011**.

4. "Experimental Studies on the Self-Shielding Effect in Fissile Fuel Breeding Measurement in Thorium Oxide Pellets Irradiated with 14 MeV Neutrons", M Abhangi, N Jain, R Makwana, S Vala, **Shrichand Jakhar**, T K Basu, C V S Rao, Plasma Science and Technology **02/2013**; 15(2):166.
5. "Measurement of neutron flux from 14 MeV D-T neutron generator using activation analysis", **Shrichand Jakhar**, C V S Rao, Anurag Shyam, B Das, Proceedings of IEEE Nuclear Science Symposium, Dresden (Germany), 19-25 Oct **2008**, 2335-2338.



(Shrichand Jakhar)

*Dedicated to my family for their
unconditional love and support*

ACKNOWLEDGEMENTS

First and foremost, I express my sincere gratitude to Dr. C. V. S. Rao for his guidance, useful discussions, and the full support in everything I needed to complete my thesis work. His role in my career can't be contained in the brief space of a few sentences.

I express my sincere gratitude to Dr. Mainak Bandyopadhyay for his help and kind support to become my thesis supervisor at the later stage.

I take immense pleasure in thanking Dr. T. K. Basu for immortal support and motivation. His help to use BARC facilities could complete my thesis work in time.

I extend my heartfelt gratitude to Prof. P. K. Kaw whose marvelous support and encouragement made my path easier to complete the work. I would like to thank Prof. S. Ganesan for useful suggestions and critical review of my work. I am thankful to my friend Shrishail for his help and motivation.

I am very much thankful to Mitul and Rajnikant for the scientific discussions, friendship and spirit of cooperation. It was a memorable time and joy to work with both of them, not only in the frame of scientific work, but personally as well. I would also like to thank other members of the IPR Neutronics Laboratory: Bhavana and Paresh for helping in the experimental work and useful discussions. I am thankful to Shailaja and Vilas for their help in the experiments. I am thankful to Chandan and Swami for useful discussions. I must extend my thanks to Dr. Asim and Dr. Arun for the motivation to complete my doctoral work. I am thankful to Mr. Shankar Joisa for his help in providing the detectors. I would like to thank Dr. R. P. Bhattacharya for his help to fill the Lead in experimental assembly. Many thanks to Aroh Srivastava for providing the data of pebble size.

I am grateful to Dr. D. N. Sharma, Dr. D. A. R. Babu, Smt. Sonali, Smt. Priyanka, Shri R. A. Kolekar of RSSD, BARC for allowing me to use the BARC facility for tritium measurement. I would also like to thank Shri S. K. Ghosh and Dr. D. Mandal from Chemical Engineering group of BARC for providing the materials required for the experiments.

I would like to thank Prof. Dhiraj Bora, Prof. Abhijit Sen, Dr. S. Mukherjee, Dr. Sudip Sen Gupta, Dr. R. Ganesh and other academic committee members for their support and encouragement.

I greatly acknowledge the help of Dr. Luciano Bertalot from ITER diagnostic division. I thank him to give me an opportunity to work at ITER where I learned a lot about the neutron diagnostics and ultimately applied them in this work. I am very much thankful to Dr. Yuri Kashchuk from Kurchatov Institute, Russia for the useful discussions on neutron diagnostics leading to success of this thesis work.

I also express my thanks to the workshop, library and administrative staff of our institute for continuous support during my thesis work.

Finally, my most sincere thanks are extended to my best friend and beloved wife, Laxmi for her unconditional love and devotion throughout. Without her care, support and love, this work could not have been completed in the last stage of the thesis. She always been a true friend to me who boosted my confidence whenever I was in midst of a tempest. I must acknowledge that my children Kavin and Tamanna have sacrificed a lot during this time.

Last but not least, I am indebted to my parents for their everlasting support and encouragement. They always encouraged and supported me throughout all stages of my education.

(Shrichand Jakhar)

CONTENTS

SYNOPSIS	IV
LIST OF FIGURES	XIV
LIST OF TABLES	XVIII
Chapter 1 Introduction	1
1.1 Nuclear fusion.....	1
1.2 D-T fusion fuels	5
1.3 Breeding blankets.....	8
1.4 Breeding blankets testing in ITER	11
1.5 Major issues for the breeding blankets	12
1.5.1 Tritium self-sufficiency	12
1.5.2 Closed tritium fuel cycle	14
1.5.3 MHD effects in liquid blankets	15
1.5.4 Radiation-hard materials	15
1.5.5 Safety issues	16
1.6 Overview of the thesis	17
Chapter 2 Characterization of source neutrons from D-T generator tube.....	21
2.1 Introduction.....	21
2.2 Neutron activation method.....	22
2.3 Calibration of HPGe γ -ray detector	27
2.3.1 Error estimate in the efficiency calibration	31
2.3.2 Full energy photo-peak efficiency function.....	32
2.4 Anisotropy of source neutrons	33
2.5 Angular distribution of source neutron spectrum	38
2.6 Neutron yield measurement	40
2.6.1 Introduction	40
2.6.2 Estimation of geometrical correction factor (k_G).....	43
2.6.3 Estimation of neutron emission anisotropy correction factor (k_A) ..	45
2.6.4 Estimation of source neutron attenuation correction factor (k_R)	45
2.6.5 Experimental details	46
2.6.6 Neutron yield results	46

2.6.7	Uncertainty estimation.....	48
2.7	Validation of the neutron tube MCNP model	49
2.8	Summary	51
Chapter 3	Development and characterization of tritium diagnostics.....	52
3.1	Introduction.....	52
3.2	Off-line tritium diagnostics	53
3.2.1	Principle	53
3.2.2	Experimental procedure	54
3.2.3	Quenching and counting efficiency calibration	55
3.3	On-line tritium measurement	58
3.3.1	Principle	59
3.3.2	Characterization of ^6Li converter layer	60
3.3.2.1	Introduction	60
3.3.2.2	Estimation of F_{Cd} , G_{th} , G_{epi} , and σ	63
3.3.2.3	Measurement of $^{197}\text{Au}(n, \gamma)^{198}\text{Au}$ reaction rates with and without Cd cover.....	64
3.3.2.4	Result of thermal flux, Φ_{th}	65
3.3.2.5	Result of epithermal flux, Φ_{epi}	66
3.3.2.6	Result of ^6Li atoms in the converter layer.....	67
3.3.3	^6Li isotope-ratio measurement	69
3.4	Summary.....	71
Chapter 4	Measurement of tritium production rate in LiAlO_2 assembly	72
4.1	Introduction.....	72
4.2	Experimental details	73
4.3	Computational model	76
4.4	Results and discussion	79
4.5	Conclusions.....	82
Chapter 5	Breeding blanket mock-up experiment containing lithium titanate ceramic pebbles and Lead	84
5.1	Introduction.....	84
5.2	Design of the experiment	86
5.3	Experimental details	89
5.3.1	Geometry of the mock-up assembly	89

5.3.2	Measurement of the neutron yield	92
5.3.3	Materials properties	93
5.3.4	Diagnostics details	95
5.4	Computational model	98
5.5	Results and discussion	99
5.5.1	TPR from ^6Li and ^7Li in breeder zones.....	99
5.5.2	Tritium measurement in multiplier zones	103
5.5.3	TPR ^6Li experimental results with SBD detector.....	105
5.5.4	Spectral distribution of tritium production	106
5.5.5	Activation foil results	108
5.6	Conclusions.....	110
Chapter 6 Neutron flux spectra investigations in breeding blanket assembly containing lithium titanate and Lead		111
6.1	Introduction.....	111
6.2	Experimental details	113
6.2.1	Geometry and irradiation parameters	113
6.2.2	Elemental composition of materials with impurities	116
6.2.3	Activation foils	118
6.3	Computational model	121
6.4	Results and discussions.....	122
6.4.1	Reaction rates	122
6.4.2	Comparison of reaction rates with FENDL-2.1 and FENDL-3.0 ..	130
6.4.3	Neutron spectra	134
6.4.4	Comparison with previous experiment / analyses.....	137
6.5	Conclusions.....	141
Chapter 7 Summary, conclusions and future outlook		143
7.1	Summary and conclusions.....	144
7.2	Future outlook.....	147
Bibliography		151

SYNOPSIS

The present thesis investigates the nuclear responses of the candidate materials for breeding blankets of a D-T fusion reactor in the form of mock-up assemblies. The measured responses are compared with calculated values obtained from the neutron transport tools used for the nuclear design of the breeding blankets. The main focus of the thesis is to validate the neutron transport physics applied in the calculation tools (code and nuclear data) and to assess the uncertainty in tritium production rate (TPR) due to uncertainties in the relevant nuclear data. The uncertainty in the TPR can eventually be linked to the tritium breeding ratio (TBR, ratio of tritium atoms produced in the breeding blankets to that consumed in the plasma). Irradiation experiments with 14 MeV neutrons were designed and performed with materials relevant to breeding blankets. Suitable measurement techniques for TPR and neutron spectra were developed, optimized, and tested in the mock-up experiments.

Tritium self-sufficiency is of critical importance to the D-T fusion power plants. There is no practical external source of tritium for fusion energy development beyond ITER. All subsequent D-T experimental devices and fusion power plants have to breed their own tritium [1]. Tritium in the future fusion power plants will be generated from lithium containing blankets surrounding the D-T plasma via ${}^6\text{Li}(n, t){}^4\text{He}$ and ${}^7\text{Li}(n, n't){}^4\text{He}$ neutron induced reactions. The nuclear design of the breeding blankets is performed with neutronics calculations utilizing 3D neutron transport codes and evaluated cross-section data libraries which are based on various physics models and approximations. The calculated TBR for a given concept of breeding blanket and first

wall is uncertain due to uncertainty associated with the system definition and the inaccuracies in predicting the TBR. The latter includes the uncertainty associated with nuclear data, the geometrical modelling, and calculation methods. The calculated achievable TBR in design analyses has to be larger than the required TBR by a margin to safely take into account the uncertainties on the requirements on the one hand, and the uncertainties in design elements, modelling and nuclear data used in the TBR calculations on the other hand. Therefore, in order to minimize the margins, high accuracy predictions of the TBR and other nuclear responses are needed for these analyses, which require validated computational tools and qualified nuclear data, including reliable uncertainty estimates. For example, an uncertainty as small as 1% translates into a shortage or a surplus of 560 g of tritium per year and per GW of fusion power [2]. This amount is quite significant in absolute terms due to safety and security issues. From last several decades, many organizations all over the world are engaged in developing nuclear data libraries especially dedicated to fusion nuclear analyses. The **Fusion Evaluated Nuclear Data Library** (FENDL) developed by **International Atomic Energy Agency** (IAEA) is widely used worldwide for neutronics calculations in the fusion applications because of the high fidelity of reliability and quality assurance. The FENDL data were selected from several libraries such as ENDF (USA), BROND (Russian Federation), JENDL (Japan) and European Fusion File (EFF) and tailored to meet the needs of the fusion community. The FENDL-2.1 version was released in 2004 for use in nuclear analyses of fusion systems [3]. FENDL-2.1 was widely used in the breeding blanket design analyses and ITER nuclear analyses. Recently IAEA has released the new version of FENDL, FENDL-3.0 [4]. Despite the high fidelity in the IAEA evaluation, the FENDL versions are far

from perfect. Integral validation of the data libraries and 3D codes used in the fusion neutronics area is an inevitable step because feedback from the integral nuclear testing in a 14 MeV neutron environment leads to significant improvements to cross-section evaluations [5].

Series of 14 MeV integral experiments were performed for measurement of tritium production rate along with other parameters at Frascati Neutron Generator (FNG), Italy, Technische Universitat Dresden (TUD), Germany, and JAEA Fusion Neutronics Source (FNS), Japan [6–15]. These experiments were basically focused on the European concepts Helium-Cooled Pebble Bed (HCPB), and Helium-Cooled Lithium Lead (HCLL) and Japanese concept Water-Cooled Ceramic Breeder (WCLL) of the breeding blankets. Mock-up experiments on HCPB breeding blanket concept indicate that the calculated tritium breeding ratio in this concept is conservative (C/E 0.9-0.95) [6, 7]. In the case of HCLL mock-up, the preliminary results show a good agreement between measurement and calculations within the total uncertainty [7]. Experiments with the mock-up of WCLL concept concluded that C/Es of the integrated tritium productions are 1.01-1.04 and 1.11-1.13 without and with the neutron reflector SS316 showing overestimation of TPR with SS316 [12].

India has proposed Lead-Lithium cooled Ceramic Breeder (LLCB) concept of breeding blanket for in-situ tritium breeding in its DEMO reactor [16]. Mock-up of the LLCB breeding blanket will be tested in ITER through Test Blanket Module (TBM) program [17]. The materials proposed for LLCB TBM are: lithium titanate ceramic pebbles enriched with ^6Li as breeder, liquid lead-lithium eutectic as breeder, coolant and multiplier, **Reduced Activation Ferritic Martinstic Steel (RAFMS)** as structural material. A set of four mock-up experiments is evolved during this work to

investigate the neutronics performance of materials used in the LLCB TBM. The first experiment whose results are discussed in this thesis uses Lead as neutron multiplier, mild steel as structural material and lithium titanate pebbles as breeder with natural lithium isotopic composition. The second planned experiment will have lithium Lead and lithium titanate pebbles with natural lithium and P91 steel as structural material. The third experiment planned will have lithium Lead in solid form and lithium titanate enriched with ^6Li and P91 steel as structural material. The fourth set of experiment will be performed with sample materials used in LLCB TBM viz. ^6Li enriched lithium lead liquid metal eutectic and lithium titanate pebbles and IN-RAFM as structural material.

In support of the LLCB TBM nuclear design, the first mock-up experimental assembly was designed and fabricated to perform measurement of various nuclear responses [18]. The measured nuclear responses include local tritium production rate (TPR) and $^{115}\text{In}(n, n')^{115\text{m}}\text{In}$ reaction rate for verification of neutron spectrum above 0.5 MeV energy in the geometry simulating radial build-up of LLCB TBM in ITER. The TPR is measured with two independent diagnostics: lithium carbonate (Li_2CO_3) pellets and on-line tritium measurement with silicon surface barrier detector (SBD) with a ^6Li to triton converter. The tritium production rates from both isotopes of lithium, ^6Li and ^7Li are measured with Li_2CO_3 pellets. The $^{115}\text{In}(n, n')^{115\text{m}}\text{In}$ reaction rate is measured by irradiating indium foils in the zones of the experimental assembly. The measured nuclear responses are compared with that of calculations performed using three-dimensional Monte Carlo code MCNP and cross-section libraries FENDL-2.1 and FENDL-3.0. The average value of C/E of tritium production in enriched Li_2CO_3 pellet is 1.11 for CB-1 (first breeder zone, **C**eramic **B**reeder) and 1.09 for CB-

2 (second breeder zone). The average value of C/E of tritium production in natural Li_2CO_3 pellets is 1.05 for CB-1 and 0.94 for CB-2. These values of C/E are on the upper bound of the estimated experimental uncertainty indicating that the calculated TPR in LLCB TBM ceramic breeder zones are slightly overestimated by calculations. The TPR in the ceramic breeding zone is mostly contributed by tritium production from ^6Li isotope in the lithium titanate (> 90%). C/E ratio for TPR- ^6Li with on-line tritium detector is close to unity (0.96). The $^{115}\text{In}(n, n')^{115\text{m}}\text{In}$ reaction rate measurement shows the tendency of underestimation by calculations in the multiplier zones up to 10%. This result indicates that the evaluated (n, 2n) cross-sections of Lead isotopes need to be improved in the nuclear data libraries.

Neutron flux spectrum is a fundamental physical quantity which is used to calculate the nuclear responses in the breeding blankets of the D-T fusion reactor. The main nuclear responses of interest in the breeding blanket technology are tritium production rate, gas production rate, nuclear heating, radiation damage, and activation. The neutron flux spectrum in the breeding blankets is calculated with the help of 3D radiation transport codes and nuclear data libraries such as FENDL-2.1. The uncertainties of design parameters are determined by uncertainties of both cross-section data and calculated neutron flux spectrum by transport codes with transport cross-section libraries. FISPACT-2007 inventory code with EAF-2007 library is widely used for the radioactive inventory calculations in the fusion reactor environment for rad-waste and occupational exposure calculations. Therefore it is necessary to validate the neutron spectra calculated by radiation transport codes with cross-section data files and the activation calculations by inventory code FISPACT-2007 performing clean benchmark experiments with the materials proposed for the

breeding blankets. An experiment was designed having Li_2TiO_3 in powder form as breeder, pure Lead as neutron multiplier, Mild Steel (MS) as structural material and high density polyethylene (HDPE) as neutron reflector and shield for room reflected neutrons [19]. The experimental assembly consists of two layers of breeder and three layers of neutron multiplier materials. The neutron spectra were measured from thermal to source energy covering the range for tritium production by ^6Li and ^7Li and neutron multiplication by Lead isotopes. Measured saturation activities in irradiated foils along-with the guess spectrum calculated with MCNP was used as input to unfold the neutron flux spectrum by code SAND-II-SNL (Spectrum Analysis by Neutron detectors-II-Sandia National Laboratory) with SNLRML (Sandia National Laboratory, Radiation Metrology Laboratory) cross-section library. SAND-II-SNL code uses an iterative perturbation method to obtain a "best fit" neutron flux spectrum for a given input set of infinitely dilute foil activities. The experimental results were analyzed with radiation transport code MCNP and nuclear data libraries FENDL-2.1 and FENDL-3.0. IRDFF-1.05 reactor dosimetry library was used for the calculation of neutron induced reaction rates. Measured reaction rates were also compared with calculated values obtained from **European Activation System (EASY-2007)** which has the inventory code FISPACT-2007 and cross-section library EAF-2007. The calculated reaction rates in the foils are in agreement with the measured reaction rates within combined uncertainty of experiment and calculations with few exceptions. The comparison of measured and calculated neutron spectrum in Lead (Pb) zones shows that measured neutron spectrum in the $\text{Pb}(n, xn)$ secondary neutron emission range is underestimated by calculations (up to 10%). The measured neutron flux in inelastic scattering range of Lead isotopes is overestimated by calculations as large as up to

80%.

Another neutronics experiment with the objective to validate the capability of neutronics codes and nuclear data to predict nuclear responses such as tritium production rate with qualified uncertainties was designed with LiAlO_2 as breeder and HDPE as neutron reflector [20]. The experimental assembly was irradiated with D-T neutrons and the tritium profile in the assembly was measured with Li_2CO_3 pellets. The experimentally measured tritium production was compared with calculated values using 3D Monte Carlo code MCNP and FENDL-2.1 cross-section library. The local TPRs were measured with small pellets detectors inside the breeding assembly. Comparison between measured and calculated (with Monte Carlo code MCNP and FENDL-2.1 cross section library) values of TPR shows agreement within the estimated uncertainty except one point.

The research work carried out and compiled here in this thesis has been published in the peer reviewed journals. An overview of the thesis content grouped under seven chapters is as follows:

Chapter-1 Introduction

This chapter begins with preamble about the nuclear fusion, confinement methods of plasmas, progress made on the magnetic confinement fusion, and fusion fuels. Further, the importance of breeding blankets to demonstrate the D-T fusion as sustainable energy source is discussed. The importance of tritium self-sufficiency and factors affecting it are described later on the chapter. Then concept of tritium breeding ratio is introduced and factors introducing uncertainty in it are explained. Major issues for the breeding blanket technology development are discussed. The chapter concludes by giving the motivation behind the work performed and the problems

addressed in the thesis.

Chapter-2 Characterization of source neutrons from D-T generator tube

This chapter describes the theoretical background, development and performance characterization of the source neutrons using activation technique. Efficiency calibration of High Purity Germanium (HPGe) γ -ray spectrometer plays an important role in the neutron flux measurement using activation technique. Therefore spectrometer was rigorously characterized for absolute efficiency as a function of γ -ray energy; coincidence correction etc. and results of these parameters are presented in this chapter. Knowledge of anisotropy and angle dependent energy spectra of the source neutrons is an essential component for the benchmark experiments and neutron yield measurement. Both these parameters were calculated using the Ti-T target model and beam parameters and results are discussed in this chapter. The results of neutron source yield along with details of various correction factors for neutron yield are presented under the purview of this chapter. Finally a calculation model for SODERN made sealed D-T neutron generator is developed and validated by measuring the neutron induced reaction rates covering the energy range from thermal to D-T source neutron energy.

Chapter-3 Development and characterization of tritium diagnostics

This chapter describes methodology and development of two techniques of the local tritium measurement. Theoretical background of both techniques and their performance characterization is described in this chapter. The first technique is based on the irradiation of Li_2CO_3 pellets in the experimental assemblies and counting of produced tritium in them using liquid scintillation technique. This technique is further extended to separate the tritium production from ^6Li and ^7Li isotopes. The other

technique is based on the direct tritium measurement using silicon surface barrier detector with ^6Li to tritium converter.

^6Li converter used in this diagnostics is characterized with ^{241}Am -Be neutron source. Other application of this diagnostics in the measurement of tritium enrichment is also discussed in this chapter.

Chapter-4 Measurement of tritium production rate in LiAlO_2 assembly

This chapter describes the experimental results on the local tritium production rate profile in the experimental assembly with LiAlO_2 breeder and HDPE as neutron reflector and shield. The experimental results are analyzed with 3D radiation transport code MCNP and nuclear data library FENDL-2.1. The ratios of calculation to experimental tritium production (C/E) in the experimental assembly are discussed in this chapter.

Chapter-5 Breeding blanket mock-up experiment containing lithium titanate ceramic pebbles and Lead

The first of the four mock-up experiments to investigate the neutronics performance of the materials used in the LLCB TBM is described in this chapter. The first part of this chapter is devoted to describe the design of the LLCB mock-up experiments. The second part of the chapter presents the tritium production (TPR) measurement results from both lithium isotopes ^6Li and ^7Li using lithium carbonate pellets in mock-up zones. The direct tritium measurement result with silicon surface barrier detector with ^6Li to tritium converter is also presented in this chapter. All the above-mentioned experimental results are compared with calculation done with MCNP and FENDL-2.1 library. The activation foil measurement results in the mock-up zones are also described.

Chapter-6 Neutron flux spectra investigation in breeding assembly containing lithium titanate and Lead

The neutron spectra results in a benchmark experiment, having three layers of neutron multiplying material lead and two layers of breeder material Li_2TiO_3 , in the geometry of LLCB TBM are discussed in this chapter. The measured neutron spectra are compared with the calculations. The measurement reaction rates in foils are also compared with the calculations with two different libraries one with dosimetry library IRDFF-1.05 and activation library EAF-02.

Chapter-7 Summary, conclusions and future outlook

This chapter gives a brief summary of the research work carried out in this thesis along with the future outlook.

LIST OF FIGURES

<i>Figure 1.1: Fusion cross-sections of the most favorable reactions as a function of projectile energy</i>	<i>3</i>
<i>Figure 1.2: The overall D-T fusion reaction. The basic fuels are deuterium and lithium; the waste product is helium</i>	<i>6</i>
<i>Figure 1.3: Excitation functions of the tritium producing reactions from lithium isotopes ${}^6\text{Li}$ and ${}^7\text{Li}$ with neutron</i>	<i>7</i>
<i>Figure 1.4: Schematic of the breeding blanket in a D-T fusion reactor</i>	<i>8</i>
<i>Figure 2.1: Foil irradiation and activity measurement sequence.....</i>	<i>25</i>
<i>Figure 2.2: Photo-peak efficiency curve of Canberra made HPGe detector GR5023 for a foil of diameter 13 mm placed on the window of detector (without self-absorption of foils).....</i>	<i>33</i>
<i>Figure 2.3: Schematic representation of a two body nuclear reaction in the laboratory frame.....</i>	<i>34</i>
<i>Figure 2.4: Differential cross-section of D-T reaction as a function of deuteron energy in center-of-mass frame calculated with DROSG2000 code.....</i>	<i>36</i>
<i>Figure 2.5: Energy loss rate (dE/dx) of D^+ beam in Ti-T target calculated with SRIM-2008 code</i>	<i>36</i>
<i>Figure 2.6: Solid angle conversion factor as a function of incident deuteron energy at three neutron emission angles (0°, 90° and 180°).....</i>	<i>37</i>
<i>Figure 2.7: Relative neutron intensity to forward direction as a function of emission angle at 150 keV D^+ beam energy.....</i>	<i>38</i>
<i>Figure 2.8: Neutron generator source spectra calculated using the target model at three emission angles 0°, 90°, and 180°</i>	<i>40</i>
<i>Figure 2.9: Measured and evaluated excitation functions of ${}^{27}\text{Al}(n, \alpha){}^{24}\text{Na}$ reaction [54].....</i>	<i>42</i>
<i>Figure 2.10: Schematic of source-foil detector geometry for neutron yield measurement.....</i>	<i>43</i>
<i>Figure 2.11: Neutron flux from disk sources and neutron flux ratio with point source ($r_s = 2, 5$, and 10 mm) as a function of r_d for $r_f = 13$ mm</i>	<i>44</i>
<i>Figure 2.12: Geometrical model of the neutron generator GENIE35.....</i>	<i>50</i>

<i>Figure 3.1: Li₂CO₃ pellets prepared by cold pressing for tritium measurement in experimental assemblies.....</i>	<i>55</i>
<i>Figure 3.2: Measured efficiencies as a function of quenching and linear fits for natural and enriched Li₂CO₃ pellets</i>	<i>58</i>
<i>Figure 3.3: Experimental set-up with ²⁴¹Am-Be source for the characterization of ⁶Li converter layer</i>	<i>61</i>
<i>Figure 3.4: Schematic of the experiment for the characterization of ⁶Li converter layer</i>	<i>62</i>
<i>Figure 3.5: Photograph of Surface Barrier Detector (SBD) with Li₂CO₃ layer.....</i>	<i>67</i>
<i>Figure 3.6: PHS spectra with and without Li₂CO₃ converter foils and gaussian fit for the triton peak.....</i>	<i>68</i>
<i>Figure 3.7: Pulse-height spectra with enriched and natural Li₂CO₃ layer placed on the charged particle detector SBD</i>	<i>70</i>
<i>Figure 4.1: Experimental assembly containing LiAlO₂ breeding material for the measurement of tritium production rate.....</i>	<i>74</i>
<i>Figure 4.2: Locations of diagnostic Li₂CO₃ pellets in the experimental assembly.....</i>	<i>76</i>
<i>Figure 4.3: Cross-section through the mid-plane of experimental assembly</i>	<i>77</i>
<i>Figure 4.4: Cross-sectional view of the MCNP model of breeding assembly with HDPE reflector</i>	<i>78</i>
<i>Figure 4.5: (a) Calculated and measured TPR radial profile at axial position 0 cm (b) radial profile of C/E ratios. The error estimate includes errors in neutron yield measurement, statistics of tritium counts and statistics of Monte Carlo calculation. .</i>	<i>80</i>
<i>Figure 4.6: (a) Calculated and measured TPR radial profiles at 16 cm axial distance from source and (b) Radial Profile of Calculated to experimental (C/E) TPR ratio. The error estimate includes errors in neutron yield measurement, statistics of tritium counts and statistics of Monte Carlo calculation.....</i>	<i>81</i>
<i>Figure 4.7: (a) Calculated and measured TPR radial profiles at 25 cm axial distance from source and (b) Radial Profile of Calculated to experimental (C/E) TPR ratios. The error estimate includes errors in neutron yield measurement, statistics of tritium counts and statistics of Monte Carlo calculation.....</i>	<i>82</i>
<i>Figure 5.1: Comparison of neutron spectra on the first wall of mock-up and LLCB TBM in ITER</i>	<i>87</i>

<i>Figure 5.2: Tritium production in mock-up zones as a function of height and width of mock-up</i>	<i>88</i>
<i>Figure 5.3: Photograph of the breeding blanket mock-up assembly ready for irradiation with 14 MeV neutrons</i>	<i>90</i>
<i>Figure 5.4: Cross-section of the mock-up assembly with HDPE reflector and tritium pellet detectors</i>	<i>91</i>
<i>Figure 5.5: Cross-sectional view of the MCNP model of breeding assembly with HDPE</i>	<i>92</i>
<i>Figure 5.6: Time profile of the 14 MeV neutron source during mock-up irradiation .</i>	<i>93</i>
<i>Figure 5.7: Size distribution of the Li_2TiO_3 pebbles used in the experiment</i>	<i>94</i>
<i>Figure 5.8: Cross-section of the mock-up assembly showing tritium measurement locations</i>	<i>95</i>
<i>Figure 5.9: Measured and calculated specific tritium activities and C/E ratios in the natural and enriched Li_2CO_3 pellets in the breeding zones</i>	<i>101</i>
<i>Figure 5.10: Measured ^6Li, ^7Li and total TPR in first and second breeding layers ..</i>	<i>102</i>
<i>Figure 5.11: Experimental & calculated tritium activity and C/E ratios for two types of diagnostic pellets in multiplier zones</i>	<i>104</i>
<i>Figure 5.12: Pulse height spectra with and without converter foil measured in breeding layer 2 (CB-2) and the gaussian fit for the triton peak</i>	<i>105</i>
<i>Figure 5.13: Tritium production as a function of neutron energy in the enriched lithium carbonate pellets in the mid of each assembly zone</i>	<i>107</i>
<i>Figure 5.14: $^{115}\text{In}(n, n')^{115m}\text{In}$ reaction rate profile and C/E ratios in the mock-up assembly</i>	<i>109</i>
<i>Figure 6.1: Cross-section of the experimental assembly used for measurement of neutron flux spectra</i>	<i>114</i>
<i>Figure 6.2: Cross-sectional view of the MCNP model of breeding assembly showing dimensions and materials</i>	<i>115</i>
<i>Figure 6.3: Measured time profile of source neutron yield from generator tube during irradiation experiment with ^3He counter</i>	<i>116</i>
<i>Figure 6.4: Excitation functions of high threshold reactions irradiated in the assembly for unfolding of neutron flux spectra</i>	<i>119</i>

<i>Figure 6.5: Excitation functions of low threshold and radiative capture reactions irradiated in the assembly for unfolding of neutron flux spectra</i>	<i>120</i>
<i>Figure 6.6: Experimental reaction rate results in assembly zones</i>	<i>124</i>
<i>Figure 6.7: C/E ratios of high threshold reactions with MCNP-IRDFF-1.05 and FISPACT-EAF2007.....</i>	<i>128</i>
<i>Figure 6.8: C/E ratios of low threshold and radiative capture reactions with MCNP-IRDFF-1.05 and FISPACT-EAF2007.....</i>	<i>129</i>
<i>Figure 6.9: Spectral response of $^{115}\text{In}(n, n')^{115m}\text{In}$ reaction in experimental assembly zones.....</i>	<i>130</i>
<i>Figure 6.10: Unfolded neutron spectra with SAND-II and calculated spectrum with MCNP and FENDL-2.1 in breeding assembly zones.....</i>	<i>135</i>
<i>Figure 6.11: Ratio of calculated and experimental neutron spectra integrated in five energy bins shown as a function of assembly zone</i>	<i>136</i>
<i>Figure 6.12: Comparison of calculated leakage neutron spectrum from Lead sphere (FENDL-2.1 and FENDL-3.0) with measurement performed at TUD, Germany</i>	<i>138</i>
<i>Figure 6.13: Leakage neutron spectrum from TUD Pb sphere experiment and neutron spectrum in zone-2 of present experiment.....</i>	<i>139</i>
<i>Figure 7.1: Measured and evaluated excitation function of $^{206}\text{Pb}(n, 2n)^{205}\text{Pb}$ reaction</i>	<i>148</i>
<i>Figure 7.2: Measured and evaluated excitation function of $^{207}\text{Pb}(n, 2n)^{206}\text{Pb}$ reaction</i>	<i>149</i>
<i>Figure 7.3: Measured and evaluated excitation function of $^{208}\text{Pb}(n, 2n)^{207}\text{Pb}$ reaction</i>	<i>149</i>

LIST OF TABLES

<i>Table 1.1 Energy yield (Q value) of the most common fusion reactions</i>	<i>4</i>
<i>Table 1.2: Physical properties of lithium compounds for tritium breeding with neutrons</i>	<i>9</i>
<i>Table 2.1: Physical characteristics of HPGe detector (Model GR5023 Canberra Industries).....</i>	<i>28</i>
<i>Table 2.2: Measured relative efficiency of HPGe detector for 1.33 MeV γ-energy (^{60}Co source) at 25 cm distance (cps = counts per second).....</i>	<i>29</i>
<i>Table 2.3: Experimental validation of optimized detector model with ^{60}Co source</i>	<i>30</i>
<i>Table 2.4: Experimental validation of optimized detector model with ^{152}Eu source ...</i>	<i>31</i>
<i>Table 2.5: Experimental validation of optimized detector model with ^{137}Cs source ...</i>	<i>31</i>
<i>Table 2.6: Maximum uncertainty in the absolute efficiency calibration of HPGe detector.....</i>	<i>32</i>
<i>Table 2.7: Ti-T target and D^+ beam parameters of GENIE35 neutron generator</i>	<i>39</i>
<i>Table 2.8: Decay properties of $^{27}\text{Al}(n, \alpha)^{24}\text{Na}$ reaction and foil details.....</i>	<i>42</i>
<i>Table 2.9: Result of the measured neutron yield by $^{27}\text{Al}(n, \alpha)^{24}\text{Na}$ reaction</i>	<i>47</i>
<i>Table 2.10: Result of the measured neutron yield by $^{93}\text{Nb}(n, 2n)^{92m}\text{Nb}$ reaction</i>	<i>48</i>
<i>Table 2.11: Uncertainty estimation in the measured neutron yield by $^{27}\text{Al}(n, \alpha)^{24}\text{Na}$ reaction.....</i>	<i>49</i>
<i>Table 2.12: Measured and calculated reaction rates in various activation foils on the surface of neutron generator (90° location).....</i>	<i>51</i>
<i>Table 3.1: Counting efficiency calibration of liquid scintillation counter for natural Li_2CO_3 pellets (Activity of tritium mixed= 1236.51 DPM*)</i>	<i>57</i>
<i>Table 3.2: Counting efficiency calibration of liquid scintillation counter for enriched Li_2CO_3 pellets (Activity of tritium mixed= 1224.95 DPM*)</i>	<i>57</i>
<i>Table 3.3: $^{197}\text{Au}(n, \gamma)^{198}\text{Au}$ reaction rates with and without Cd cover.....</i>	<i>65</i>
<i>Table 3.4: Result of measured thermal flux at the irradiation location of ^{241}Am-Be source set-up</i>	<i>66</i>
<i>Table 3.5: Result of measured epithermal flux at the irradiation location of ^{241}Am-Be source experimental setup.....</i>	<i>67</i>
<i>Table 3.6: Measured ^6Li atoms in Li_2CO_3 converter foil used for on-line tritium measurement (cps = counts per second).....</i>	<i>68</i>

<i>Table 3.7: Measured ^6Li isotopic abundance in enriched Li_2CO_3 converter foil</i>	<i>70</i>
<i>Table 5.1: Color coding of the material used in the MCNP model of mock-up assembly</i>	<i>90</i>
<i>Table 5.2: Elemental composition of materials with impurities used in the experiment</i>	<i>94</i>
<i>Table 5.3: Experimental and calculated TPR-^6Li in the second breeder zone (CB-2) with on-line tritium diagnostics.....</i>	<i>106</i>
<i>Table 6.1: Elemental composition of materials with impurities used in the experiment</i>	<i>117</i>
<i>Table 6.2: List of foils irradiated in the breeding assembly zones and neutron induced reactions used in the study for neutron spectra measurement</i>	<i>119</i>
<i>Table 6.3: Uncertainties on measured neutron induced reaction rates in foils.....</i>	<i>123</i>
<i>Table 6.4: Measured (E) and calculated (C) reaction rates and C/E ratios in zone-1</i>	<i>125</i>
<i>Table 6.5: Measured (E) and calculated (C) reaction rates and C/E ratios in zone-2</i>	<i>125</i>
<i>Table 6.6: Measured (E) and calculated (C) reaction rates and C/E ratios in zone-3</i>	<i>126</i>
<i>Table 6.7: Measured (E) and calculated (C) reaction rates and C/E ratios in zone-4</i>	<i>126</i>
<i>Table 6.8: Measured (E) and calculated (C) reaction rates and C/E ratios in zone-5</i>	<i>127</i>
<i>Table 6.9: Comparison of neutron induced reaction rates in assembly zone-1 with FENDL-2.1 and FENDL-3.0 libraries</i>	<i>132</i>
<i>Table 6.10: Comparison of neutron induced reaction rates in assembly zone-2 with FENDL-2.1 and FENDL-3.0 libraries</i>	<i>132</i>
<i>Table 6.11: Comparison of neutron induced reaction rates in assembly zone-3 with FENDL-2.1 and FENDL-3.0 libraries</i>	<i>133</i>
<i>Table 6.12: Comparison of neutron induced reaction rates in assembly zone-4 with FENDL-2.1 and FENDL-3.0 libraries</i>	<i>133</i>
<i>Table 6.13: Comparison of neutron induced reaction rates in assembly zone-5 with FENDL-2.1 and FENDL-3.0 libraries</i>	<i>134</i>

<i>Table 6.14: Measured and calculated neutron multiplication (partial and total) in TUD Lead sphere experiment</i>	<i>138</i>
<i>Table 6.15: Neutron leakage multiplication in OSAKA experiment (0.017-15 MeV) 140</i>	
<i>Table 6.16: Neutron leakage multiplication in OSAKA experiment (0.3-15 MeV).... 140</i>	
<i>Table 7.1 : Summary of the future experiments in support of the LLCB TBM nuclear design</i>	<i>147</i>

Chapter 1

Introduction

The ultimate goal of the nuclear fusion research is to gain sufficient scientific and engineering knowledge so that the process of energy production in stars and sun can be recreated on the Earth in controlled manner. As per our current understanding, magnetically confined fusion is the most promising method of achieving a fusion power plant. The easiest way to realize the nuclear fusion in controlled manner is the reaction between two isotopes of hydrogen: deuteron and triton. This reaction is popularly known as D-T reaction. Deuterium is abundant in nature and can be extracted from sea water. Tritium is not available on earth owing to its radioactive nature and will have to be bred in-situ from the nuclear reaction of fusion neutrons with lithium isotopes: ${}^6\text{Li}$ and ${}^7\text{Li}$.

Nuclear fusion is in an ideal and promising energy source to replace coal, oil and gas fired power plants around the world. It has no carbon footprint, except that carbon which is produced during construction and manufacturing of the plant.

1.1 Nuclear fusion

Energy is an integral part of the everyday life of modern civilization. The absence of the energy in everyday life brings the civil society centuries back. In current scenario, our energy supply comes mainly from fossil fuels, with nuclear power and renewable

sources rounding out the mix. Known resources to produce energy through these means as on today are not sufficient to provide the needs of the future generations for their sustainable development apart from their effect on the environment degradation. Therefore it is utmost important to develop a method which can provide inexhaustible and environment friendly source of energy. Nuclear fusion is such a promising energy production method which can provide the inexhaustible and environment friendly source of energy. Development of the fusion technology to demonstrate that this process can be used as power source is an important research field.

Nuclear fusion is a process in which two light elements fuse together to form a heavier atom having mass smaller than the combined mass of their parents and the mass difference is released in the form of energy. The resulting energy from fusion reaction is released in the form of kinetic energies of outgoing particles which can then ultimately be converted into electrical energy. In order to have short ranged strong nuclear interaction between two fusing nuclei, they must have sufficient kinetic energy to overcome the electrostatic coulomb repulsion between them i.e. the fusing nuclei must penetrate through the coulomb barrier via quantum mechanical tunneling process. In more general term, the fuel atoms must be heated to thermonuclear temperatures for initiating fusion process. The typical temperature required to initiate the fusion reactions is in the order of several tens of keV ($1 \text{ eV} = 11604 \text{ }^0\text{K}$). At such high temperatures the fuel mixture is converted into the fourth stage of matter called plasma. The biggest challenge in achieving fusion in a controlled manner is confinement of plasma at thermonuclear temperatures in the steady state, which can then be used for electricity production. Tokamak based fusion devices based on the magnetic confinement concept are the most promising to realize the fusion process as

future source of energy.

Lawson criterion is an important measure of a system that defines the conditions needed for a fusion reactor to reach ignition, i.e. the heating of the plasma by the fusion products is sufficient to maintain the temperature of the plasma against all losses without any external power input. Lawson criterion gives a minimum required value for the product of the plasma density (n) and the "energy confinement time" (τ_E). Lawson criterion often refers to this inequality for D-T fusion reaction at 10 keV temperature [21].

$$n\tau_E > 10^{20} \text{ s/m}^3 \quad (1.1)$$

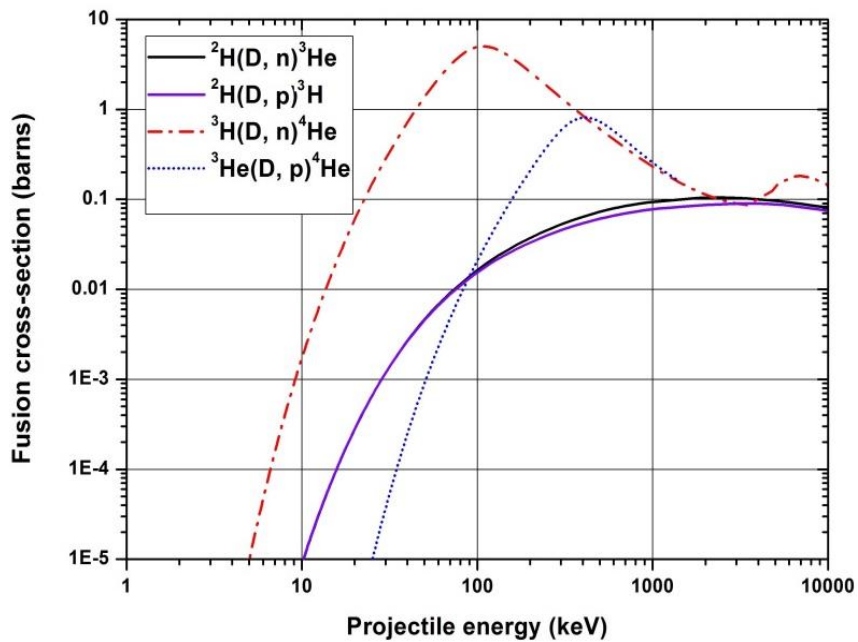


Figure 1.1: Fusion cross-sections of the most favorable reactions as a function of projectile energy [22]

There are number of fusion reactions which can be realized for terrestrial fusion. The desirable requirements for the terrestrial fusion reactions are that they should occur at low temperatures i.e. the input power required to heat the atoms should be low, and the energy release per reaction must be highest i.e. Q value of the reaction should be

high. The nuclear cross-sections of the most favorable fusion reactions as a function of the projectile energy are given in *Figure 1.1*. It can be seen from *Figure 1.1* that the cross-section of the D-T fusion reaction is the highest among all other reactions and it occurs at the lowest temperature. Due to this reason D-T reaction is foreseen as candidate reaction for the first generation fusion reactors.

Table 1.1 Energy yield (*Q* value) of the most common fusion reactions [23]

Fusion reaction	Abbreviated form	Energy yield (MeV)
${}^2_1\text{H} + {}^3_1\text{H} \rightarrow {}^4_2\text{He} + {}^1_0\text{n}$	T(d, n) ${}^4\text{He}$	17.60
${}^2_1\text{H} + {}^2_1\text{H} \rightarrow {}^3_2\text{He} + {}^1_0\text{n}$	D(d, n) ${}^3\text{He}$	3.27
${}^2_1\text{H} + {}^2_1\text{H} \rightarrow {}^3_1\text{He} + {}^1_1\text{p}$	D(d, p)T	4.03
${}^3_1\text{H} + {}^3_1\text{H} \rightarrow {}^4_2\text{He} + 2{}^1_0\text{n}$	T(t, 2n) ${}^4\text{He}$	11.3
${}^2_1\text{H} + {}^3_2\text{He} \rightarrow {}^4_2\text{He} + {}^1_1\text{p}$	${}^3\text{He}$ (d, p) ${}^4\text{He}$	18.3
${}^1_1\text{p} + {}^6_3\text{Li} \rightarrow {}^4_2\text{He} + {}^3_2\text{He}$	${}^6\text{Li}$ (p, α) ${}^3\text{He}$	4.02
${}^1_1\text{p} + {}^{11}_5\text{B} \rightarrow 3{}^4_2\text{He}$	${}^{11}\text{B}$ (p, 2 α) ${}^4\text{He}$	8.68

List of the most common fusion reactions with their energy yield per reaction (*Q* value) is given in *Table 1.1*. It can be seen from *Table 1.1* that the D-T reaction yields the second highest energy per reaction after ${}^3\text{He}$ (d, p) ${}^4\text{He}$. ${}^3\text{He}$ (d, p) ${}^4\text{He}$ reaction has advantage that it is aneutronic i.e. there is no concern of activation caused by neutrons like D-T reaction. Disadvantages of ${}^3\text{He}$ (d, p) ${}^4\text{He}$ reaction as source of fusion energy include: it requires much higher temperatures than D-T reaction (*Figure 1.1*), one of the fuel of this reaction deuteron produces neutrons via D-D reaction and ${}^3\text{He}$ resources are scarce on the earth.

Tokamak based magnetic confinement fusion research has registered good progress in key areas of reactor relevance in the last several decades. A number of improved

confinement regimes were discovered; as a result, the fusion triple product $n.T.\tau_E$ and Q_{DT} equivalent (ratio of the fusion power to the input power) have increased to about 1.5×10^{21} keV.s.m⁻³ and about 1.25 respectively in separate plasma discharges in JT-60U [24]. Many D-T experiments have been conducted on JET and TFTR, which has produced fusion powers of 16 MW and 11 MW respectively in these two machines [24]. This progress in the fusion research has resulted into the start of the construction of 500 MW fusion power machine called **International Thermonuclear Experimental Reactor (ITER)**. ITER device based on tokamak concept of magnetic confinement is a collaborative project among seven partners viz. European Union, China, India, Japan, the Republic of Korea, the Russian Federation and the USA. ITER is aimed at demonstrating the scientific and technical feasibility of fusion reactors and intends to operate largely at $Q = 10$ conditions [25]. ITER is designed to produce 500 MW of fusion power from 50 MW input power: the first of all fusion experiments to produce net energy. During its operational lifetime, ITER will test key technologies necessary for the next step: the demonstration fusion power plant that will prove that it is possible to capture fusion energy for commercial use.

1.2 D-T fusion fuels

The reaction between deuterium and tritium requires the lowest temperature (*Figure 1.1*) to get it started and therefore is considered to be the best candidate reaction for a fusion power plant. Tritium does not occur naturally on our planet Earth because it is radioactive, decaying with a half-life of 12.3 years. Therefore tritium will have to be manufactured in-situ in the fusion reactor itself. In principle this can be done by allowing the neutron that is produced in the D-T reaction to react with the two

isotopes of lithium: ${}^6\text{Li}$ and ${}^7\text{Li}$. Both lithium isotopes interact with neutrons to produce tritium and helium. Thus the basic fuels for a fusion power plant burning deuterium and tritium will be ordinary water and lithium salts. Deuterium will be extracted from water (abundance of deuterium isotope in natural hydrogen is 0.0115%), and tritium will be produced from lithium salts. Both basic fuels are relatively cheap, abundant, and easily accessible. The waste product will be the inert gas helium. The overall D-T fusion reaction is shown schematically in *Figure 1.2*.

The two tritium producing reactions from lithium isotopes ${}^6\text{Li}$ and ${}^7\text{Li}$ with fusion neutron are:

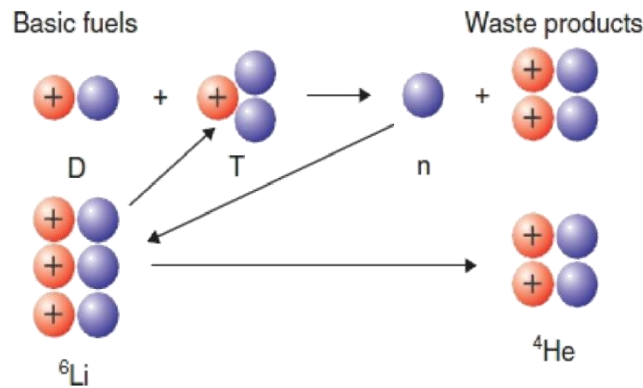
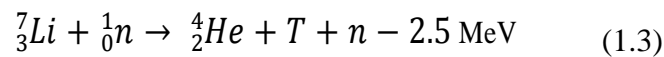
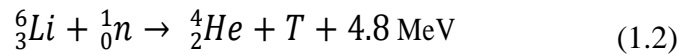


Figure 1.2: The overall D-T fusion reaction. The basic fuels are deuterium and lithium; the waste product is helium

The neutron interaction with ${}^6\text{Li}$ is most probable with a low energy neutron; it is exothermic, releasing 4.8 MeV of energy. The neutron reaction with ${}^7\text{Li}$ is an endothermic reaction, only occurring with a fast neutron and absorbing 2.5 MeV of energy but it generates an additional low energy neutron which can produce tritium with ${}^6\text{Li}$. Release of 4.8 MeV energy by the tritium producing reaction of ${}^6\text{Li}$ with

neutron provides energy multiplication in addition to the energy released in the fusion core. Natural lithium is composed of 92.6 percent of ${}^7\text{Li}$ and 6.4 percent of ${}^6\text{Li}$ in atom fraction unit. The raw fuel material required for D-T fusion reaction, one kilogram of lithium can produce 1×10^5 GJ of electricity [26]. The reaction cross-sections of neutrons with both lithium isotopes as a function of neutron energy are plotted in *Figure 1.3*.

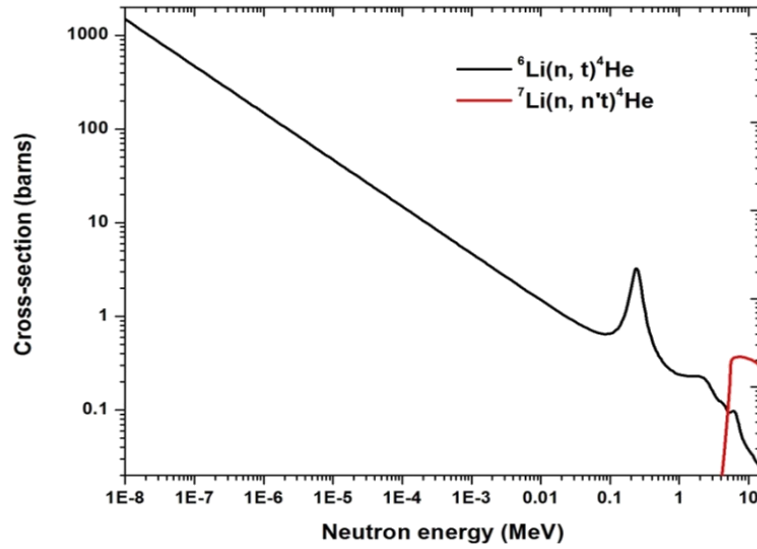


Figure 1.3: Excitation functions of the tritium producing reactions from lithium isotopes ${}^6\text{Li}$ and ${}^7\text{Li}$ with neutron [22, 27]

It can be seen from *Figure 1.3* that the tritium production by ${}^6\text{Li}$ with neutron is very high at thermal energies (in the order of few thousand barns) and shows $1/v$ behavior (v being the velocity of the neutron). The tritium production by ${}^7\text{Li}$ needs neutrons of energy above 2.5 MeV i.e. it is a threshold reaction but it produces one low energy neutron which can produce the tritium with ${}^6\text{Li}$ isotope. Hence both isotopes are useful for the tritium production in D-T fusion environment. Tritium production by 14 MeV neutrons is dominant by ${}^7\text{Li}$ isotope. However ${}^7\text{Li}$ cross-section with neutron at 14 MeV is not enough to multiply the neutrons to achieve the tritium self-sufficiency.

1.3 Breeding blankets

As discussed earlier, one of the fuel tritium, required for the D-T fusion reactors, will have to be produced in-situ due to its non-availability in nature. This function is provided by a layer, i.e. breeding blanket, containing lithium salts with other materials surrounding the fusion core. Main functions of the breeding blanket in the fusion reactor include generation of tritium, conversion of neutron energy (both from primary and secondary reactions) into heat, extraction of nuclear heat to produce electrical energy and to provide the shielding of critical components of reactor against the nuclear radiation. Several concepts of breeding blankets have evolved using different breeder and multiplier materials. They can be broadly classified into two main categories, liquid and solid breeding blankets. The liquid blanket concepts use liquid metals such as Pb-Li eutectic as breeder and multiplier. The solid concepts use ceramic breeders containing lithium as breeder and beryllium as neutron multiplier. The schematic of the breeding blanket in a D-T fusion reactor is shown in *Figure 1.4*.

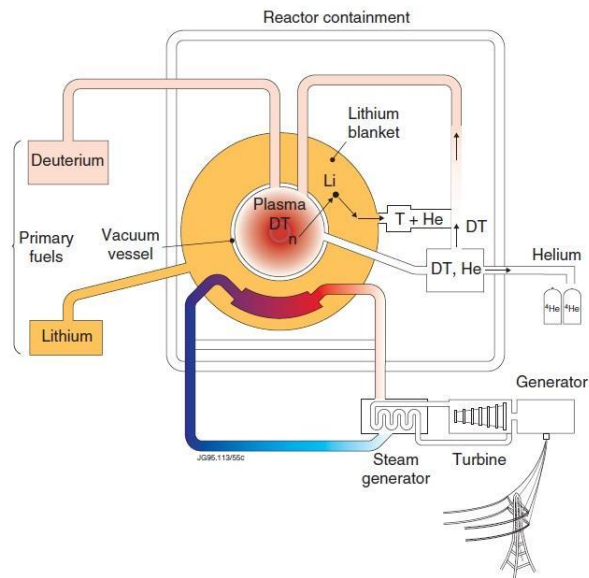


Figure 1.4: Schematic of the breeding blanket in a D-T fusion reactor

A typical breeding blanket in a fusion reactor consists of breeder, multiplier, coolant and structural materials. The most common solid breeder materials are Li_2TiO_3 , Li_2ZrO_3 , Li_2O , LiAlO_2 , and Li_4SiO_4 . The liquid breeder materials are lithium metal and Pb-Li eutectic. Physical and tritium breeding properties of the some breeding materials are given in *Table 1.2*.

Table 1.2: Physical properties of lithium compounds for tritium breeding with neutrons [28]

Material	Properties					
	Breeding yield	Melting point	Gram density	Li density	Heat capacity	Thermal conductivity
		$^{\circ}\text{C}$	g/cc	g/cc	J/(g.mol.K)	W/m.K
Li_2O	Good	1430	2.01	0.93	54	4-6
Li_2SiO_3	Fair	1200	2.53	0.39	100-150	2-5.5
Li_2TiO_3	Fair	1533	3.43	0.44	110-185	1-1.5
Li_4SiO_4	Fair	1250	2.39	0.55	140	2-5.5
LiAlO_2	Fair	1610	2.56	0.27	-	3.5-4.7
Li	Good	180	0.50	0.50	4140	50
$\text{Li}_{17}\text{Pb}_{83}$	Very good	235	9.40	0.06	170	17

The desired properties of a breeder material in the fusion reactor blankets are as follows: high concentration of lithium atoms, low tritium retention, tritium release at low temperatures, low radiation damage & neutron activation of functional and structural materials, mechanically stable at reactor operating temperatures, high thermal conductivity etc. The other critical component of a breeding blanket is neutron multiplier material. It is mandatory to increase the number of neutrons in the blanket region by neutron multiplication reactions to ensure the availability of neutrons to compensate for the leakage through blankets and loss due to parasitic

reactions. Desirable properties of the multiplying materials include high (n, xn) cross-sections, low neutron absorption cross-sections, low activation for occupation exposure and rad-waste purposes, etc. The most common neutron multiplying materials proposed for fusion breeding blankets are Lead and beryllium. Lead has higher (n, xn) cross-section than beryllium but the threshold of neutron reaction with beryllium is lower. Due to this reason beryllium can have multiplication reactions with the secondary neutrons produced by fusion neutrons. Both multiplier and breeder materials are contained in the structural materials. Structural materials also have impact on the neutronics performance of the breeding blanket i.e. Tritium Breeding Ratio (TBR) is affected by amount of structural material. The most common structural materials proposed for the blankets are ferritic steels. Extraction of tritium produced and cooling of the blanket region is performed by deploying coolants. These coolants and extractors are mixture of different gases. The few examples of the extraction and coolant gases are hydrogen and helium.

As shown in *Figure 1.4* that the bred tritium will have to be extracted from the blanket region and stored for fueling the plasma. This cycle is termed as fuel cycle. There will be some losses in this cycle due to permeation, retention in the vessel and incomplete extraction of the bred tritium. Due to its radioactive nature it will keep on decaying till it is used in the plasma. There are no external sources for the tritium breeding, so tritium will have to be produced for the next generation plants. All these factors impose a requirement on the design of breeding blanket to produce more tritium than it consumes in the plasma. This parameter is expressed as **tritium breeding ratio (TBR)** i.e. the average number of tritium atoms produced in the blanket per tritium atom consumed by plasma. For tritium self-sufficiency **TBR must be greater than**

unity to compensate for the losses in fuel cycle, radioactive decay, inventory for the next generation plants and reserve inventory in case of failure of fuel cycle.

1.4 Breeding blankets testing in ITER

ITER is an experimental fusion reactor with 500 MW fusion power. The goal of ITER is to demonstrate the scientific and technological feasibility of fusion power for peaceful purposes. Approximately 400 MW power will be carried by the neutrons emitted from D-T fusion reactions in ITER. A small portion of these neutrons in ITER will be used for tritium breeding in testing modules called Test Blanket Modules (TBM). The main objective of TBM program is to provide the first experimental data on the performance of integrated breeding blankets in real fusion environment [29]. The ITER TBM program is aiming to demonstrate that fusion reactors can be self-sufficient in tritium and extract high grade heat for electricity generation. The TBM program involves six breeder blankets that have been designed by various collaborations between ITER members. These test blanket systems (TBS) are classified as follows [29]:

- Helium Cooled Lithium Lead (HCLL) TBS and the Helium Cooled Pebble Bed (HCPB) TBS;
- Water Cooled Ceramic Breeder (WCCB) TBS and the Dual Coolant Lithium;
- Dual Coolant Lithium Lead (DCLL) TBS;
- Helium Cooled Ceramic Breeder (HCCB) TBS and the Lithium Lead Ceramic Breeder (LLCB) TBS

Each of the six breeder blanket designs to be tested on ITER has a slightly different design and these are subject to change. Overviews of each of these blanket designs are

available in the references [17, 30–33]. Each of the six blanket design teams will have the opportunity to create four modules to test various aspects of their design [34]. Each of these modules will be inserted into one of three dedicated equatorial ports at different times.

1. **Electromagnetic transient test blanket module (EM-TBM):** As the blankets have large amounts of ferromagnetic material they are expected to affect the plasma behavior. The EM-TBM will be used to investigate the consequences of electromagnetic transients inside the blankets.
2. **Neutronics and tritium production test blanket module (NT-TBM):** These modules will be installed prior to the D-T phase and will test the blankets tritium production.
3. **Thermo-mechanics test blanket module (TM-TBM):** They will test the thermal mechanical behavior of the breeder materials.
4. **Plant integration test blanket module (INT-TBM):** They will demonstrate the blankets ability to produce tritium, extract tritium and extract heat under different plasma conditions.

1.5 Major issues for the breeding blankets

In this section several issues linked with tritium breeding blanket technology are discussed.

1.5.1 Tritium self-sufficiency

Self-sufficiency is a key issue for the breeding blanket design as the world supply of tritium is limited and current civil inventory will be exhausted by ITER operations.

Therefore the breeding blanket design must demonstrate that they can generate sufficient tritium for its own use and inventory for the future reactors. Tritium self-sufficiency is affected by the plasma physics and technology conditions of the fusion systems. These include plasma configuration, operation modes and parameters, control systems for plasma stability, heating and exhaust systems embedded in blanket and tritium processing systems [1]. To ensure self-sufficiency, the calculated achievable tritium breeding ratio (TBR) should be larger than the required TBR. The required TBR should exceed unity by a margin that compensates for tritium losses, radioactive decay, tritium inventory in plant components, and supplying inventory for start-up of other plants [1]. The latter two have the largest impact on the TBR. Amount of on-line reserve tritium inventory required is uncertain and need to be assessed. Tritium fractional burn-up impacts tritium inventory. High burn-up fractions are desirable to reduce the required TBR. An effort should be made to reduce the amount of structural material particularly in the first wall (FW) and front 10 cm of blanket. Uncertainties in calculating the achievable TBR could be as high as 30% due to uncertainties in system definition, modelling and calculation methods and nuclear data [1]. An aggressive effort is required to reduce the uncertainty as low as possible. The achievable overall TBR depends on the confinement scheme due to the impact on breeding blanket coverage and possible limitation on blanket thickness. Tritium self-sufficiency in D-T fusion power plants cannot be assured unless specific plasma and technology conditions are met. The uncertainty in calculated TBR can also lead to surplus tritium generation. Surplus tritium production is also issue for handling the surplus tritium than the capacity of the plant system [2].

1.5.2 Closed tritium fuel cycle

In the D-T fusion reactor, the amount of tritium to be handled is 10^{17} Bq (30 g) under accountancy of a few tens of Bq [35]. The form of tritium handled includes solid pellets and gas (both for fueling), energetic neutrals and ions (for neutral and ion beam heating) and plasmas, having temperatures ranging from 10 to 10^9 K. Therefore the physics and chemistry of the interactions of tritium with materials used in the reactor or tritium confinement systems are very complex. The high levels of radioactivity of tritium generate additional problems due to emission resulting in the decay heat i.e. all the pellets can't be kept together. Furthermore defect formation by electron excitation and helium-3 production (decay product of tritium after decay) result in various damages in materials. This, in turn, influences basic process of hydrogen-materials interactions such as adsorption, solution, diffusion and permeation in materials. The tritium burn-up rate in the plasma is very low (few % of injected tritium) and the majority has to be recovered by pumping out from the reactor vessel. Since the recovered tritium includes H, D, T, He and other impurities, it should be purified and then recycled. The reactor is surrounded by blanket systems to realize power generation and tritium production simultaneously. To enhance the recovering rate of T produced in the blanket, addition of water vapor is well known to be effective, but T diluted in H_2O is very hard or need lots of energy to be recovered, which increases fusion energy cost. In addition, tritium produced in the blanket easily permeates into coolant. The permeated tritium readily reacts with surface contaminants to produce hazardous tritiated water. In particular, ferrite, a low activation structure candidate material, has very high tritium permeability and needs permeation barrier with the permeation reduction of 5-6 orders of magnitude [35].

Tritium injected into the plasma can be permeated to the coolant water easily producing HTO, resulting diluted tritiated water from which tritium recovery is very cost consuming.

1.5.3 MHD effects in liquid blankets

Blanket designs utilizing liquid breeder materials (molten lithium salts or eutectic alloys) have problem of the magneto-hydrodynamic (MHD) pressure drop, flow modifications, additional joule heating etc. due to metal flow under strong magnetic fields. The MHD effects, being coupled with heat and mass transfer, have a profound impact on the blanket performance, operation and safety, which can be either positive or negative depending on the specific issue. If MHD effects on blanket operation are better understood and predicted in normal and off-normal conditions, fusion blanket designs can be significantly improved [36].

1.5.4 Radiation-hard materials

In fusion power reactor, the breeding blanket materials will be subjected to very high fluences of nuclear radiation (neutrons, gammas, betas etc.) due to its proximity to the plasma core and its function of tritium breeding. High energy neutrons will produce displacement damage via displacement cascade and gases i.e. hydrogen and / or helium through transmutation reactions. This damage and gas production in materials will result into the degradation of the mechanical properties of the materials. High temperatures of the blanket will further deteriorate the mechanical properties. Therefore in order to ensure the proper functioning of the blanket materials, radiation resistant materials suitable to function in the breeding blankets environment need to

be developed. For the breeding blankets, the materials that need to be developed include beryllium and/or beryllium-titanium alloys for neutron multiplication, lithium bearing compounds for tritium generation, and the liquid metal coolants like Lead-lithium eutectic as breeder and multiplier. The critical issues related to the first wall materials include their transmutation and displacement damage due to the high energy neutrons, manufacturing the large sized intricate shapes and their joining and codes for qualification of the materials for use in fusion environments [37]. Helium produced in the materials due to (n, α) reactions of the neutrons with the atoms constituting the first wall is an issue that is difficult to deal with. The rate of production of helium in the material due to its irradiation is very high (in the range of 200-600 appm/yr for steel) and, therefore, in its lifetime of several years, the material is likely to accumulate huge amounts of helium. Since the solubility of helium in any metallic matrix is known to be zero, the high temperature helium embrittlement is an issue of major concern. Furthermore, this helium, under thermal fatigue likely to be experienced by the first wall of a tokamak, limits the life of the first wall austenitic steel severely [37].

1.5.5 Safety issues

In addition to the functional requirements, breeding blanket must demonstrate safe operation in normal and off-normal conditions, low environmental impacts in terms of radioactive and other waste materials (over the life of the plant and after shutdown / decommissioning).

The use of the radioactive tritium in fusion reactors is one of the key concerns with regard to the safety for workers and the public. The amount of tritium burnt in fusion

reactor is approximately 1.8 mg/s to generate 1 GW of fusion power. Since only a small fraction of injected tritium is burnt in the fusion reaction. Therefore the amount of the tritium to be handled in the fuel cycle will be huge. Safe, reliable and efficient tritium management in the breeder blanket faces unique technological challenges. DEMO will require a continuous operation of the tritium fuel cycle involving very high tritium amounts to be handled in the blanket systems. Important requirements are high tritium extraction efficiency from the blanket, low tritium permeation into the coolant, and an accurate, fast and reliable tritium analytics. To cope with the increased requirements for DEMO one need to find improved and may be even new processes for the tritium extraction system and the coolant purification system [38]. In addition, the development of techniques and concepts for tritium accountancy is one of the key issues to be solved in the future.

The other safety issues to be handled in the breeder blankets are radioactivity release due to failure of the cooling system and hydrogen generation in the liquid metals when water is mixed with liquid metal in an accidental scenario.

1.6 Overview of the thesis

The first part of the thesis deals with the development and performance characterization of the diagnostics for the measurement of source neutrons, on-line & off-line tritium, and neutron spectra in assembly zones. Source neutron absolute yield of tube manufactured by M/s SODERN [39] was measured by deploying activation technique and its time profile with ^3He counter cross-calibrated against activation measurements [40–43]. In order to include the neutron emission anisotropy and angle dependent energy spectra of D-T reaction, a calculation model (source neutron

definition) was developed using the codes SRIM-2008, NeuSDesc [44, 45]. Calculated anisotropy and angle-dependent neutron spectra along-with the generator geometry are modelled in 3D radiation transport code MCNP. The source model developed for the neutron generator was validated by measuring the spectral indices of various neutron induced reactions in the foils placed at the surface of tube. High Purity Germanium (HPGe) detector was used for the measurement of γ -activity in the foils and was absolutely calibrated for absolute efficiency in wide energy range with point sources and Monte Carlo calculations. The detector model developed for Monte Carlo calculations can be used to obtain the absolute efficiencies for activated foils [46]. Two kinds of tritium diagnostics were developed for the tritium profile measurement in the mock-ups containing breeding blanket materials. First diagnostics is based on the Li_2CO_3 pellets irradiated in the mock-ups and then tritium counting using liquid scintillation technique. The second diagnostic method is to measure the tritium on-line in the mock-ups and it is based on the charged particle detector covered with ^6Li to triton converter. Both these diagnostics methods were characterized and calibrated to measure the tritium profile in the mock-ups.

In the second part of the thesis, analysis results of the irradiation experiments with the breeding blanket materials are discussed. The measured nuclear responses in the breeding blanket assemblies were compared with the calculated values with the neutron transport tools applied for the design of fusion breeding blankets. The 3D radiation transport code MCNP and nuclear data libraries FENDL-2.1 and FENDL-3.0 were used for the calculation of nuclear responses. The main focus of this part is to experimentally validate the calculation tools applied for breeding blanket nuclear design and to quantify the uncertainty in tritium production rate due to uncertain

nuclear data. Benchmark irradiation experiments are reported for three kind of breeder material assemblies LiAlO_2 , Li_2TiO_3 pebbles, and powder. The experiment with LiAlO_2 breeding material was performed by measuring the tritium production rate profile inside the assembly and comparison with the calculations [20]. The second mock-up experiment was performed by measuring tritium production with two kinds of diagnostics in the geometry simulating the LLCB TBM in ITER [18]. Neutron spectral index of $^{115}\text{In}(n, n')^{115\text{m}}\text{In}$ reaction is also measured and compared with calculations to study the prediction capability of $(n, 2n)$ reaction cross-section data in the FENDL-2.1 library. The third experiment with Li_2TiO_3 powder and same geometry used in the second experiment is focused to measure the neutron spectrum in the whole range from thermal to source neutron energy [19]. The objective of this experiment was to validate the neutron spectrum prediction capability of the calculation tools in the neutron energy range which is of interest to breeding blankets.

The structure of the thesis is as follows;

1. **Chapter one** introduces the preamble to the nuclear fusion and breeding blankets research. Later in the chapter motivation of the research work reported in this thesis is discussed.
2. **Chapter two** describes the characterization and validation of the source neutrons from D-T neutron generator. This chapter also describes the calibration of HPGe detector used for the measurement of γ -activities in the foils.
3. **Chapter three** describes the development and performance characterization of two kinds of tritium measuring diagnostics. These diagnostics are developed for the mock-up experiments with breeding blanket materials.

4. **Chapter four** reports the experimental tritium production rate results in the LiAlO_2 assembly and these results are compared with the calculated values obtained with 3D radiation transport code MCNP and nuclear data library FENDL-2.1.
5. **Chapter five** presents the design, experimental and calculation results of the mock-up assembly with Li_2TiO_3 breeder material in the ITER LLCB TBM geometry.
6. **Chapter six** discusses the experimental measurement of neutron spectra in the breeding assembly containing Li_2TiO_3 powder in the energy range from thermal to source neutrons relevant to breeding blankets. Measured spectra are compared with the calculated spectra and discrepancy between them is discussed. The cross-section data responsible for the discrepancy are identified.
7. **Chapter seven** gives a brief summary of the research work carried out in this thesis along with future outlook.

Chapter 2

Characterization of source neutrons from D-T generator tube

2.1 Introduction

Nuclear responses in a neutronics benchmark experimental assembly are strongly dependent on the source neutron emission i.e. absolute yield, anisotropy, and angular spectra. The absolute neutron yield is required for the normalization of measured tritium and foil saturation activities to determine tritium production rate, and neutron induced reaction rates respectively. Accurate angular spectra and anisotropy of source neutrons are required for the transport code used for analysis of benchmark experiment. Therefore source neutrons must be well characterized in terms of absolute intensity, energy and angular emission with qualified uncertainty. The neutron source used for the experiments reported in the thesis is a sealed neutron tube manufactured by M/s Sodern, France (Model GENIE35) [39]. This sealed neutron generator tube is based on the accelerator concept in which accelerated deuteron beam is bombarded on the Ti-T target to produce D-T neutrons. Being a sealed tube, it is impossible to perform any in-situ measurement on it. Therefore associated α -particle method, widely used for the absolute measurement of neutron yield in the D-T generators,

can't be employed in this source [47-48]. Therefore activation technique has been employed for the measurement of source neutrons from this sealed neutron generator tube.

A mathematical expression is derived later in this chapter for the absolute neutron yield estimation from the measured neutron induced activities in the activated foils. Various correction factors required for the measurement of neutron yield are discussed. Thereafter calibration of HPGe γ -ray spectrometer used for the activated samples is described. Then characterization of source neutrons is performed in terms of absolute neutron yield, anisotropy of source emission and angular spectra of 14 MeV neutrons from D-T neutron generator. Finally a 3D model for neutron transport calculations in the GENIE35 generator geometry is developed and validated.

2.2 Neutron activation method

D-T fusion reaction in the neutron generator tube produces two energetic particles: α -particle and neutron. The α -particles being short-ranged can't come out of the neutron generator tube. Most of the source neutrons, being high energetic and penetrating particles, can pass through the tube material without any collision. Activation method is best suited to measure these un-collided neutrons using threshold reactions having threshold energy close to the source neutrons. Virgin neutrons by interacting with the foil isotopes produce gamma emitting radio-nuclides in the foil material. By measuring the gamma rays in the activated foils or samples, the activation rate of the target nuclide in the foil can be estimated and hence the number of neutrons passing through the foil at that particular location. The relationship between incident neutron flux on the foil and activity produced in the foils is derived in the following

discussion.

Let a target "A" of mass m being irradiated in a neutron flux $\phi(E)$ producing radioactive product "B".

Let:

$\sigma_A(E)$: cross-section for producing the nuclide B at energy E

λ_B : decay constant of the nuclide B

$\sigma_B(E)$: neutron absorption cross-section of nuclide B at energy E

$N_A(t)$: number of atoms of nuclide A with atomic mass A_A present at time t.

The neutron induced reaction on target "A" producing radioactive nuclide "B" (decay constant λ_B) with subsequent decay to nuclide "C" can be written as:



The generation rate of nuclide "B" is proportional to the activation cross section σ_A , neutron flux $\phi(E)$, and the number of target atoms N_A . During irradiation, the radioactive nuclide "B" decays as well as it can be destroyed by the neutron absorption. Therefore net production rate of the nuclide B can be written as:

$$\frac{dN_B(t)}{dt} = N_A(t)\sigma_A\phi - N_B(t)\sigma_B\phi - \lambda_B N_B(t) \quad (2.2)$$

In mathematical expression 2.2, $\sigma\phi$ is equal to

$$\sigma\phi = \int_0^\infty \sigma(E)\phi(E)dE = \bar{\sigma} \int_0^\infty \phi(E)dE = \bar{\sigma} \phi \quad (2.3)$$

In mathematical expression 2.3, $\bar{\sigma}$ is spectrum averaged cross-section. The spectrum averaged cross-section should be determined using expression 2.3 for the neutron flux measurement using activation technique. Hereafter, spectrum averaged cross-section is represented without bar on σ for convenience.

With the initial condition $N_B(0) = 0$ i.e. number of radio-isotopes in the target are zero

before irradiation, the analytical solution of the first order differential equation 2.2 is given by:

$$N_B(t) = \frac{\sigma_A N_A(0)\phi}{\lambda_B + \sigma_B\phi - \sigma_A\phi} \{e^{-\sigma_A\phi t} - e^{-(\lambda_B + \sigma_B\phi)t}\} \quad (2.4)$$

The total activity of nuclei "B" produced in the target, $A_B(t_{ir})$ during irradiation time t_{ir} can be calculated by:

$$A_B(t_{ir}) = N_B(t_{ir})\lambda_B = \frac{\sigma_A N_A(0)\phi}{1 + \frac{(\sigma_B - \sigma_A)\phi}{\lambda_B}} \{e^{-\sigma_A\phi t_{ir}} - e^{-(\lambda_B + \sigma_B\phi)t_{ir}}\} \quad (2.5)$$

Equation 2.5 is the general expression of the activation process in the irradiated samples. In practice, irradiation targets are selected in such a way that:

1. The fraction of the target nuclei destroyed by neutron irradiation is negligible, i.e. $\sigma_B\phi t \ll 1$.
2. The radioisotope produced has a neutron absorption cross-section such that $\lambda_B \gg \sigma_B\phi$.

Under above-mentioned two assumptions, equation 2.5 reduces to:

$$A_B(t_{ir}) = \sigma_A N_A(0)\phi \{1 - e^{-\lambda_B t_{ir}}\} \quad (2.6)$$

From equation 2.6, neutron flux can be determined from measured activity, $A_B(t_{ir})$ of the neutron irradiated target.

The foil or sample irradiation and subsequently activity measurement process in the activated samples is systematically depicted in *Figure 2.1*.

The irradiated foil or sample is counted after some time when irradiation process is over. This time is termed as cooling time (*Figure 2.1*). The radioactivity in the activated sample at time t after irradiation ($t = 0$ at the end of irradiation) is given by:

$$A_B(t) = A_B(t_{ir})e^{-\lambda_B t} = \sigma_A N_A(0)\phi \{1 - e^{-\lambda_B t_{ir}}\}e^{-\lambda_B t} \quad (2.7)$$

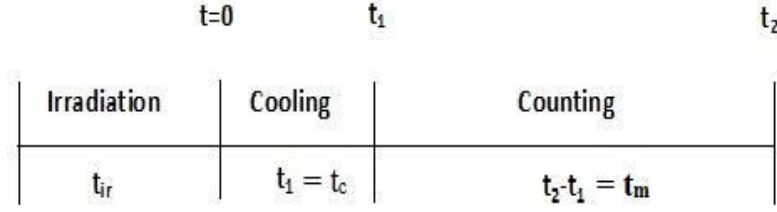


Figure 2.1: Foil irradiation and activity measurement sequence

Activated samples are counted for time, $t_m = t_2 - t_1$ to measure the radioactivity produced by neutron irradiation process. This process is termed as counting time t_m . Total measured disintegrations during counting time (t_m) can be obtained by integrating equation 2.7 between times t_1 to t_2 :

$$\begin{aligned}
 D(t_1, t_2) &= \int_{t_1}^{t_2} A_B(t) dt = \sigma_A N_A(0) \phi \{1 - e^{-\lambda_B t_{ir}}\} \int_{t_1}^{t_2} e^{-\lambda_B t} dt \\
 &= \frac{\sigma_A N_A(0) \phi}{\lambda_B} \{1 - e^{-\lambda_B t_{ir}}\} \{e^{-\lambda_B t_1} - e^{-\lambda_B t_2}\}
 \end{aligned} \tag{2.8}$$

One of the option to deduce the radioactivity in the activated samples is the counting of gamma rays resulting from the decay of neutron induced reaction product. Another option for the measurement of radioactivity in the activated sample is counting of beta rays. The latter option is not preferred for those samples which emit gamma rays because of difficulties in measuring beta rays from metal or solid samples. In the current work, the foil activities are deduced from first option i.e. counting of gamma rays form activated samples. Hence, the methodology is developed considering this option in the subsequent discussion.

The number of emitted gamma rays of energy E_k per unit disintegration is known as branching ratio (I_γ). Thus this factor is considered when converting counted gamma

rays into radioactivity produced by neutrons. Only a fraction of the emitted gamma rays from activated sample result in the photo-peak counts in the detector. This factor is known as intrinsic photo-peak efficiency of gamma ray detector (ϵ). The number of gamma rays incident on the detector depends on the distance between irradiated foil and detector. This factor is known as geometrical efficiency (Ω). Introducing these factors in to equation 2.8 give the total number of photo-peak counts detected in the gamma ray detector during counting time $t_2 - t_1$.

$$P_k = \frac{I_\gamma \epsilon \Omega \sigma_A N_A(0) \phi}{\lambda_B} \{1 - e^{-\lambda_B t_{ir}}\} \{e^{-\lambda_B t_1} - e^{-\lambda_B t_2}\} \quad (2.9)$$

Let $t_1 = t_c$ (cooling time) and $t_2 - t_1 = t_m$ (measuring time). On substitution of these values, equation 2.9 can be used to determine the photo-peak counts detected in the detector in terms of irradiation, cooling and counting times.

$$P_k = \frac{I_\gamma \epsilon \Omega \sigma_A N_A(0) \phi}{\lambda_B} \{1 - e^{-\lambda_B t_{ir}}\} e^{-\lambda_B t_c} \{1 - e^{-\lambda_B t_m}\} \quad (2.10)$$

By rearranging equation 2.10 in terms of neutron flux, ϕ :

$$\phi = \frac{P_k \lambda_B}{I_\gamma \epsilon \Omega \sigma_A N_A(0) \{1 - e^{-\lambda_B t_{ir}}\} e^{-\lambda_B t_c} \{1 - e^{-\lambda_B t_m}\}} \quad (2.11)$$

Equation 2.11 is the most convenient form for the estimation of neutron flux from measured gamma counts in the neutron activated samples. It is clear from mathematical expression 2.11 that the neutron activation method can be used to determine the absolute neutron flux.

Absolute neutron flux can be used to determine the neutron yield of a source with the appropriated corrections due to emission anisotropy, source properties (point, surface or volume), source-foil geometry etc. Neutron yield Y_n , of a point source, can be linked to flux at distance r by following expression:

$$Y_n = 4\pi r^2 \phi \quad (2.12)$$

Generally, the geometry of the accelerator based D-T neutron source is in the form of a disk. The foil used to measure the neutron flux also has the shape of disk. Let the correction factor due to both these factors is k_G . The neutron emission from D-T neutron generators in laboratory frame is not isotropic due to bombardment of mono-directional energetic deuteron beam. It depends on the energy of the incident deuteron beam and tritium target parameters. Let the anisotropy factor be k_A due to neutron emission anisotropy. The neutrons emitted from target are also attenuated by target, neutron generator tube and foil materials. Let the correction factor due to absorption of virgin neutrons in these materials be k_R . By introducing these factors into equation 2.12, the neutron yield expression takes the form.

$$Y_n = \frac{4\pi r^2 \phi}{k_G k_A k_R} \quad (2.13)$$

Equation 2.13 can be used for the estimation of neutron yield by using data of measured neutron flux and various correction factors.

2.3 Calibration of HPGe γ -ray detector

High-Purity Germanium (HPGe) detector is widely used to measure γ -rays from activated samples due to its very good energy resolution, peak-to-valley ratio, high photo-peak efficiency etc. To determine the neutron induced activity in the activated foils, it is essential to calibrate it absolutely for photo-peak efficiency in a wide energy range. Activated foils used for neutron flux measurement are extended (volumetric) γ -ray sources. The sources available for efficiency calibration of HPGe detector are usually point sources. Therefore it is difficult to determine the photo-peak efficiency

precisely for extended sources using these point sources. A method was developed to address this problem. This method has following three steps: (1) Experimental photo-peak (PP) efficiencies for point sources are determined and compared with calculated PP efficiencies by Monte Carlo code (2) Detector dimensions in Monte Carlo (MC) model is changed in such a way that the calculated efficiencies match with experimental values (3) Optimized MC model is validated in the whole energy range and different source-to-detector distances using calibrated point sources. This MC model then can be used to find the photo-peak efficiency for any kind of source geometry at desired energy. Advantage of this methodology is that the self-shielding of the activated samples is built-up in the model by defining the geometry of it and the real source-detector geometry can be considered in the model.

Table 2.1: Physical characteristics of HPGe detector (Model GR5023 Canberra Industries)

Property	Value
Crystal active diameter	67.5 mm
Crystal thickness	69.5 mm
Crystal-window distance	5 mm
Window thickness	500 μ m
Window material	Be

Reverse electrode coaxial germanium detector model GR5023 manufactured by M/s Canberra industries, USA was used for the measurement of γ -rays in the neutron activated samples. Physical characteristics of this detector are given in *Table 2.1*. It can be seen from *Table 2.1* that the detector has crystal thickness of 67.5 mm and has beryllium window towards source position.

HPGe detectors are usually characterized by relative efficiency to NaI(Tl) detectors. Relative efficiency is defined as the ratio of efficiencies of HPGe and 3" \times 3" right

cylindrical NaI(Tl) detectors at 1.33 MeV γ -ray energy from a point ^{60}Co source at 25 cm from the face of both detectors as per IEEE test procedures for Germanium detectors for ionizing radiation [49]. In order to measure relative efficiency of the HPGe detector, a ^{60}Co point source was placed 25 cm from the windows of both NaI(Tl) (3" \times 3") and HPGe detectors. Result of measured relative efficiency at 1.33 MeV γ -ray energy from a point ^{60}Co source at 25 cm distance with 3" \times 3" NaI(Tl) and HPGe detectors are given in *Table 2.2*.

Table 2.2: Measured relative efficiency of HPGe detector for 1.33 MeV γ -energy (^{60}Co source) at 25 cm distance (cps = counts per second)

Measured count rate (cps)		Relative efficiency
NaI(Tl)	HPGe	%
34.96	52.34	66.8

The relative efficiency of HPGe detector was also measured by manufacturer and was quoted to be 64.9%. The present measurement shows quite good agreement with the manufacturer value (difference between two measurements is 2.8%). The absolute efficiency of 3" \times 3" NaI(Tl) detector at 1.33 MeV energy is well measured and is found to be 1.21×10^{-3} [49]. Product of NaI(Tl) absolute and HPGe relative efficiencies gives absolute efficiency of HPGe at 1.33 MeV energy. Therefore absolute efficiency of the Canberra made HPGe detector model GR5023 is calculated to be 8.08×10^{-4} at 25 cm from detector window at 1.33 MeV energy. The efficiency of the HPGe detector was also calculated with Monte Carlo code MCNP by modelling the detector geometry parameters given in *Table 2.1*. The MCNP calculated value was overestimated with respect to the measurement by 8%. The reasons for this overestimation could be shrinking of crystal due to application of high-voltage and presence of dead layer on the detector [50]. Therefore crystal was modelled in the

calculation by shrinking it by 1 mm in diameter and 1.8 mm in length. The calculated efficiency after this change matched with the measured efficiency. This model will be called optimized detector model for rest of the calculations in the thesis.

The optimized detector model was experimentally validated at different gamma ray energies and detector-source distances using calibrated point sources for their activities. Experimental validation results of the optimized detector MC model with ^{60}Co source at three detector-to-source distances are given in *Table 2.3*. Results of the experimental validation with ^{152}Eu source are given in *Table 2.4*. Source-to-detector distances chosen in *Table 2.3* and *Table 2.4* are such that the true coincidence effect in the detector is negligible i.e. loss of counts in the photo-peaks due to simultaneous detection of one of the gamma rays from ^{60}Co / ^{152}Eu and other gamma ray from same source or its secondary radiation. The experimental validation results with ^{137}Cs source are given in *Table 2.5*. It can be concluded from these results (*Table 2.3*, *Table 2.4* and *Table 2.5*) that the Monte Carlo optimized detector model is able to predict the absolute efficiency of HPGe detector within 3% difference with the experiment. This model will be used throughout the thesis to estimate the absolute efficiency of the various gamma rays arising from the activated foils by modelling the geometry of the foil of interest.

Table 2.3: Experimental validation of optimized detector model with ^{60}Co source

Distance cm	Efficiency @ 1.17 MeV			Efficiency @ 1.33 MeV		
	Exp. (E)	Cal. (C)	C/E	Exp. (E)	Cal. (C)	C/E
15	2.17E-03	2.15E-03	0.99	1.97E-03	1.97E-03	1.00
25	9.03E-04	8.93E-04	0.99	8.14E-04	8.19E-04	1.01
30	6.46E-04	6.44E-04	1.00	5.94E-04	5.90E-04	0.99

Table 2.4: Experimental validation of optimized detector model with ^{152}Eu source

Energy MeV	Detector-source dist. 25 cm			Detector-source dist. 30 cm		
	Exp. (E)	Cal. (C)	C/E	Exp. (E)	Cal. (C)	C/E
0.122	3.51E-03	3.61E-03	1.03	2.48E-03	2.54E-03	1.03
0.245	2.63E-03	2.70E-03	1.03	1.86E-03	1.92E-03	1.03
0.344	2.09E-03	2.13E-03	1.02	1.46E-03	1.51E-03	1.03
0.779	1.14E-03	1.18E-03	1.03	8.23E-04	8.46E-04	1.03
0.964	9.87E-04	1.02E-03	1.03	7.12E-04	7.36E-04	1.03
1.112	8.93E-04	9.24E-04	1.03	6.46E-04	6.68E-04	1.03
1.408	7.68E-04	7.89E-04	1.03	5.53E-04	5.68E-04	1.03

Table 2.5: Experimental validation of optimized detector model with ^{137}Cs source

Distance cm	Efficiency ($E_\gamma = 0.662$ MeV)		
	Experiment	Calculation	C/E
10	6.02E-03	6.12E-03	1.02
15	3.15E-03	3.19E-03	1.01
25	1.31E-03	1.32E-03	1.01
30	9.39E-04	9.47E-04	1.01

2.3.1 Error estimate in the efficiency calibration

Maximum error in the absolute efficiency calibration of the HPGe detector was estimated including relative uncertainty in the activity of ^{152}Eu source, statistical error of the measured photo-peak counts, photo-peak area determination uncertainty and difference in experiment and model calculation i.e. the maximum difference in predicting the absolute efficiency by MC detector model.

Values of these errors and overall uncertainty in the efficiency calibration of HPGe detector is given in *Table 2.6*.

Table 2.6: Maximum uncertainty in the absolute efficiency calibration of HPGe detector

Uncertainty type	Uncertainty Value
¹⁵² Eu Activity	1.5%
Statistics of counts	0.5%
Photo-peak area	2%
C/E	3%
Overall	3.94%

Because all the errors in *Table 2.6* are random in nature and independent to each other therefore maximum uncertainty in the HPGe detector absolute efficiency calibration is estimated to be 3.94% using quadratic law of combination of errors. The systematic errors such as positioning of the source with respect to detector, pulse-pile up etc. in the efficiency calibration process were kept as minimum as possible.

2.3.2 Full energy photo-peak efficiency function

The full energy photo-peak efficiency (product of intrinsic and geometrical efficiencies) curve for the Canberra made HPGe detector model GR5023 with foil diameter 13 mm placed on the window and calculated with the optimized calculation model is shown in *Figure 2.2*.

The energy range of the calibration covers the gamma rays emitted from various activated foils used in the present thesis. As the self-absorption of gamma rays in foil material is distinct for each of the foils therefore the results shown in *Figure 2.2* don't include the self-absorption of gamma rays in foil material. However, the self-absorption by foils is included in the results shown later in the thesis. In some of the cases, foils were not put on the window of the detector. For those cases, the distance between foil and detector along-with foil self-absorption was included to estimate the

efficiency. The purpose of calibration curve here is to demonstrate the feasibility of the proposed method, energy range coverage and approximate values of the efficiency.

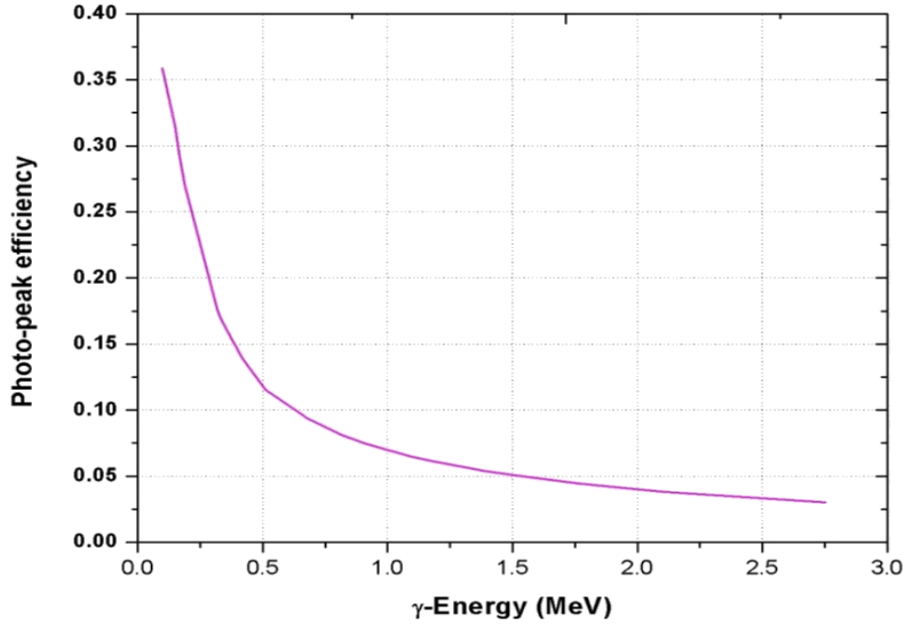


Figure 2.2: Photo-peak efficiency curve of Canberra made HPGe detector GR5023 for a foil of diameter 13 mm placed on the window of detector (without self-absorption of foils)

2.4 Anisotropy of source neutrons

As stated earlier, the neutron emission from D-T reaction in accelerator based neutron generators is anisotropic in the laboratory frame. It depends on the energy of the incident D^+ beam, ratio of Ti and T atoms in target, thickness and energy loss of deuteron in the target. Generally targets used in D-T neutron generators have thicknesses more than the range of the incident deuteron i.e. the targets are thick targets. This section is focused to quantify the neutron emission anisotropy from the Sodern made D-T neutron generator tube.

Schematic representation of a two body nuclear reaction in the laboratory frame is

shown in *Figure 2.3*. In *Figure 2.3*, the subscript “*a*” denotes the incident particle (deuteron), “*b*” the target particle (tritium), “*1*” the emitted neutron and “*2*” the emitted alpha particle. Letters *p* and θ represent the momenta in the laboratory frame and the angles between the outgoing particle and the deuteron direction.

The energy of the outgoing neutron (E_1) in lab frame is calculated according to the relativistic kinematic equation 2.14 [51]:

$$E_1 = \{(E_a + m_b)^2 - p_a^2 \cos^2 \theta\}^{-1} \times \left[(E_a + m_b) \left\{ m_b E_a + \frac{1}{2} (m_a^2 + m_b^2 + m_1^2 - m_2^2) \right\} + p_a \cos \theta_n \left[\left\{ m_b E_a + \frac{1}{2} (m_a^2 + m_b^2 - m_1^2 - m_2^2) \right\}^2 - m_1^2 m_2^2 - m_1^2 p_a^2 \sin^2 \theta_n \right]^{1/2} \right] \quad (2.14)$$

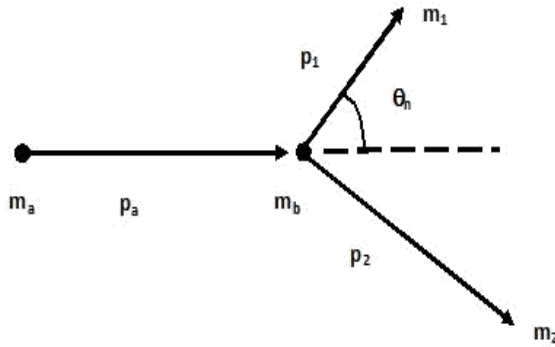


Figure 2.3: Schematic representation of a two body nuclear reaction in the laboratory frame

Units of particle masses and momenta in equation 2.14 are expressed in terms of energy i.e. unit of mass is E/c^2 and momenta E/c (E is the energy and c is the speed of light). Kinetic energy of the outgoing neutron can be obtained using value of E_1 from equation 2.14.

$$E_n = E_1 - m_1 \quad (2.15)$$

Momentum of the outgoing particle “1” (neutron) can be obtained from following expression by substituting the value of E_1 from equation 2.14.

$$p_1 = (E_1^2 - m_1^2)^{1/2} \quad (2.16)$$

Relative intensity of neutron emitted in the direction of emission angle θ_n normalized to the intensity for $\theta_n = 0^0$ is given by the following expression [52]:

$$\frac{I(\theta)}{I(0^0)} = \frac{\int_0^{E_d} \left(\frac{d\sigma}{d\Omega'} \right) \left(\frac{dE}{dx} \right)^{-1} \left(\frac{d\Omega'}{d\Omega} \right) (E, \theta_n) dE}{\int_0^{E_d} \left(\frac{d\sigma}{d\Omega'} \right) \left(\frac{dE}{dx} \right)^{-1} \left(\frac{d\Omega'}{d\Omega} \right) (E, 0^0) dE} \quad (2.17)$$

Where:

$\frac{d\sigma}{d\Omega'}$ = Differential cross-section in centre-of-mass (CM) frame

$\frac{dE}{dx}$ = Rate of energy loss of deuteron in Ti-T target

$\frac{d\Omega'}{d\Omega}$ = Solid angle conversion factor from CM to laboratory frame

Differential cross-section of D-T reaction ($\frac{d\sigma}{d\Omega'}$) can be calculated using DROSG2000 code [53] developed by IAEA to calculate neutron energies, differential cross-sections and differential yields, thick-target yields and white neutron spectra from mono-energetic neutron producing reactions. The calculated values of differential cross-section with DROSG2000 code as a function of D^+ energy in the center-of-mass (CM) frame is given in Figure 2.4.

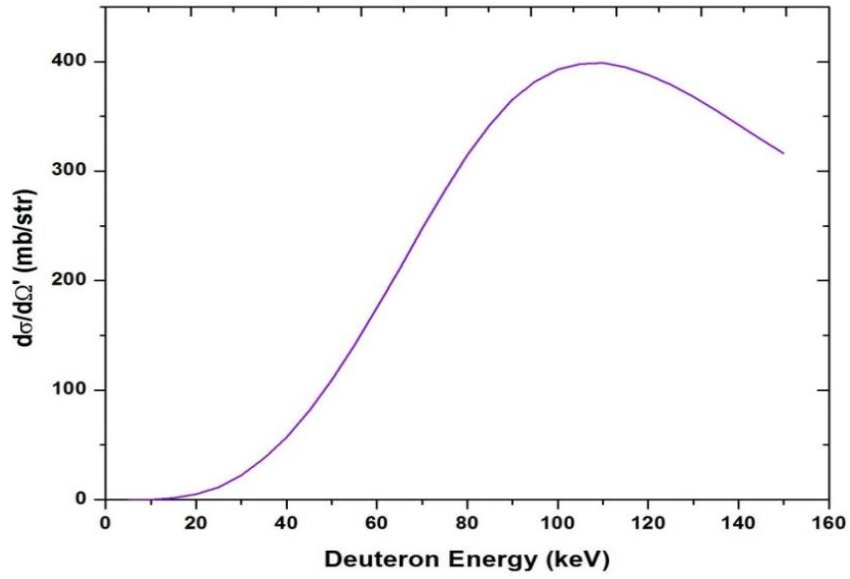


Figure 2.4: Differential cross-section of D-T reaction as a function of deuteron energy in center-of-mass frame calculated with DROSG2000 code

D^+ beam energy loss rate in Ti-T target (dE/dx) can be calculated with Monte Carlo code SRIM-2008 [44] which simulates physical processes of incident ion beam with the solid target atoms. SRIM-2008 calculated dE/dx is given in *Figure 2.5*. Ratio of the T and Ti atoms in the dE/dx calculation was assumed to be 1.5.

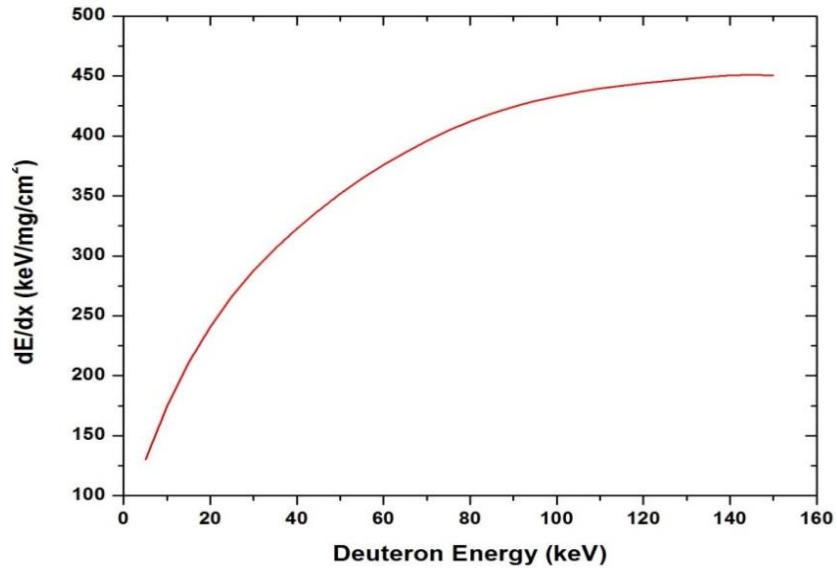


Figure 2.5: Energy loss rate (dE/dx) of D^+ beam in Ti-T target calculated with SRIM-2008 code

Following relativistic kinematics, solid angle conversion factors from the center-of-mass to the laboratory frame $d\Omega'/d\Omega$ can be written as for a two body reaction:

$$\frac{d\Omega'}{d\Omega}(E_d, \theta_n) = \frac{p_1^2}{(E_a + m_b)p_1 - p_a E_1 \cos\theta_n} \quad (2.18)$$

Solid angle conversion factor from the center-of-mass to the laboratory was calculated as a function of deuteron energy and neutron emission angle using equation 2.18. Results of the calculation at three emission angles 0° , 90° , and 180° are given in *Figure 2.6*.

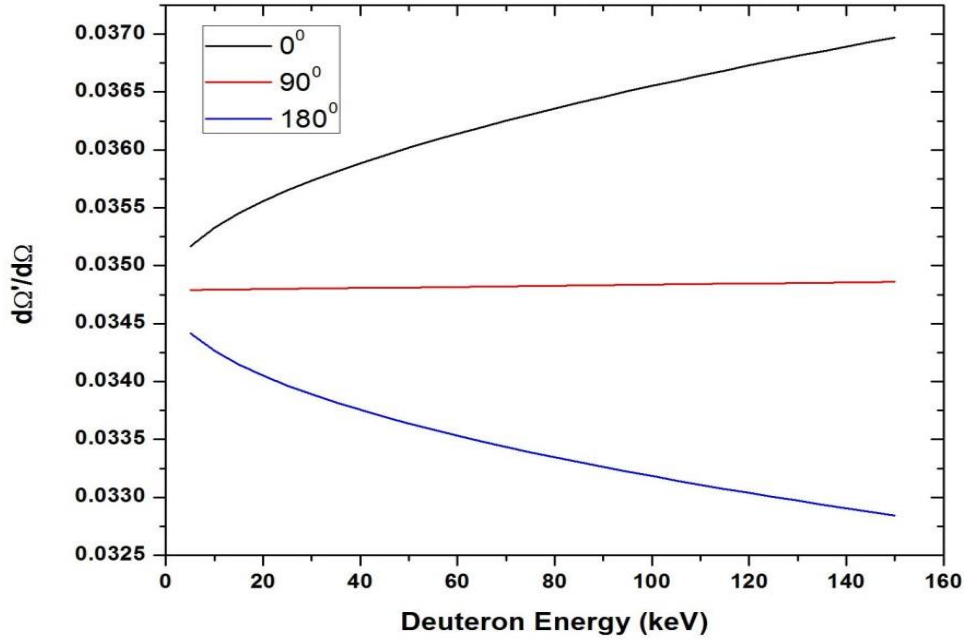


Figure 2.6: Solid angle conversion factor as a function of incident deuteron energy at three neutron emission angles (0° , 90° and 180°)

The results in *Figure 2.6* are given only up to 150 keV because the operating voltage in the Sodern neutron generator tube was kept at 150 keV for the experiments reported in this work. However this methodology is valid for higher deuteron energies also. It can be seen from *Figure 2.6* that the solid angle conversion factor and hence neutron anisotropy is almost independent of deuteron energy at 90° emission direction.

Relative intensity of neutrons at an angle with respect to 0^0 was calculated using mathematical equation 2.17. The result of the relative intensity as a function of neutron emission angle is shown in *Figure 2.7*.

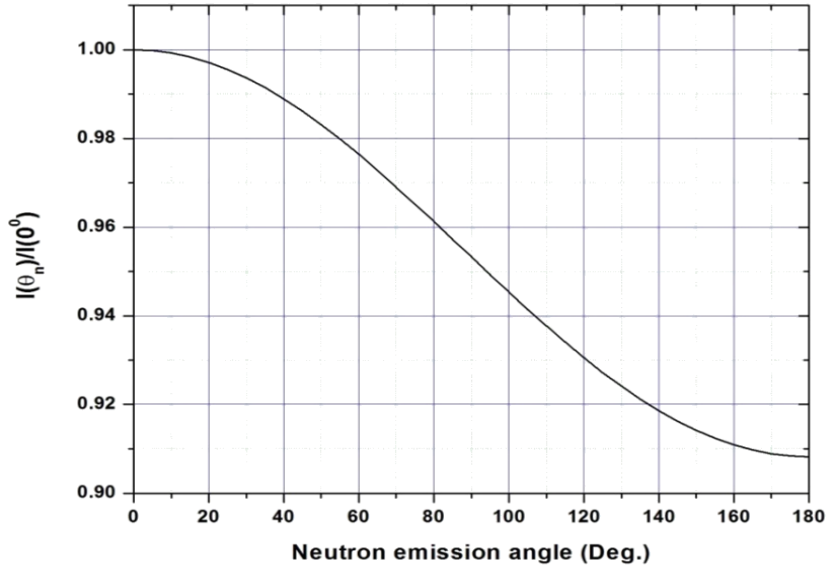


Figure 2.7: Relative neutron intensity to forward direction as a function of emission angle at 150 keV D^+ beam energy

It can be seen from *Figure 2.7* that the neutron emission is peaked in the direction of incident beam (forward) and it is least in the backward direction. The shape of anisotropy curve is approximately symmetrical with respect to 90^0 . The anisotropy factor at 150 keV is 1.05 in forward direction and 0.95 in backward direction. Anisotropy factor at 90^0 is 1.0. The angular distribution of neutrons shown in *Figure 2.7* was modelled in the calculation model used for the analysis of neutronics experiments reported later in the thesis.

2.5 Angular distribution of source neutron spectrum

Energy of the source neutron from D-T reaction varies with respect to the emission angle due to mono-directional deuteron beam and reaction kinematics (equation 2.14).

If the energy loss rate of the D^+ ions in the target and the double differential cross-section of the D-T reaction are known, neutron spectrum as a function of emission angle can be estimated. Since accurate modelling of neutron spectra is indeed important for neutronics experiments, several programs have been developed for this purpose. Examples are the DROSG2000 and NeuSDesc codes. DROSG2000 code doesn't give the spectral information as a function of energy for thick targets. NeuSDesc (Neutron Source Description) considers intrinsic peak broadening effects such as energy and angular straggling of the ions in the beam, energy spread of incident ion beam. It uses SRIM-2008 which simulates the stopping of ions in materials using Monte Carlo calculations. Input required for this program are incident D^+ ion beam energy, thickness of the Ti-T target, and T/Ti ratio in target. Values of these parameters for SODERN GENIE35 neutron generator (NG) tube are listed in *Table 2.7*.

Table 2.7: Ti-T target and D^+ beam parameters of GENIE35 neutron generator

Parameter	Value
Beam energy (keV)	150
Target thickness ($\mu\text{g}/\text{cm}^2$)	2200
T/Ti atom ratio	1.5

The angular resolution for the neutron spectra calculation was kept 1° . Using beam and tritium target parameters in GENIE35 NG tube, calculated neutron spectra at three neutron emission angles (0° ; 90° ; 180°) are shown in *Figure 2.8*.

The calculated spectra at these angles include the anisotropy factors described in the previous section. Source neutron peak broadening at 90° has nearly gaussian shape and non-gaussian at other angles. Peak broadening is minimum at 90° and maximum at 0° . The source neutron spectra were calculated at total 180 angles (0 - 180°) and

modelled in the MCNP.

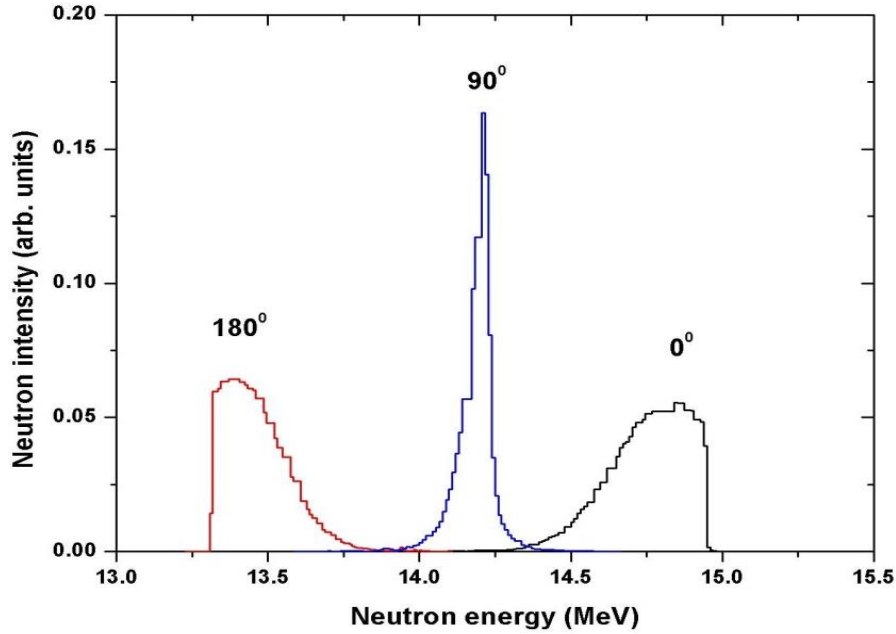


Figure 2.8: Neutron generator source spectra calculated using the target model at three emission angles 0° , 90° , and 180°

2.6 Neutron yield measurement

This section discusses the application of activation technique for the measurement of neutron yield in a sealed neutron generator tube manufactured by Sodern, France.

2.6.1 Introduction

For the accurate measurement of neutron yield by foil activation technique, the selection of the appropriate neutron induced nuclear reaction is of utmost importance. Selection of an appropriate foil and reaction should be made considering following physical and nuclear properties:

- The neutron induced reaction should have threshold energy close to the source;

- The cross-section of neutron induced threshold reaction should be high enough to produce measurable counts;
- Uncertainty in cross-section value should be as small as possible;
- Half-life of the product should neither be too long nor too short but of the same order or larger than the irradiation times;
- Isotopic abundance should be known accurately i.e. foils having single isotopes are preferred;
- Purity of foil material should be very high to avoid interference from other neutron induced reactions from impurity nuclei;
- The foil mass should be such that it doesn't perturb the neutron flux i.e. the self-attenuation of source neutrons should be negligible by foil material;

There are several neutron induced reactions which can serve the purpose of neutron yield estimation using activation technique. Aluminum has some ideal characteristics for experiments with D-T neutron sources. Aluminum occurs as one isotope of mass 27 which has good cross-section for fast neutrons in the form of $^{27}\text{Al}(n, \alpha)^{24}\text{Na}$ reaction. This reaction is used as standard in the neutron dosimetry for the determination of other reaction cross-sections. Half-life of the product of this reaction is 14.95 hours giving sufficient counts in the irradiation for few hours. The product of this reaction gives two gamma rays (1.369 and 2.754 MeV) with almost 100% emission probability per decay. The decay properties of this reaction are listed in *Table 2.8*.

Table 2.8: Decay properties of $^{27}\text{Al}(n, \alpha)^{24}\text{Na}$ reaction and foil details

Half-life	Threshold (MeV)	E_γ (keV)	Thickness (μm)
14.95 h	5.0	1368.6	250

The evaluated and measured excitation functions of this reaction are compared in *Figure 2.9*.

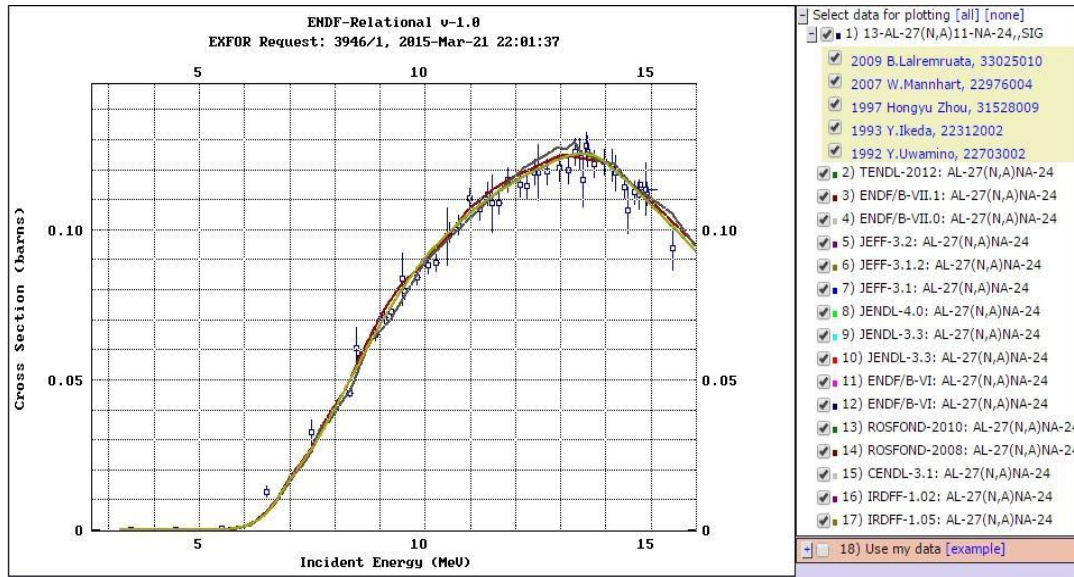


Figure 2.9: Measured and evaluated excitation functions of $^{27}\text{Al}(n, \alpha)^{24}\text{Na}$ reaction [54]

It can be seen from *Figure 2.9* that the IRDF-02 and other evaluated cross-section curves are closely following the measured cross-section points i.e. the excitation function of this reaction is very well known. It should be kept in mind that the 1.369 MeV and 2.754 MeV gamma rays from product of $^{27}\text{Al}(n, \alpha)^{24}\text{Na}$ reaction are emitted in coincidence to each other i.e. there will be some losses in the counts measured in the detector (depends on the distance between detector and foil). Therefore appropriate coincidence correction factor should be calculated for the real geometry of the detector and foil and applied in the results.

Neutron yield can be estimated using equation 2.13 and substituting the value of

neutron flux from equation 2.11. After this substitution neutron yield expression has the following form:

$$Y_n = \frac{4\pi r^2 P_k \lambda_B}{k_G k_A k_R I_\gamma \varepsilon \Omega \sigma_A N_A(0) \{1 - e^{-\lambda_B t_{ir}}\} e^{-\lambda_B t_c} \{1 - e^{-\lambda_B t_m}\}} \quad (2.19)$$

In equation 2.19, product of intrinsic photo-peak efficiency ε and solid angle factor (geometrical efficiency) Ω can be replaced with full-energy peak efficiency (ε_f). Number of target isotope atoms in the un-irradiated foil having mass m can be obtained using expression $N_A(0) = (L.m.a)/A$. Where L is Avogadro's constant, a is abundance of target isotope and A is the atomic mass of the target isotope. After substituting these two factors, neutron yield expression takes the following form:

$$Y_n = \frac{4\pi r^2 P_k \lambda_B A}{k_G k_A k_R I_\gamma \varepsilon_f \sigma_A L m a \{1 - e^{-\lambda_B t_{ir}}\} e^{-\lambda_B t_c} \{1 - e^{-\lambda_B t_m}\}} \quad (2.20)$$

Mathematical expression 2.20 is the final form for neutron yield estimation using foil activation technique based on gamma counting in the activated foils. The meaning of the terms used in this expression is already given in the earlier discussion.

2.6.2 Estimation of geometrical correction factor (k_G)

Geometrical correction factor k_G which takes into account the disk shape of the D^+ beam and foil is estimated in the following discussion. Schematic of the source-detector geometry is depicted in *Figure 2.10*.

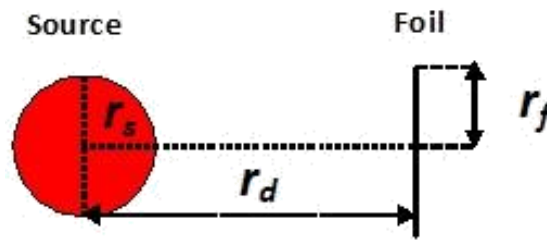
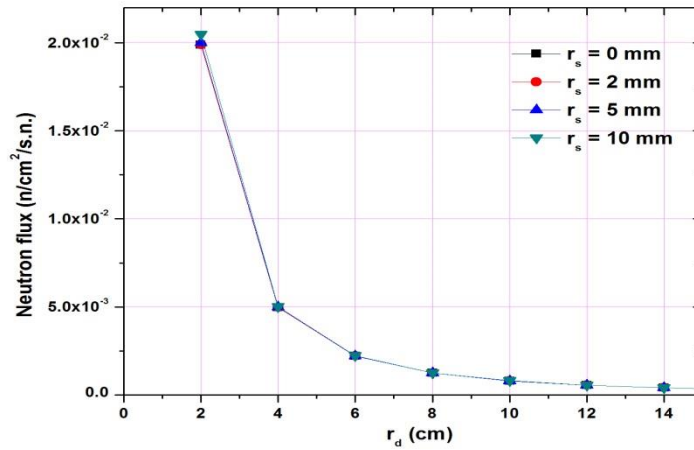
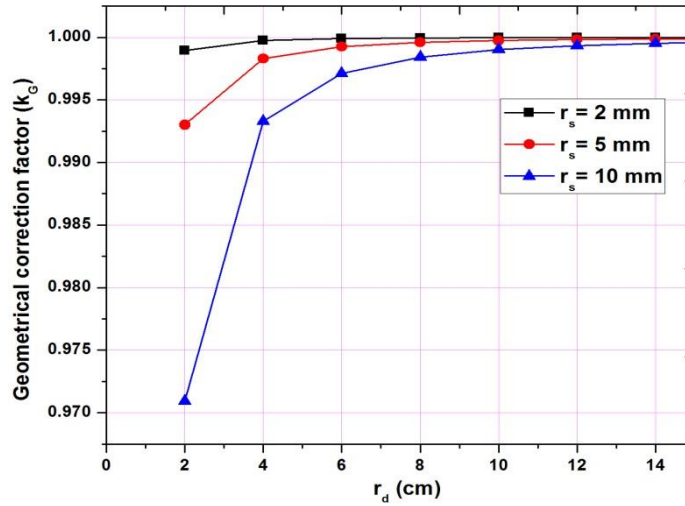


Figure 2.10: Schematic of source-foil detector geometry for neutron yield measurement

The D-T neutron source in the Sodern tube can be considered as surface source owing to cylindrical shape of the incident beam. The radius of the D^+ beam on Ti-T target (r_s) is 1 mm. The foil radius (r_f) is 6.5 mm. The foil was placed on the outer surface of the neutron generator tube which has 6 cm distance from the source center (r_d).



(a) Neutron flux



(b) Ratio of neutron fluxes with point source

Figure 2.11: Neutron flux from disk sources and neutron flux ratio with point source ($r_s = 2, 5$, and 10 mm) as a function of r_d for $r_f = 13$ mm

In order to study the disk geometry of source and foil, schematic shown in *Figure 2.10* was modelled in the Monte Carlo code MCNP and neutron flux in the foil region was

calculated for four values of source radius. Results of the calculated neutron fluxes as a function of distance between source and foil are given in *Figure 2.11a*. Results of the neutron fluxes ratio with point source as a function of distance between source and foil are given in *Figure 2.11b*. The maximum correction factor is 1.03 for $r_s = 10$ mm and $r_d = 20$ mm. The correction factor due to the disk shape of source and detector for the GENIE35 neutron generator is estimated to be 1.0 (*Figure 2.11b*).

2.6.3 Estimation of neutron emission anisotropy

correction factor (k_A)

The aluminum foil used for time integrated yield measurement was irradiated at 90° position with respect to incident deuteron beam. As discussed earlier in the source neutron anisotropy section 2.4 that the correction factor due to anisotropy at experimental position (90°) is also 1.0. It can be seen from section 2.4 that the anisotropy correction factors are different from unity at the angles other than 90° angle.

2.6.4 Estimation of source neutron attenuation

correction factor (k_R)

There are materials between the source and foil location in the GENIE35 neutron generator tube. The attenuating material between source and foil from source side are as follows: 2mm oil + 28 mm SS. The correction factor due to source neutron attenuation / collision with these materials was estimated to be 0.707 with Monte Carlo calculations.

2.6.5 Experimental details

An ultra-pure aluminum foil was irradiated on the surface of neutron generator tube for 30 minutes. The irradiated foil was counted with HPGe detector for gamma rays. The same foil was counted for different durations to ensure that no other interfering reaction is being measured. Foil was also counted at different distances from the detector window to validate the coincidence calibration of the detector. Branching ratio of both gamma rays was also checked. A niobium foil was also irradiated with aluminum foil to cross-check the results. Time profile of the neutron emission was measured with ^3He counter covered with HDPE.

2.6.6 Neutron yield results

In this section, results of the neutron yield estimation by $^{27}\text{Al}(n, \alpha)^{24}\text{Na}$ reaction and its cross-check with $^{93}\text{Nb}(n, 2n)^{92\text{m}}\text{Nb}$ reaction are discussed. The cross-calibration of ^3He counter (for time profile measurement of neutron emission) with $^{27}\text{Al}(n, \alpha)^{24}\text{Na}$ measurement is performed.

Neutron yield measurement result using mathematical expression 2.19 and correction factors with $^{27}\text{Al}(n, \alpha)^{24}\text{Na}$ reaction is given in *Table 2.9*. The full-peak efficiency in *Table 2.9* is given at 5 cm distance from the detector window for 1368 keV gamma energy from ^{24}Na . Photo-peak counts are corrected for background and loss due to coincidence events in the detector. The physical constants used for the neutron yield estimation are taken from National Institute of Standards and Technology (NIST) database [55]. Nuclear decay data of the reaction product is taken from National Nuclear Data Center, Brookhaven National Laboratory, which are based on ENSDF and the Nuclear Wallet Cards [56]. Excitation function of $^{27}\text{Al}(n, \alpha)^{24}\text{Na}$ reaction was

taken from references [57, 58]. The measured neutron yield during above-mentioned experiment with $^{27}\text{Al}(n, \alpha)^{24}\text{Na}$ reaction was $8.90 \times 10^9 \text{ n/s}$.

Table 2.9: Result of the measured neutron yield by $^{27}\text{Al}(n, \alpha)^{24}\text{Na}$ reaction

Parameter	Value
Source-detector distance (r) cm	6.01
Photo-peak counts (P_k)	4635
Decay constant (λ_B) s^{-1}	1.284×10^{-5}
Atomic mass (A) amu	26.982
Geometrical corr. factor (k_G)	1.0
Anisotropy corr. factor (k_A)	1.0
Attenuation corr. factor (k_R)	0.707
γ -ray intensity (I_γ)	1.0
Peak efficiency (ϵ_f) @ 1368 keV	9.36×10^{-3}
Spectrum averaged cross-section (σ_A) b	0.129
Avogadro constant (L)	6.022×10^{23}
Foil mass (m) g	8.14×10^{-2}
Isotopic abundance (a)	1.0
Irradiation time (t_{ir}) s	1.80×10^3
Cooling time (t_c) s	1.01×10^4
Counting time (t_m) s	8.00×10^3
Neutron yield (Y_n) n/s	8.90×10^9

Result of the neutron yield measurement with niobium foil ($^{93}\text{Nb}(n, 2n)^{92m}\text{Nb}$ reaction) is given in *Table 2.10*. The foil was kept at 2 cm from the detector i.e. the full-peak efficiency in *Table 2.10* is given at 2 cm for 935 keV. Both neutron yield measurements agree within 3% difference i.e. $^{27}\text{Al}(n, \alpha)^{24}\text{Na}$ reaction is most suitable for neutron yield measurement. Time averaged count rate in ^3He counter during this experiment was 27.16 cps (count per second). Therefore the calibration factor for the neutron yield measurement by this counter was determined to be $3.05 \times 10^{-9} \text{ cps per source neutron}$. This calibration factor is valid as long as the materials around the

neutron generator are unchanged and counter is also kept at the location where this calibration was performed.

Table 2.10: Result of the measured neutron yield by $^{93}\text{Nb}(n, 2n)^{92m}\text{Nb}$ reaction

Parameter	Value
Source-detector distance (r) cm	6.01
Photo-peak counts (P_k)	4513
Decay constant (λ_B) s^{-1}	7.904×10^{-7}
Atomic mass (A) amu	92.906
Geometrical corr. factor (k_G)	1.0
Anisotropy corr. factor (k_A)	1.0
Attenuation corr. factor (k_R)	0.71
γ -ray intensity (I_γ)	0.9915
Peak efficiency (ϵ_f) @935 keV	3.06×10^{-2}
Spectrum averaged cross-section (σ_A) b	0.476
Avogadro constant (L)	6.022×10^{23}
Foil mass (m) g	2.4×10^{-1}
Isotopic abundance (a)	1.0
Irradiation time (t_{ir}) s	1.80×10^3
Cooling time (t_c) s	4.25×10^5
Counting time (t_m) s	1.39×10^4
Neutron yield (Y_n) n/s	9.19×10^9

2.6.7 Uncertainty estimation

Uncertainty in the neutron yield measurement was estimated by combining the uncertainties in the various parameters used for this purpose. The major parameters giving uncertainty in the neutron yield are calibration of the HPGe detector, reaction cross-section, foil mass, peak area and statistical error. The uncertainty in each of these parameters as well as overall uncertainty in the neutron yield is given in *Table 2.11*.

Table 2.11: Uncertainty estimation in the measured neutron yield by $^{27}\text{Al}(n, \alpha)^{24}\text{Na}$ reaction

Error component	Value %
Statistical error	1.49
HPGe calibration	3.94
Reaction cross-section	1.04
Foil mass	0.12
Photo-peak area	2
Neutron yield	4.78

All these errors are independent and random in nature and therefore they can be added using quadratic law.

2.7 Validation of the neutron tube MCNP model

For analysis of integral benchmark experiments with transport codes, accurate modelling of the neutron source anisotropy, spectra, geometry, material around the source, materials in the target etc. are required. For this reason, the neutron generator tube GENIE35 was accurately modelled in the MCNP. The source anisotropy and spectra described in sections 2.4 and 2.5 were also implemented in the calculation model. This calculation model (geometry, material composition and source description) needs to be experimentally validated so that integral measurements can be fairly compared with the calculated responses. Validation of calculation model was performed by measuring the neutron reaction rates by irradiating various foils with nine nuclear reactions. The responses of these neutron induced reactions in the foil material cover the whole energy range from thermal to fusion neutron source.

The neutron generator tube GENIE35 is equipped with a copper backed Ti-T (titanium-tritium) target cooled with mineral oil. The generator has high-voltage insulation material resina in the vicinity of the target. The other materials in the

vicinity of the target are target support structure, cooling oil and high-voltage (HV) insulating material. The neutron generator systems are enclosed within a 5.5 mm thick SS316 tube of diameter 12cm. All these features of the neutron generator are important for experiments performed with the neutrons emerging from this tube. These features were implemented in the calculation model for neutron transport with code MCNP. Top view of the MCNP model is shown in *Figure 2.12*.

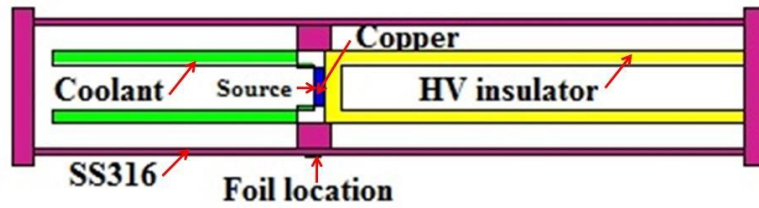


Figure 2.12: Geometrical model of the neutron generator GENIE35

Neutron source described in section 2.4 and 2.5 was also implemented in the calculation model. The calculated energy-angle distributions of the source neutrons were modelled in calculation model with angular resolution of 1° . The neutron generator setup was modelled as accurately as possible in the model. In order to validate the calculation model (materials around the source and source definition), several foils were irradiated on the outer surface of tube at 90° location. Results of the experimental (E) and calculated (C) reaction rates of various reactions are given in *Table 2.12*. The dosimetry file used for the calculation of reaction rates in *Table 2.12* was IRDF-2002 [59, 60]. The error estimates on C/E ratios shown in *Table 2.12* include uncertainty in HPGe calibration, neutron yield error, peak area determination error, statistical error, foil mass and statistical error in reaction rate calculation by MCNP. The C/E ratios for all the high threshold reactions are close to unity implying that the source and materials around the source are well described in the calculation model. The C/E ratio for the thermal neutron reaction is also close to unity.

Table 2.12: Measured and calculated reaction rates in various activation foils on the surface of neutron generator (90° location)

Reaction	Reaction rate (r/s.n./nuclide)		C/E	C/E Error
	Experimental (E)	Calculation (C)		
$^{27}\text{Al}(n, \alpha)^{24}\text{Na}$	2.04E-28	2.01E-28	0.98	0.066
$^{93}\text{Nb}(n, 2n)^{92\text{m}}\text{Nb}$	7.27E-28	7.36E-28	1.01	0.070
$^{59}\text{Co}(n, 2n)^{58}\text{Co}$	1.04E-27	1.06E-27	1.02	0.068
$^{90}\text{Zr}(n, 2n)^{89}\text{Zr}$	9.57E-28	9.33E-28	0.98	0.066
$^{27}\text{Al}(n, p)^{27}\text{Mg}$	1.24E-28	1.33E-28	1.08	0.071
$^{64}\text{Zn}(n, p)^{64}\text{Cu}$	3.16E-28	3.32E-28	1.05	0.071
$^{58}\text{Ni}(n, 2n)^{57}\text{Ni}$	3.45E-29	3.55E-29	1.03	0.069
$^{58}\text{Ni}(n, p)^{58}\text{Co}$	6.75E-28	7.24E-28	1.07	0.070
$^{59}\text{Co}(n, \gamma)^{60}\text{Co}$	8.16E-27	7.66E-27	0.94	0.062

2.8 Summary

In this chapter, absolute efficiency calibration of the HPGe detector used for the measurement of gamma rays from activated samples was performed with uncertainty less than 4%. A methodology based on the activation technique was developed to measure the neutron yield of the Sodern made GENIE35 neutron generator. Time profile of source neutron emission was measured with ^3He counter cross-calibrated with activation measurements. Using this methodology, neutron yield was measured with uncertainty 4.78%. Neutron emission anisotropy and angular distribution of source spectra were calculated using the model calculations. A MCNP model including neutron source definition and geometry of GENIE35 tube was developed. The MCNP model was validated with the experimental measurements using activation foils placed on the surface of neutron tube at 90°.

Chapter 3

Development and characterization of tritium diagnostics

3.1 Introduction

Measurement of tritium production rate (TPR) in the blanket mock-up assemblies is one of the important nuclear responses to validate the capability of neutronics codes and nuclear data with qualified uncertainties. The requirements for the TPR diagnostics are as follows: it must be able to measure tritium as low as few Bq/g i.e. measurement sensitivity must be very high, high accuracy, good spatial resolution, and the diagnostic detectors must not perturb the thermal neutron field. Non-perturbation of thermal neutron field and good spatial resolution are particularly important for local TPR measurements inside the breeder layer where steep gradients of thermal neutron flux exist. There are several methods which can be employed for this purpose. The tritium measuring diagnostics can be broadly classified into two categories: off-line and on-line measurements. Widely used off-line technique is the irradiation of lithium containing compounds in the experimental assembly and thereafter tritium measurement with liquid scintillation technique. On-line technique utilizes the charged particle detector with lithium layer to measure the tritons

produced in the converter layer. This chapter describes the details of both tritium measuring techniques and characterization of these diagnostics.

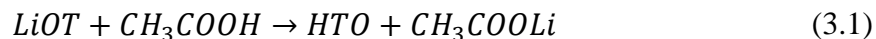
3.2 Off-line tritium diagnostics

3.2.1 Principle

In this method, lithium containing pellets are irradiated with neutrons in the experimental assembly and tritium produced in them is measured off-line either by ionization chambers or liquid scintillation counters. Liquid scintillation counting technique is most reliable and convenient for detection of tritium because well calibrated liquid scintillation counters are commercially available. Tritium nuclide is a β^- emitter having end point energy 18 keV and average energy 5 keV. Therefore in order to measure it, tritium produced in the pellets need to be in contact with liquid scintillator to avoid the loss of counts. Generally, lithium compounds are not compatible in terms of solubility with liquid scintillation cocktails. To overcome this problem pellets are dissolved in the appropriate solvent and then part of it is mixed with liquid scintillation cocktail. This procedure is known as wet chemistry treatment. Wet chemistry treatment consists of three steps [61]: (1) dissolution of pellet in acetic acid (CH_3COOH), (2) removal of lithium salts from the pellet solution by hydrofluoric acid, (3) incorporation of the pellet solution in the liquid scintillator. Lithium carbonate (Li_2CO_3) is most commonly used as pellet material due to its non-hygroscopic nature and solubility in acetic acid.

When a neutron interacts with the lithium nucleus present in the Li_2CO_3 molecule, it is broken into two molecules LiOT and CO_2 . Therefore during irradiation, tritium generated in the Li_2CO_3 pellet is contained in the chemical form of LiOT [61]. LiOT can't escape from the pellet at room temperature conditions and hence storage

stability of tritium in pellet is high even for long durations. When pellet is dissolved in CH_3COOH , tritium in LiOT is converted into HTO through following chemical reaction.



Tritium in HTO (tritiated water) form is most stable. It can't be removed from tritiated water at ambient temperature conditions. Part of the dissolved solution is mixed into scintillation cocktail to produce the light from tritium beta rays. The light emitted by scintillator is subsequently detected by the photo-multiplier tubes in the counter. Finally detected light in liquid scintillator can be converted to the total tritium activity present in the pellet considering various factors involved in the above-mentioned process from pellet dissolution to light detection.

3.2.2 Experimental procedure

Lithium carbonate (Li_2CO_3) pellets used in the irradiation experiments were prepared by mixing Li_2CO_3 powder with polyvinyl alcohol (PVA) binder and then compressed to 5 tons of pressure. After that, the pellets were slightly heated to remove the binder material PVA. Photograph of the pellets (with pellet diameter) used in irradiation experiment is shown in *Figure 3.1*.

Irradiated pellets were mixed with binary-acids: nitric (HNO_3) and acetic (CH_3COOH) acids. HNO_3 dissolves the Li_2CO_3 very well in it but its excessive amount gives strong quenching effect in the liquid scintillator. So, an optimized amount of nitric acid should be added into the solution and quenching effect must be quantified. An appropriate volume ratio of strong and weak acid was found in the reference [61] for per unit mass of Li_2CO_3 . The binary-acid solvent was prepared with 70% concentrated HNO_3 and 100% concentrated CH_3COOH . The volume ratio of the

HNO₃ and CH₃COOH in the solvent was 3:10. The amount of binary-acid was 6 ml to dissolve 1 g of Li₂CO₃. The pellets were kept in this solution for 10 hours to dissolve them completely. Part of the pellet solution (approximately 0.5 ml) was mixed with commercially available liquid scintillation cocktail Optiphase HISAFE-3 in HDPE counting vials. Beta counting from tritium activity in the samples were performed with ultra-low level liquid scintillation counter model Quantulus 1220 manufactured by M/s Perkin Elmer limited [62]. The minimum detectable activity of this counter is typically less than 0.2 Bq/g in lithium carbonate pellets.



Figure 3.1: Li₂CO₃ pellets prepared by cold pressing for tritium measurement in experimental assemblies

3.2.3 Quenching and counting efficiency calibration

There can be two types of quenching effects in the liquid scintillator solution due to presence of foreign solvents: chemical and color quench. Chemical quench occurs when the energy of the tritium beta (β^-) particle is absorbed by compounds that will not re-emit the energy during the transfer to the solvent molecules. Hence, the energy

of the beta particle will not reach the scintillator and consequently, no light will reach to the detector. Color quench occurs when the emitted light is absorbed by color in the sample. The energy transmission can occur correctly, but once the light is emitted by the scintillator it is absorbed by color in the sample. As a consequence, the signal detected at the photomultiplier tube will not represent the total quantity of light truly emitted i.e. due to quenching effect number of detected beta counts are less than the real beta activity in the sample. Presence of acid in the pellet solution generates both chemical and color quenching. Therefore this quenching effect needs to be quantified to correct the measured beta activity in the samples. The measured counting efficiency expresses the level of quench in a sample and is the ratio of the measured disintegrations to the disintegration events from sample. Increase in quench levels reduces the counting efficiency.

Liquid scintillation counter Quantulus 1220, manufactured by M/s Perkin Elmer limited, generates a parameter to represent the quenching effect. This effect is represented by Special Quench Parameter (SQP(E)). SQP(E) is generated from the external standard spectra [62]. An un-irradiated pellet was dissolved in the binary-acid solution as per the procedure described in the previous section. Known tritium activity was introduced in this solution by mixing calibrated tritiated water from North American Scientific. Six samples were prepared by taking equal amount of pellet solution in each. Varying amounts of acid were introduced in them to include the different amount of quenching. SQP(E) and net counts from each sample were determined using liquid scintillation counter. Counting efficiency of each sample was determined from the ratio of the measured net counts to the activity of tritium in the tritiated water. A linear fit was performed between SQP(E) and recovery efficiency.

Results of the quench and recovery efficiency calibration are given in *Table 3.1* and *Table 3.2* for natural and enriched pellets respectively.

Table 3.1: Counting efficiency calibration of liquid scintillation counter for natural Li_2CO_3 pellets (Activity of tritium mixed= 1236.51 DPM*)

SQP(E)	Net count rate (cpm)	Efficiency
781.33	59.56	0.25
753.90	49.43	0.21
713.62	29.87	0.13
708.55	29.26	0.12
704.50	26.99	0.11
669.66	16.69	0.07

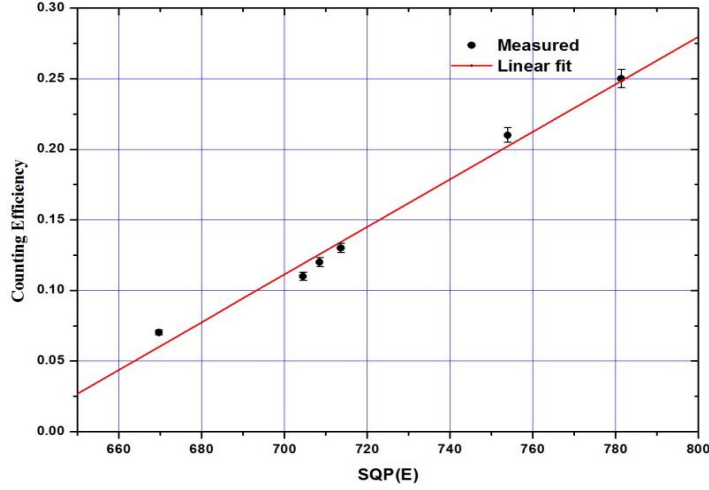
Table 3.2: Counting efficiency calibration of liquid scintillation counter for enriched Li_2CO_3 pellets (Activity of tritium mixed= 1224.95 DPM*)

SQP(E)	Net count rate (cpm)	Efficiency
781.82	60.34	0.26
757.00	50.14	0.22
729.00	36.90	0.16
711.06	29.67	0.13
658.96	21.21	0.09
656.15	13.06	0.06

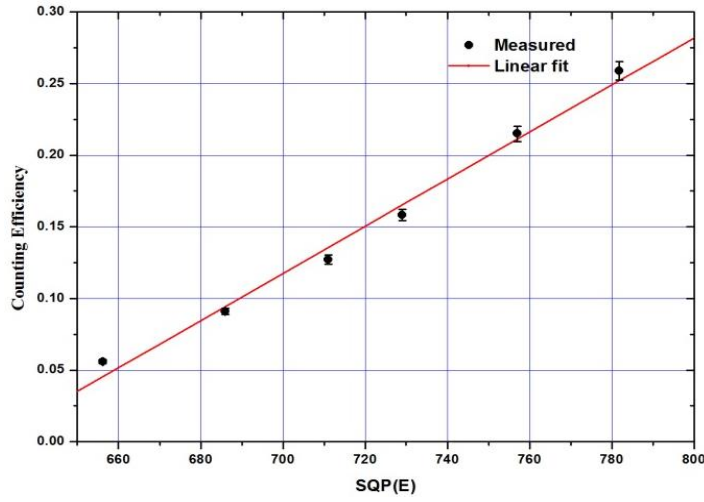
*DPM - Disintegration per minute

The quench calibration curves for both types of pellets are plotted in *Figure 3.2*.

The experimental error in the efficiency calibration was estimated considering uncertainty in the activity of the tritiated water (2.3%), statistical error in measured counts (0.88%) and error in linear fit (0.87%). Because all these errors are random in nature and independent to each other therefore they can be combined to obtain the total error using quadratic square law. The overall relative uncertainty in the efficiency calibration was estimated to be 2.6%



(a) Natural Li_2CO_3



(b) Enriched Li_2CO_3

Figure 3.2: Measured efficiencies as a function of quenching and linear fits for natural and enriched Li_2CO_3 pellets

3.3 On-line tritium measurement

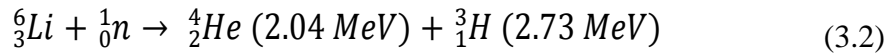
Although tritium production rate (TPR) measurement by diagnostic pellet method as described in previous section is well established and widely used for the breeding blanket mock-up experiments. Pellet method has disadvantages in terms of the systematic errors introduced by the off-line measurement and it requires long

irradiations to get enough counts in the pellets. However, given the importance of the TPR measurement in breeding blanket technology, it is quite important to cross-check the diagnostic pellet measurement with another independent technique. An on-line tritium measurement technique with charged particle detector and ^6Li to triton converter was developed for this purpose. The charged particle detector was silicon surface barrier detector (SBD) and lithium carbonate enriched with ^6Li was converter layer.

This section describes the development and characterization of the on-line tritium measurement diagnostic based on the surface barrier detector with ^6Li converter.

3.3.1 Principle

There are two tritium producing nuclear reactions with neutrons in the fusion breeding blanket environment: one is with ^6Li isotope and another with ^7Li . Majority of tritium in the breeder layers is produced by ^6Li through following nuclear reaction with thermal neutron:



Thermal neutron reaction with isotope ^6Li is an exothermic reaction releasing total energy of 4.77 MeV per reaction. The resultant energy is carried by triton (2.73 MeV) and α -particle (2.04 MeV). Direct measurement of these product particles can give the information about the tritium production reaction rate from ^6Li isotope in breeder materials. Charged particle detector such as silicon surface barrier detector (SBD) can be employed to measure the product particles on-line. In order to provide the ^6Li atoms for this reaction, a very thin layer of lithium compounds enriched with ^6Li can be provided on the window of the SBD detector. Thickness of this converter layer

should be such that the energy loss of outgoing particles in the nuclear reaction 3.2 is negligible.

3.3.2 Characterization of ^6Li converter layer

3.3.2.1 Introduction

Number of ^6Li atoms in the converter layer must be known accurately for the estimation of tritium production rate from measured counts at a particular location inside the experimental assembly. Therefore the converter layer must be characterized for the number of ^6Li atoms in it. The product particles of nuclear reaction 3.2 are emitted back-to-back i.e. either of the particle is detected in the detector per reaction. The energy loss of 2.04 MeV α -particle in the aluminum window (equivalent thickness 2300 Å of Si) and Li_2CO_3 layer is estimated to be 975 keV using SRIM-2008 Monte Carlo code. The energy loss of the α -particle is significant in comparison to source α -energy (2.04 MeV) therefore alpha particles will not show any peak in the pulse-height spectra (PHS). The energy loss of 2.73 MeV tritons in detector window is 80 keV which is negligible with respect to their source energy and clear peak will be available in the PHS. Due to absorption of α -particles in the converter layer and detector, only half of the tritons are detected (half tritons are emitted in opposite direction to the detector). Hence a correction factor of 0.5 is required to consider this effect.

Numbers of ^6Li atoms in the converter foil ($N_{\text{Li-6}}$) in terms of neutron flux (Φ), microscopic cross-section (σ), solid angle correction factor (K) and triton count rate (C) are given by:

$$N_{Li-6} = \frac{c}{\sigma \phi K} \quad (3.3)$$

Number of ${}^6\text{Li}$ atoms in the converter layer can be estimated with mathematical expression 3.3 by putting the layer in a well characterized thermal neutron field.

${}^6\text{Li}$ converter foil was characterized with the help of ${}^{241}\text{Am}$ -Be neutron source of intensity 3.8×10^7 n/s. Fast neutrons in this source are produced by ${}^9\text{Be}(\alpha, n){}^{12}\text{C}$ reaction. ${}^{241}\text{Am}$ provides alpha particles required for the above reaction from the spontaneous fission. Neutron spectrum from this source is poly-energetic with maximum energy up to 10 MeV. Fast neutrons from ${}^{241}\text{Am}$ -Be were thermalized by 7 cm thick High Density Polyethylene (HDPE) moderator.

The setup and schematic of experiment used for the characterization of converter layer is shown in *Figure 3.3* and *Figure 3.4* respectively.

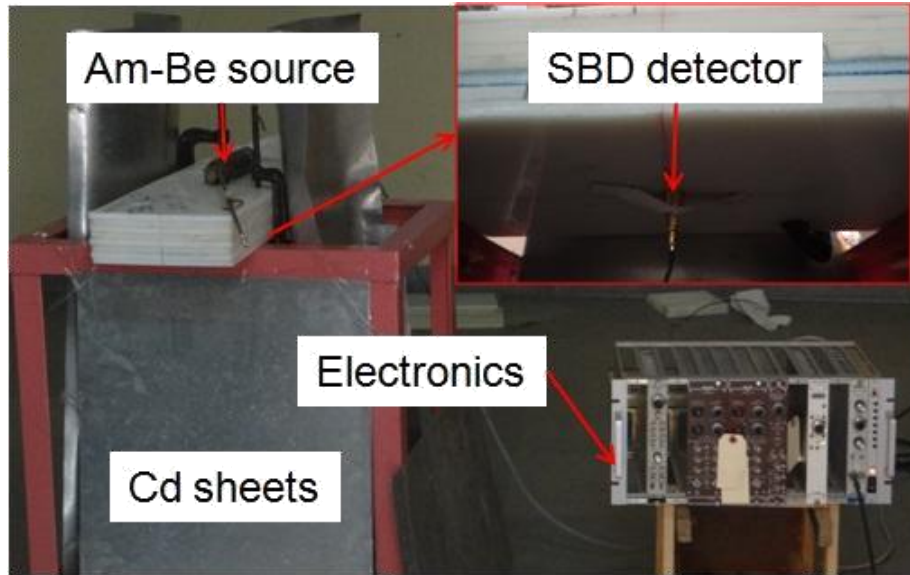


Figure 3.3: *Experimental set-up with ${}^{241}\text{Am}$ -Be source for the characterization of ${}^6\text{Li}$ converter layer*

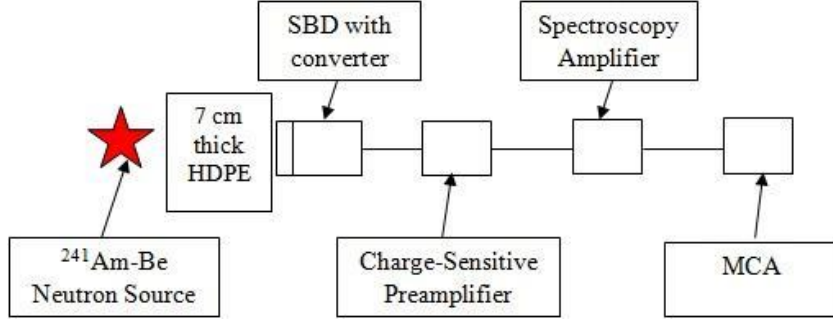


Figure 3.4: Schematic of the experiment for the characterization of ^6Li converter layer

Thermal plus epithermal neutron flux was measured with the help of $^{197}\text{Au}(n, \gamma)^{198}\text{Au}$ activation reaction with cadmium ratio technique [63]. Mathematical expression for the thermal neutron flux can be written as:

$$\phi_{th} = \frac{R_s - F_{Cd}R_{s,Cd}}{g\sigma G_{th}} \quad (3.4)$$

Where:

R_s and $R_{s,Cd}$ are the reaction rates of bare and cadmium covered gold foil irradiation;

g is the correction for departure from cross-section behavior;

G_{th} is the self-shielding factor for thermal neutrons,

σ is the spectrum averaged thermal neutron cross-section and

F_{Cd} is the cadmium correction factor

R_s and $R_{s,Cd}$ are determined by the following mathematical expressions:

$$R_s \text{ or } R_{s,Cd} = \frac{A_{sp} F_g M}{a N_A I_\gamma \epsilon_f} \quad (3.5)$$

With

$$A_{sp} = \frac{N_p \lambda}{m(1 - e^{-\lambda t_{ir}})e^{-\lambda t_c}(1 - e^{-\lambda t_m})} \quad (3.6)$$

Where:

N_p = net number of counts under full energy peak during time t_m

λ = decay constant

m = mass of the irradiated foil

t_{ir} = irradiation time

t_c = cooling time

M = atomic weight

a = isotopic abundance

N_A = Avogadro's constant,

I_γ = gamma emission probability of peak

ϵ_f = full-energy peak detection efficiency,

F_g = correction factor for self-attenuation of γ -rays in the foil

In a mixed thermal and epithermal neutron field, the epithermal neutrons flux can be calculated by using following mathematical expression [63]:

$$\phi_{epi} = \frac{\phi_{th} g \sigma G_{th}}{(R - F_{Cd}) I_0(\alpha) G_{epi}} \quad (3.7)$$

Where

R is the cadmium ratio, $I_0(\alpha)$ resonance integral cross-section, G_{epi} self-shielding factor for epithermal neutrons

3.3.2.2 Estimation of F_{Cd} , G_{th} , G_{epi} , and σ

Presence of cadmium cover over gold foil attenuates most of the neutrons below 0.55 eV. This cover results in the lesser activation of gold foil with cadmium cover than it would have been if cutoff was at thermal energy. F_{Cd} is the factor which accounts for this effect and was calculated by modelling the experiment in the Monte Carlo code MCNP. It is the ratio of the $^{197}\text{Au}(n, \gamma)^{198}\text{Au}$ reaction rate integrated below Cd cutoff

(0.55 eV) to the reaction rate between thermal energy to Cd cutoff. The calculated factor (F_{Cd}) for the current experiment with code MCNP was 2.93.

G_{th} and G_{epi} are the self-shielding factors in gold foil for thermal and epithermal neutrons respectively. These factors represent the perturbation of thermal and epithermal neutron field due to presence of gold foil detector. Both of them were estimated with MCNP by taking the ratios of the $^{197}\text{Au}(n, \gamma)^{198}\text{Au}$ reaction rate with and without foil material in their respective energy ranges. The calculated values are $G_{th} = 0.83$ and $G_{epi} = 0.91$.

Spectrum averaged cross-section for $^{197}\text{Au}(n, \gamma)^{198}\text{Au}$ reaction in the spectrum at irradiation location was estimated to be 95.24 barn with neutron transport calculations.

3.3.2.3 Measurement of $^{197}\text{Au}(n, \gamma)^{198}\text{Au}$ reaction rates with and without Cd cover

In order to measure the $^{197}\text{Au}(n, \gamma)^{198}\text{Au}$ reaction rates with and without Cd cover, two gold foils were irradiated in the experimental setup (*Figure 3.3*) separately: one bare and another covered with Cd. The gamma activities in the irradiated gold foils were determined by measuring the 412 keV gammas emitted from ^{198}Au with the help of HPGe detector. Thickness of the Cd cover was 0.25 mm. The experimental results of measured activities and $^{197}\text{Au}(n, \gamma)^{198}\text{Au}$ reaction rates in both foils with and without Cd cover are given in *Table 3.3*.

The measured Cd ratio which physically represents the ratio of the thermal plus epithermal flux to fast flux was 5.34.

Table 3.3: $^{197}\text{Au}(n, \gamma)^{198}\text{Au}$ reaction rates with and without Cd cover

Parameter	Without Cd	With Cd
Foil mass (g)	0.6586	0.6592
Full-peak eff. @ 412 keV	8.18×10^{-2}	8.18×10^{-2}
Isotope abundance	1.0	1.0
I_γ	0.9562	0.9562
Avogadro No.	6.02×10^{23}	6.02×10^{23}
λ (s ⁻¹)	2.98×10^{-6}	2.98×10^{-6}
Full-peak counts	6.32×10^3	1.25×10^4
Irradiation time (s)	7.20×10^3	8.52×10^4
Cooling time (s)	1.80×10^2	4.20×10^2
Counting time (s)	3.60×10^3	3.60×10^3
Atomic mass (a.m.u.)	196.97	196.97
Specific activity (Bq/g)	1615.96	302.38
Reaction rates (R_S, $R_{S,Cd}$) (r/nuclei)	5.28×10^{-19}	9.89×10^{-20}
Cadmium ratio, R	5.34	

3.3.2.4 Result of thermal flux, Φ_{th}

All the parameters required for the estimation of the thermal flux (eq. 3.4) are obtained in earlier discussion. Values of these parameters along-with the thermal flux value at the irradiation location of the experimental setup (*Figure 3.3*) are given in *Table 3.4*.

Experimental error in the thermal flux measurement was estimated by considering the error in HPGe detector calibration (3.94%), statistical error in the counts (0.89%), error in the cross-section of $^{197}\text{Au}(n, \gamma)^{198}\text{Au}$ reaction (0.67%) and uncertainty in peak area determination (2%). Addition of all the errors using quadratic law gives 4.56% error in the thermal flux measurement.

Table 3.4: Result of measured thermal flux at the irradiation location of $^{241}\text{Am-Be}$ source set-up

Parameter	Value
R_S (r/nuclei)	5.28×10^{-19}
$R_{S,Cd}$ (r/nuclei)	9.89×10^{-20}
F_{Cd}	2.93
σ (barn)	95.24
G_{th}	0.83
Φ_{th} (n.cm $^{-2}$.s $^{-1}$)	3.02×10^3

3.3.2.5 Result of epithermal flux, Φ_{epi}

For experimental determination of epithermal neutron flux using mathematical expression 3.7, value of resonance integral $I_0(\alpha)$ is required. α is known as neutron shaping factor which takes into account the non-ideal shape of the epithermal flux [64]. Resonance integral as a function of α is defined as follows [63]:

$$I_0(\alpha) = \left(\frac{I_0 - 0.429\sigma}{E_\gamma^\alpha} + \frac{0.429\sigma}{(2\alpha + 1)E_{Cd}^\alpha} \right) E_a^\alpha \quad (3.8)$$

Where:

I_0 = Resonance integral for $^{197}\text{Au}(n, \gamma)^{198}\text{Au}$ reaction (1550 barns)

σ = $^{197}\text{Au}(n, \gamma)^{198}\text{Au}$ cross-section at thermal energy

E_γ^α = Effective resonance energy (5.65 eV)

E_{Cd}^α = Cd cutoff energy (0.55 eV)

E_a^α = Arbitrary energy (1 eV)

Value of α was assumed to be 1.0. The value of $I_0(\alpha)$ using equation 3.8 was calculated to be 25 barn. Epithermal flux along-with the parameters used for calculation at the irradiation location of the experimental setup (*Figure 3.3*) is given in

Table 3.5. Value of epithermal flux at the irradiation site is determined to be 4.33×10^3 n/cm²/s.

Table 3.5: Result of measured epithermal flux at the irradiation location of ²⁴¹Am-Be source experimental setup

Parameter	Value
R	5.34
Φ_{th} (n.cm ⁻² .s ⁻¹)	3.02×10^3
F _{Cd}	2.93
σ (barn)	95.24
$I_0(\alpha)$ (barn)	25.0
G _{th}	0.83
G _{epi}	0.91
Φ_{epi} (n.cm ⁻² .s ⁻¹)	4.33×10^3

3.3.2.6 Result of ⁶Li atoms in the converter layer

SBD with Li₂CO₃ layer on its window was kept at the location where thermal and epithermal flux was determined in previous discussion. Li₂CO₃ used in the layer was enriched with ⁶Li isotope. Photograph of the SBD with Li₂CO₃ layer is given in Figure 3.5.

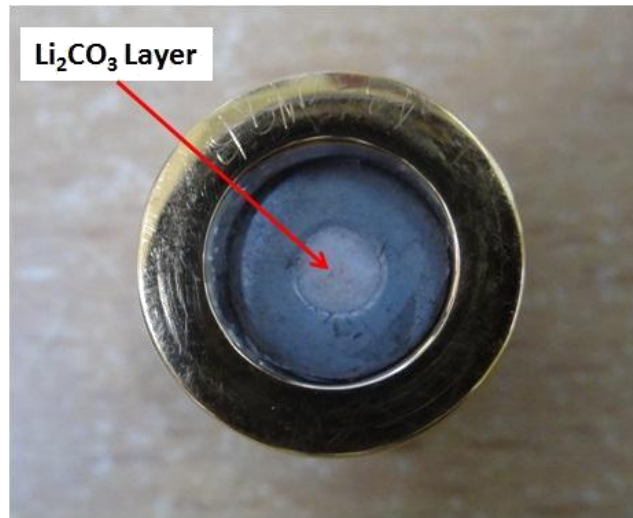


Figure 3.5: Photograph of Surface Barrier Detector (SBD) with Li₂CO₃ layer

The pulse-height spectra from SBD were recorded in 16k multichannel analyzer (MCA) using standard nuclear instrumentation (Pre-amplifier, spectroscopy amplifier, HV power supply, NIM bin etc.). In order to take the background of charged particles emerging from detector and nearby materials, PHS was recorded without Li_2CO_3 layer. The PHS spectra of SBD taken with and without converter layer and gaussian fit for tritium peak are shown in *Figure 3.6*.

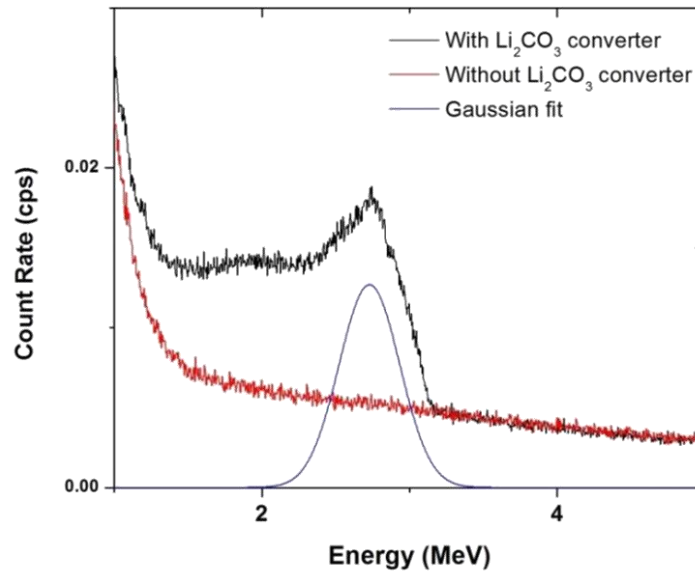


Figure 3.6: PHS spectra with and without Li_2CO_3 converter foils and gaussian fit for the triton peak

Result of the number of ^6Li atoms in the converter foil are shown in *Table 3.6*.

Table 3.6: Measured ^6Li atoms in Li_2CO_3 converter foil used for on-line tritium measurement (cps = counts per second)

Parameter	Value
Count rate (C) cps	1.42
σ (barn)	613
$\Phi_{\text{th}} + \Phi_{\text{epi}}$ (n/cm ² /s)	7.36×10^3
Geometry corr. factor (K)	0.5
$N_{\text{Li-6}}$	6.30×10^{17}

Experimental uncertainty in the ${}^6\text{Li}$ atoms measurement includes uncertainty in the count rate, cross-section, and flux measurement. The statistical error in the triton counts is 0.27%, error in cross-section is 0.67% and in flux measurement 4.56%. The combined error in ${}^6\text{Li}$ atom measurement at 1σ level is estimated to be 4.62%.

3.3.3 ${}^6\text{Li}$ isotope-ratio measurement

Another application of this on-line technique is the measurement of ratio of ${}^6\text{Li}$ isotopes in two samples having varying ${}^6\text{Li}$ fractions. From equation 3.3, triton count rate measured in the SBD detector is proportional to the number of ${}^6\text{Li}$ atoms in the converter foil. Therefore the count rate ratio will be equal to the ratio of the ${}^6\text{Li}$ atoms in the converter foils having different fractions of ${}^6\text{Li}$. Let A_N be the fraction of ${}^6\text{Li}$ in natural Li (Li_2CO_3 sample), A_E be the fraction of ${}^6\text{Li}$ in enriched Li (Li_2CO_3 sample), C_N triton count rate from natural Li sample, and C_E triton count rate from enriched Li sample. Using equation 3.3, isotope ratio of ${}^6\text{Li}$ in enriched and natural Li sample can be written as:

$$\frac{A_E}{A_N} = \frac{C_E}{C_N} \quad (3.9)$$

If isotopic abundance of ${}^6\text{Li}$ in natural lithium is known, isotopic abundance of the enriched lithium sample can be calculated using following expression:

$$A_E = A_N \frac{C_E}{C_N} \quad (3.10)$$

In order to measure the isotopic abundance of ${}^6\text{Li}$ in the enriched Li_2CO_3 sample, experimental setup of *Figure 3.3* was used. Pulse-height spectra with two kinds of converter foils, one with Li_2CO_3 having natural Li isotopic composition and another Li_2CO_3 sample having enriched ${}^6\text{Li}$ composition, were recorded. The recorded PHS

spectra for two types of layers with background are shown in *Figure 3.7*.

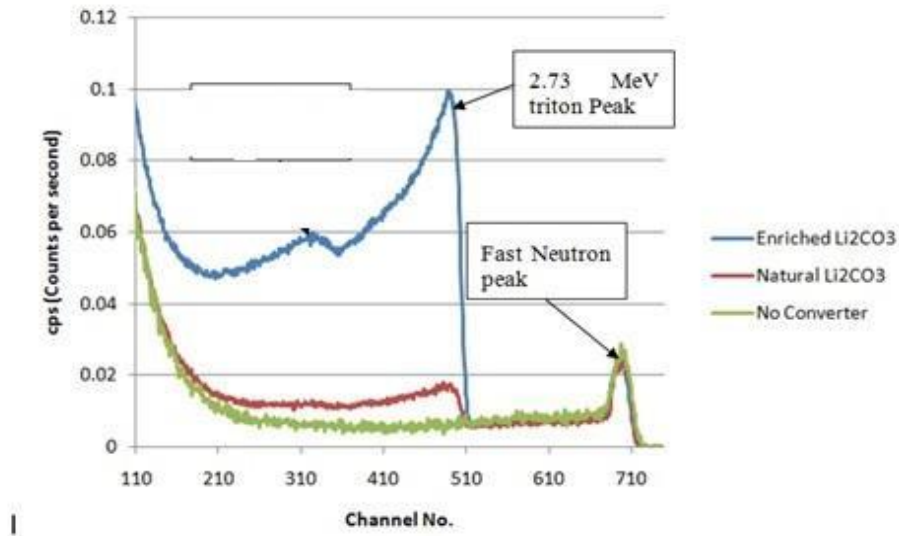


Figure 3.7: Pulse-height spectra with enriched and natural Li_2CO_3 layer placed on the charged particle detector SBD

It can be seen from *Figure 3.7* that the introduction of converter layers changes the pulse-height spectra in the energy range of the emerging particles from tritium producing reaction with ^6Li . Result of the ^6Li isotopic abundance in the enriched Li_2CO_3 sample is given in *Table 3.7*.

Table 3.7: Measured ^6Li isotopic abundance in enriched Li_2CO_3 converter foil

Parameter	Value
Count rate with nat. Li_2CO_3 layer (C_N) cps	1.19
Count rate with en. Li_2CO_3 layer (C_E) cps	9.76
Abundance of ^6Li in nat. Li_2CO_3	7.54%
Abundance of ^6Li in en. Li_2CO_3	61.84%

The isotopic abundance of the same sample was also determined with Inductively Coupled Plasma Mass Spectroscopy (ICPMS) and the result was 60.69% of ^6Li . Both results agree within 1.8%.

3.4 Summary

Two independent techniques for the measurement of tritium production rate in the breeding blanket mock-up experiments were developed and characterized in this chapter. These diagnostics will be employed to measure the TPR in the breeding blanket mock-ups and are reported in the later part of the thesis. Another application of the on-line method was shown to be in the measurement of the ^6Li ratio determination in the samples having varying fractions of ^6Li .

Chapter 4

Measurement of tritium production rate in LiAlO_2 assembly

4.1 Introduction

Tritium self-sufficiency is a key issue in the development of a fusion reactor based on the D-T reaction [1]. In order to assess the realistic margins for such self-sufficiency, the tritium breeding capability has to be calculated for the blanket concepts under development taking into account the uncertainties due to the nuclear data and codes used in the calculations [65, 86]. Radiation transport code MCNP and nuclear data library FENDL-2.1 [3] are adopted as a reference tool in fusion reactor nuclear analyses. FENDL-2.1 is a collection of the best evaluation for fusion applications from the world-wide nuclear data libraries such as ENDF/B-VI.8, JEFF-3.0, Brond-2.1 and JENDL-3.3 fusion files.

In the most current designs of D-T fusion reactor, lithium-containing ceramics such as Li_2O , LiAlO_2 , Li_2TiO_3 , Li_2ZrO_3 and Li_4SiO_4 are considered to be as the candidates of tritium breeding materials [11–15, 67–71]. Several experiments were conducted to validate the tritium production rate (TPR) in the breeding assemblies [7, 11, 13–15, 68]. A neutronics experiment with the objective to validate the capability of MCNP

and nuclear data library FENDL-2.1 to predict nuclear responses such as tritium production rate with qualified uncertainties was designed and performed with lithium aluminate (LiAlO_2) as breeder and High Density Polyethylene (HDPE) as neutron reflector. However LiAlO_2 was considered a candidate breeding material in the past but is not proposed in the current designs of the breeding blankets. Therefore current experiment was performed to test the experimental techniques and validation of the computational tools with available breeding material LiAlO_2 so that further experiments with relevant materials can be done applying these techniques.

The experimental assembly was irradiated with D-T neutrons from neutron generator tube and the spatial distribution of tritium profile was measured with Li_2CO_3 pellets having natural lithium isotopic composition. The experimental tritium production rates were compared with calculated values of Monte Carlo code MCNP and FENDL-2.1 cross-section library.

4.2 Experimental details

The experimental assembly consists of LiAlO_2 breeder material surrounded with neutron reflecting material HDPE, diagnostic pellets and neutron generator tube at the center. *Figure 4.1* shows the photograph of the LiAlO_2 assembly used for the 14 MeV irradiation experiment. The tritium breeding assembly has hexagonal cross-section with central hexagonal hole to insert the neutron tube. The radial thickness of the LiAlO_2 breeder zone was 78 mm. The γ -phase LiAlO_2 (natural Li isotopic composition) ceramic pellets were filled inside 1 mm thick aluminum tubes. Role of aluminum rods was to provide the container for the pellets so that they can be assembled easily. These aluminum rods were arranged in rows to make the breeding

assembly shown in *Figure 4.1*. The experimental assembly was surrounded with HDPE to reflect neutrons (simulation of reflected neutrons in fusion breeding blanket environment) and to shield the room returned neutrons into the assembly.

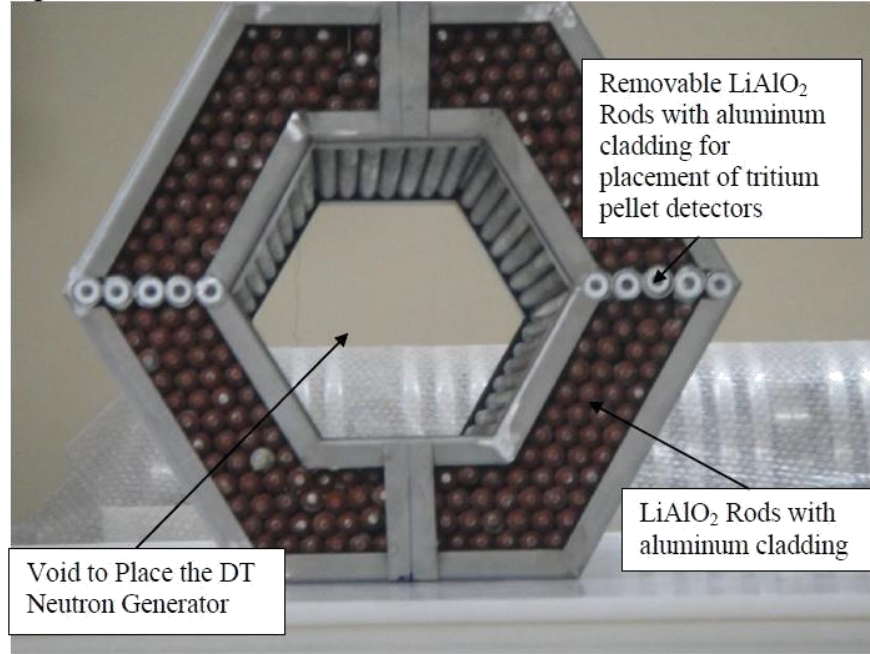


Figure 4.1: *Experimental assembly containing LiAlO₂ breeding material for the measurement of tritium production rate*

The assembly was irradiated continuously for five hours with 14-MeV neutrons generated from the D-T neutron tube manufactured by M/s SODERN, France [39]. The neutron tube was inserted inside the assembly keeping the neutron source at the center of the assembly. The source neutron yield during the experiment was measured with 13 mm dia. ultra-pure copper foil (99.999% purity) using $^{63}\text{Cu}(n, 2n)^{62}\text{Cu}$ threshold reaction with radiometric technique. The measured neutron yield during the experiment was $9.12 \times 10^9 \text{ n/s}$ ($\pm 6.99 \%$). The time evolution of the neutron emission during the irradiation was monitored with ^3He proportional counter covered with HDPE and the neutron emission count rate was varying 5% from the average count rate.

The tritium distribution profile in the breeding assembly was measured using cold pressed Li_2CO_3 (natural Li isotopic composition) pellets with diameter 10 mm and thickness 2.6 mm. The masses of Li_2CO_3 diagnostic pellets were in the range 236.7-332.5 mg. The isotopic compositions of lithium isotopes (^6Li and ^7Li) in both Li_2CO_3 and LiAlO_2 were determined by mass spectroscopy. The measured atom percentage of ^6Li and ^7Li in Li_2CO_3 were 7.56% and 92.44% respectively and ^6Li and ^7Li in LiAlO_2 were 7.56% and 92.44% respectively. The Li_2CO_3 pellets were wrapped in aluminum foils to avoid the contamination from surrounding LiAlO_2 pellets. Tritium activity in irradiated diagnostic pellets was measured with liquid scintillation spectrometer after wet chemistry treatment procedure [61]. Firstly, the irradiated pellets were dissolved in the binary acid solvent. The binary acid solvent was prepared with 70% HNO_3 and 100% CH_3COOH ($\text{HNO}_3:\text{CH}_3\text{COOH}$ ratio in the binary acid mixture was 3:10). The pellets were kept in this solution for 10 hours at room temperature to dissolve them completely. The pellet solution was mixed gravimetrically to the commercially available liquid scintillation cocktail Optiphase Hisafe-3 (10 ml) in polyethylene vials. Tritium measurement in pellets were performed with Ultra Low Level liquid scintillation counter model LKB wallac Quantulus 1220 manufactured by M/s Perkin Elmer Limited. The Minimum Detectable Activity (MDA calculated as 3 of background) achieved was 0.0147 Bq/g of acid solvent for a background count rate of 1.102 cpm and counting time of 500 min (50 min 10 cycles). The statistical error (1σ) in the tritium measurement was in the range of 1.65-7.5%. The liquid scintillation counter was calibrated for tritium detection efficiencies and recoveries corresponding to various quench levels.

Li_2CO_3 pellet detectors were placed inside the removable aluminum pipes. After

placing the pellet detectors at their respective positions, the empty space was filled with LiAlO_2 pellets to avoid direct scattered neutrons from the HDPE to the central pellet detectors. There were five such aluminum tubes for the positioning of the detectors. Locations of these channels from source were 10, 11.5, 13.0, 14.5 and 16.0 cm respectively. In each measuring channel there were two Li_2CO_3 pellets. There were total 10 measurement locations in the whole assembly. Positions of these pellets with respect to source position are shown in *Figure 4.2*.

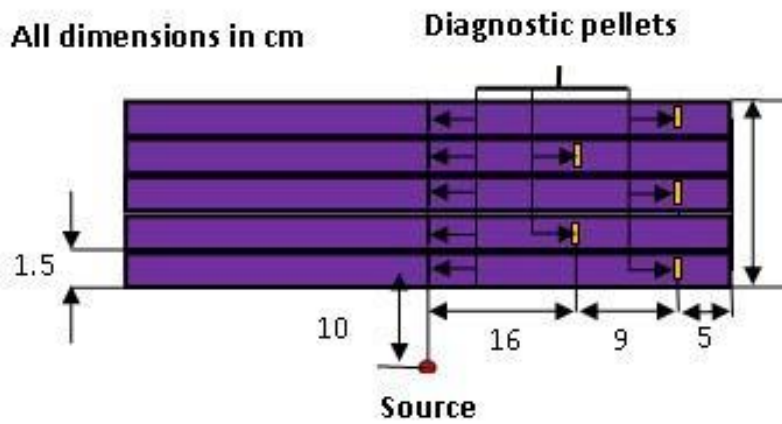


Figure 4.2: Locations of diagnostic Li_2CO_3 pellets in the experimental assembly

4.3 Computational model

The experimental assembly which includes breeder material LiAlO_2 , neutron reflector HDPE, aluminum tubes, support structure of the experimental assembly, neutron generator tube, diagnostic pellets etc. were modelled in the calculation model to calculate the tritium production rate in the diagnostic pellets. Lattice card in MCNP was used to create the hexagonal breeding assembly filled with an element made of LiAlO_2 with aluminum cladding.

Neutron generator tube model described in Chapter 2 which includes tritium target, cooling circuit, HV insulator and NG tube, was modelled in the calculation. Neutron

source model described in Chapter 2 which includes angle dependent source spectra and emission anisotropy was implemented in the calculation model. *Figure 4.3* shows the top view of the experimental assembly at source plane exhibiting the location of diagnostic pellets. *Figure 4.4* show the cross-sectional view of MCNP the model displaying materials used in the experiment.

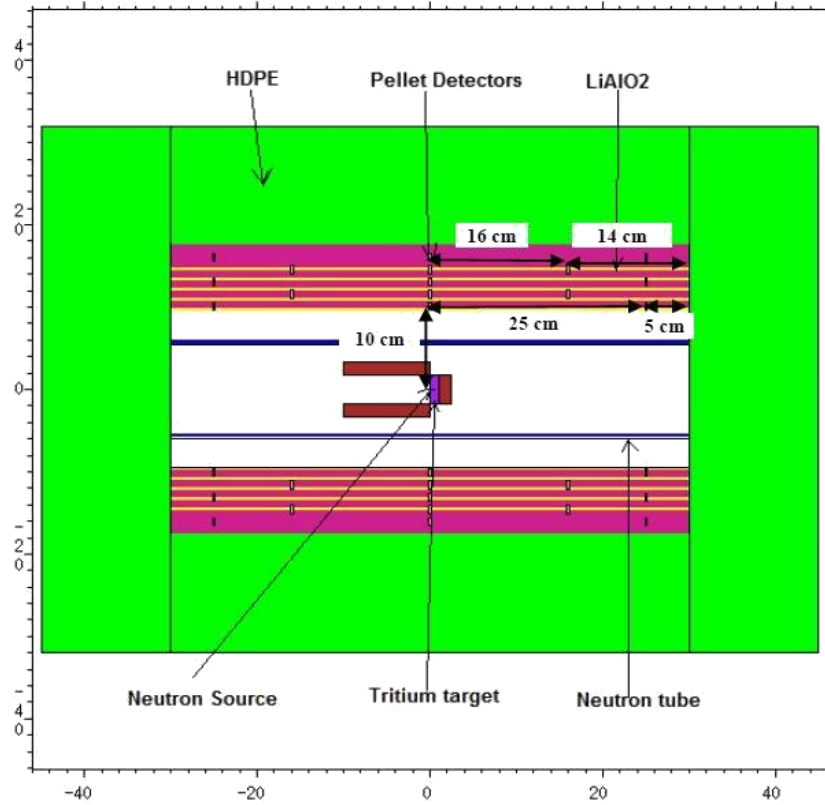


Figure 4.3: Cross-section through the mid-plane of experimental assembly

The experiment was analyzed with Monte Carlo code MCNP and FENDL-2.1 neutron transport library. Significant amount of tritium atoms are produced by ^6Li isotopes and low energy neutrons below 1 eV. So, it is necessary to know the low energy neutron population precisely in the breeding assembly. Hence, the $S(\alpha, \beta)$ thermal neutron tables from the ENDF-VI.5 (poly.60t) library were used for the neutron transport below 1 eV. This special cross-section library considers the low energy neutron interaction with hydrogen atoms present in the HDPE molecule i.e. motion of free

hydrogen atoms differs from the atoms bonded in a molecule and hence the neutron interaction.

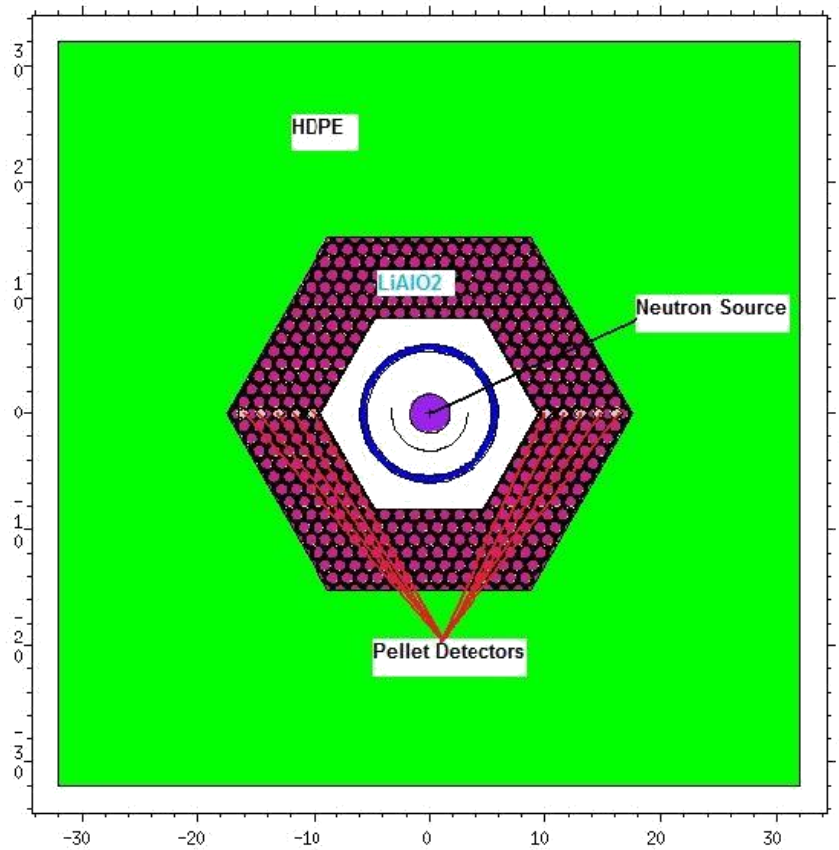


Figure 4.4: Cross-sectional view of the MCNP model of breeding assembly with HDPE reflector

Cell averaged tallies called F4 in MCNP were used to calculate the tritium production in diagnostic pellets since they can model the self-shielding effect adequately. Reaction number (widely known as MT number) 105 was used to calculate the tritium production from ^6Li isotope and MT number 205 for tritium production calculation from ^7Li isotope. Total tritium production rate was the sum of the contribution from both isotopes after normalization to their atomic ratio in the natural lithium. The maximum statistical error (fractional standard deviation) in the MCNP calculated tritium production reaction rates was 1.76%.

4.4 Results and discussion

Radial profiles of tritium production rate (TPR) in the breeding assembly were measured at three axial positions (1) axial position 0 cm from the source with 1.5 cm radial resolution (2) axial position 16 cm from source with 3 cm radial resolution (3) axial position 25 cm from source with 3 cm radial resolution. There were total 10 points where TPR was measured and calculated with MCNP and FENDL-2.1. Schematic of all the measurement positions is shown in *Figure 4.2*. TPR in the assembly was measured with the help of lithium carbonate pellets.

The experimental (E) and calculated (C) TPR radial profile along-with C/E ratios at axial position 0 cm, is shown in *Figure 4.5*. Tritium production rate shows almost flat profile up to 4.5 cm depth from source in the assembly. It increases in the penetration depth beyond 4.5 cm due to vicinity of the HDPE neutron reflector. The detector near the neutron reflector shows higher TPR ($\times 4$) than the detectors near to the source due to higher thermal flux built-up by reflection from HDPE and breeder material. The calculation results predict the TPR very well except one point which overestimates measured TPR beyond the experimental error bar (point close to source). The average value of the C/E ratios for measurement locations at axial distance 0 cm is 1.08.

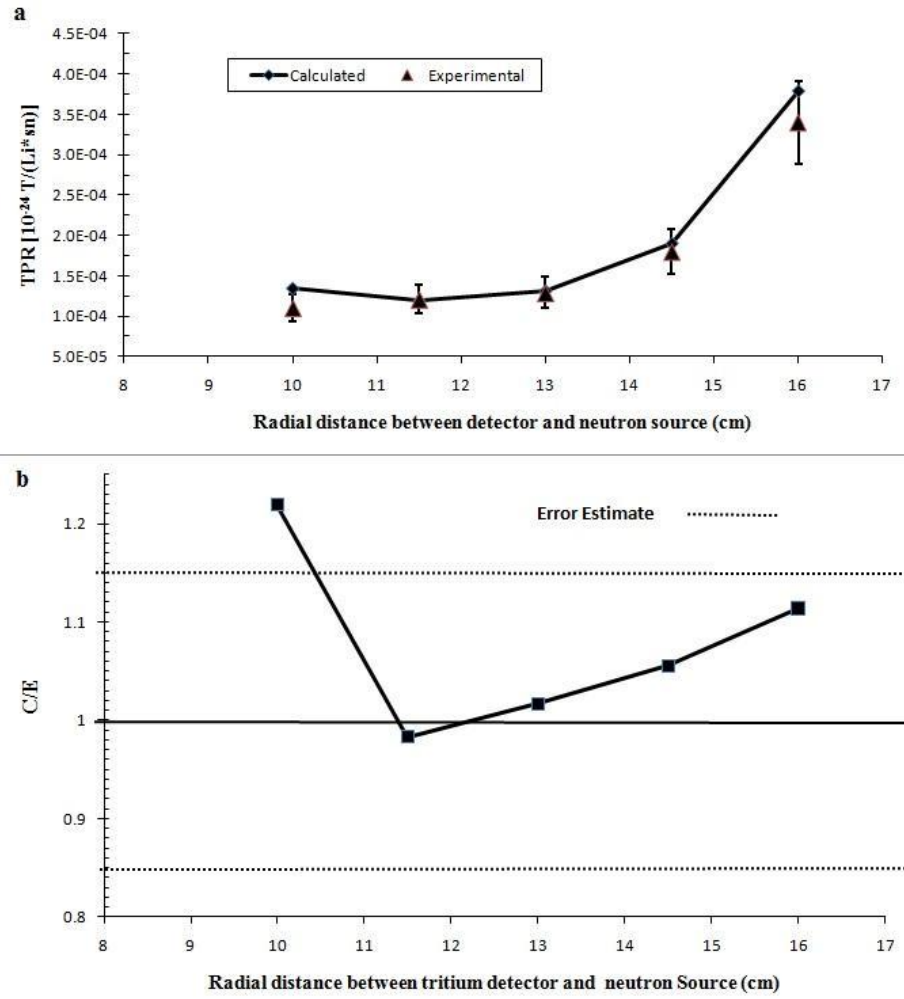


Figure 4.5: (a) Calculated and measured TPR radial profile at axial position 0 cm (b) radial profile of C/E ratios. The error estimate includes errors in neutron yield measurement, statistics of tritium counts and statistics of Monte Carlo calculation.

Measured and calculated tritium production rate radial profile along-with C/E ratios at 16 cm axial distance is given in *Figure 4.6*. The average value of the C/E ratios for 16 cm axial position is 0.91. The calculated and measured TPR profiles for this case agree well within the estimated error bar.

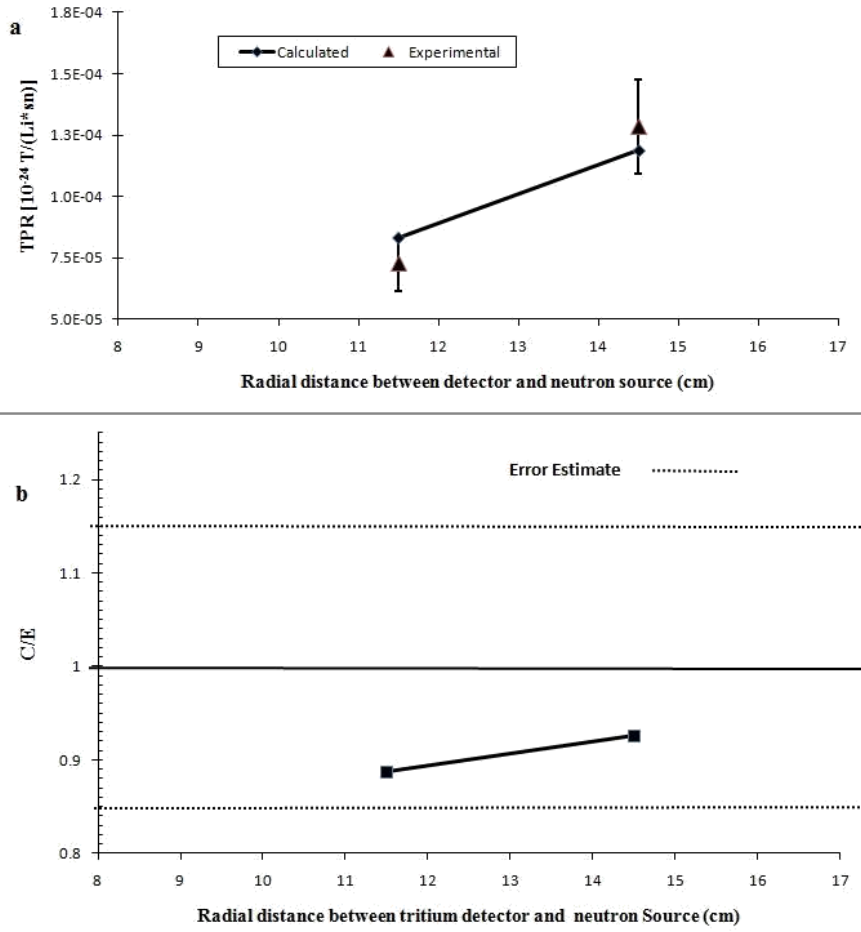


Figure 4.6: (a) Calculated and measured TPR radial profiles at 16 cm axial distance from source and (b) Radial Profile of Calculated to experimental (C/E) TPR ratio. The error estimate includes errors in neutron yield measurement, statistics of tritium counts and statistics of Monte Carlo calculation

Measured and calculated TPR profiles and C/E ratios for 25 cm axial position are shown in *Figure 4.7*. The average value of the C/E ratios for this axial position is 1.01. The C/E ratios are close to unity within the estimated error bar. The pellet detector near to the HDPE shows higher tritium production rate ($\times 2$) than the points near to the source due to reflected neutrons from HDPE and softening of neutron spectrum due to presence of breeding material LiAlO_2 . It can be seen from *Figure 4.7* that the middle point shows lower TPR than the edge points due to presence of HDPE reflector.

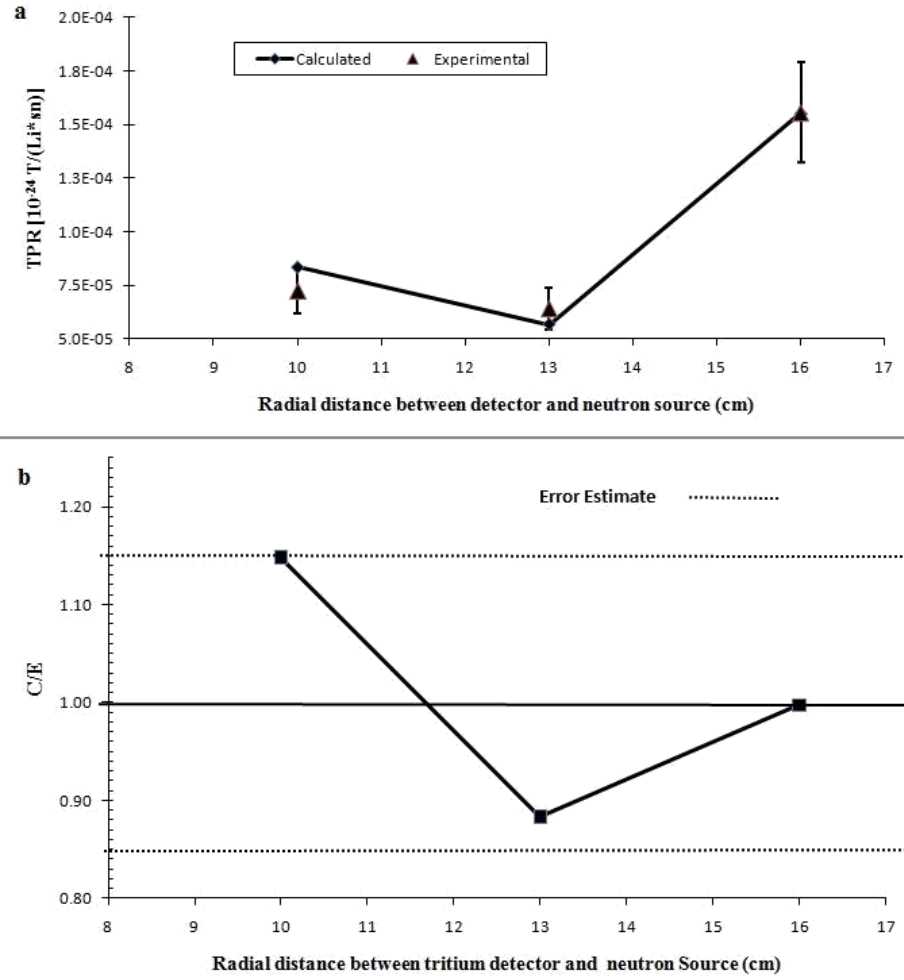


Figure 4.7: (a) Calculated and measured TPR radial profiles at 25 cm axial distance from source and (b) Radial Profile of Calculated to experimental (C/E) TPR ratios. The error estimate includes errors in neutron yield measurement, statistics of tritium counts and statistics of Monte Carlo calculation.

4.5 Conclusions

A benchmark experiment for tritium production rate was performed with an assembly having LiAlO_2 as breeder and HDPE as reflector. The local TPR was measured with small Li_2CO_3 pellet detectors inside the breeding assembly. Measured tritium production rates were compared with the calculated values. Comparison between measured and calculated (with Monte Carlo code MCNP and FENDL-2.1 cross section

library) values of TPR shows good agreement in the LiAlO_2 assembly. However the calculated TPR at a location very near to the source was found to be overestimating the measured value. This experiment was an attempt to develop all the necessary experimental techniques and calculation tools to perform the benchmark experiments with candidate breeding materials. Experience gained from this experiment will help to improve the experimental uncertainties in the TPR measurement and source neutron yield in the forthcoming experiments.

Chapter 5

Breeding blanket mock-up experiment containing lithium titanate ceramic pebbles and Lead

5.1 Introduction

To ensure tritium self-sufficiency in the D-T fusion reactor, the calculated achievable tritium breeding ratio (TBR) must be equal to or greater than the minimum required TBR [1]. TBR in the fusion reactor blankets is calculated with the help of neutron transport codes and cross-section data libraries. The cross-section data libraries are collection of evaluated data based on various physics models and approximations. The evaluated cross-section data have uncertainties and therefore it results in the uncertain calculated TBR. There-fore neutronics integral experiments with breeding blanket mock-up are an important research activity to validate the evaluated cross-section data files so that cross-section files can be upgraded and uncertainty in TBR due to cross-sections can be reduced. Several neutronics benchmark experiments with blanket mock-ups are reported in the literature for different breeding blanket concepts [5, 11, 12, 15, 20, 65, 67, and 68].

India has proposed Lead-Lithium cooled Ceramic Breeder (LLCB) concept of breeding blanket for in-situ tritium production in its DEMO reactor [16]. Mock-up of the LLCB breeding blanket will be tested in ITER through Test Blanket Module (TBM) program [17]. The materials proposed for LLCB TBM are: lithium titanate enriched with ^6Li in ceramic pebble form as breeder, liquid Lead-lithium eutectic as breeder, coolant and multiplier, Reduced Activation Ferritic Martinstic Steel (RAFMS) as structural material. A set of four mock-up experiments is planned to investigate the neutronics performance of materials used in the LLCB TBM. The first experiment whose results are discussed in this chapter uses Lead as neutron multiplier, mild steel (MS) as structural material and lithium titanate pebbles as breeder with natural lithium isotopic composition. MS used in the experiment was of grade 55 as per ASTM (American Society for Testing and Materials) A516 standard. The second planned experiment will have Pb-Li and lithium titanate pebbles with natural lithium and P91 steel as structural material. The third experiment planned will have Pb-Li in solid form and lithium titanate enriched with ^6Li and P91 steel as structural material. The fourth set of experiment will be performed with sample materials used in LLCB TBM viz. ^6Li enriched Pb-Li liquid metal eutectic and lithium titanate pebbles and IN-RAFMS as structural material. The first mock-up experimental assembly was designed and fabricated to perform measurements of the nuclear responses (TPR and $^{115}\text{In}(n, n')^{115m}\text{In}$ reaction rate) in the geometry simulating radial build-up of LLCB TBM in ITER. The TPR is measured with two kinds of diagnostics: Li_2CO_3 pellets and on-line tritium measurement with silicon surface barrier detector (SBD) having ^6Li to triton converter. The $^{115}\text{In}(n, n')^{115m}\text{In}$ reaction rate is measured by irradiating indium foil in the zones of experimental assembly. The measured nuclear responses

are compared with that of calculations done using the three-dimensional Monte Carlo code MCNP and cross-section libraries FENDL-2.1 and FENDL-3.0 [3, 4].

5.2 Design of the experiment

Design of a mock-up experiment requires neutronics conditions to be similar to the nuclear environment of LLCB TBM in ITER. The conditions equivalent to the ITER nuclear environment are the neutron spectrum, tritium production rate, nuclear heating, damage etc. The basic parameters on which the other parameters (total tritium production, nuclear heating, damage etc.) depend is the neutron spectrum and flux. The neutron spectrum can be approximately reproduced using D-T neutron generator with combination of materials and hence the tritium production rate (TPR). It is the neutron fluence which is impractical to be produced in the neutron generator environment and hence it is impossible to study the other nuclear parameters like radiation damage, gas production and nuclear heating with neutron generators i.e. these parameters are not measurable while TPR is measurable with neutron generators.

Radial build-up of the mock-up was kept similar to the first five zones of LLCB TBM in ITER. LLCB TBM will be installed in one of the equatorial ports of ITER. The first wall of LLCB TBM will see the reflected neutrons from the torus. In order to create ITER LLCB TBM first wall like spectra, a cavity, with reflecting material HDPE, around the neutron generator is formed. The dimension of this cavity was optimized to approximately match the neutron spectra on the first wall of mock-up. The optimized dimension of the cavity was $17(\text{length}) \times 25(\text{width}) \times 25(\text{height}) \text{ cm}^3$.

Comparison of neutron spectra on the mock-up first wall and LLCB TBM first wall is

shown in *Figure 5.1*.

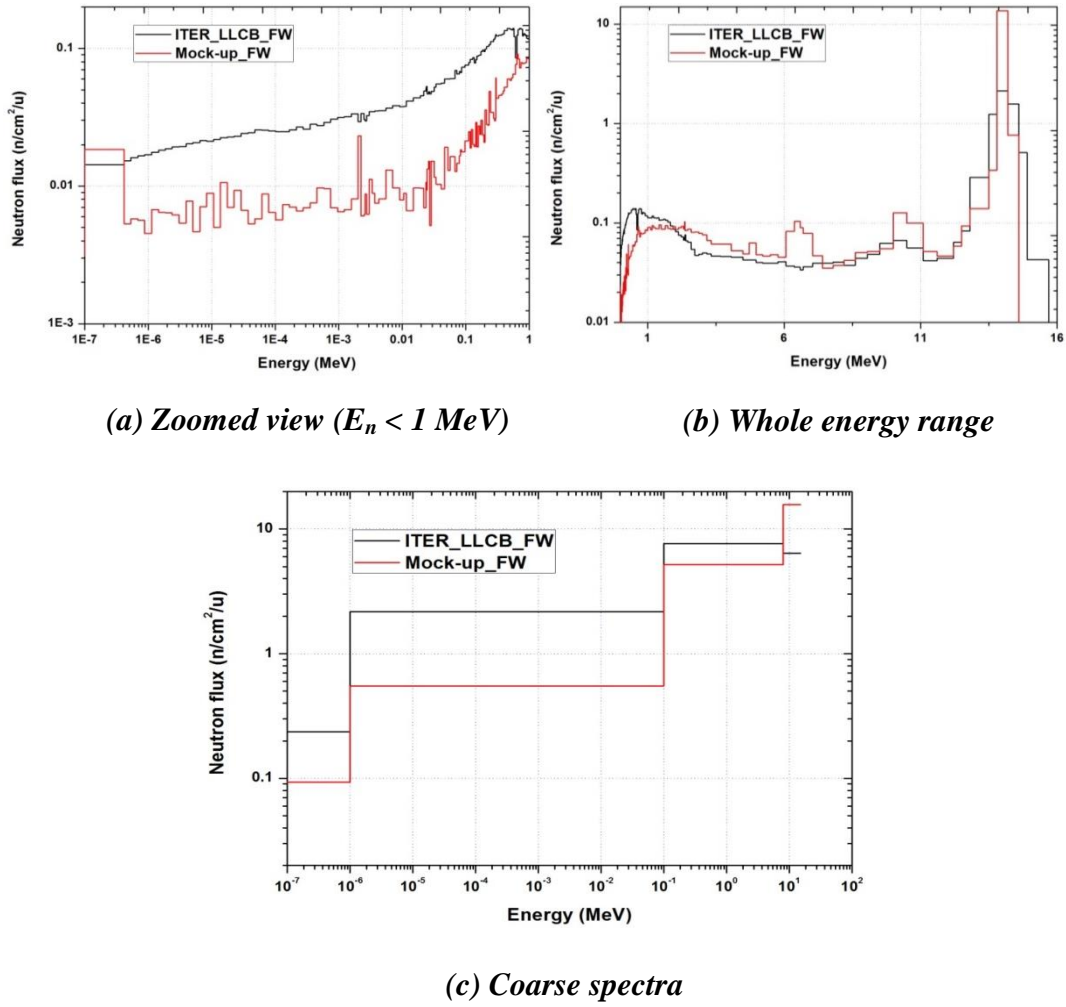


Figure 5.1: Comparison of neutron spectra on the first wall of mock-up and LLCB TBM in ITER

It can be seen from *Figure 5.1* that the mock-up first wall fast neutron spectra show quite reasonable matching (within few tens of percent) with the LLCB TBM first wall spectrum in the fast and thermal neutron energy range. Maximum difference is in the intermediate energy range (0.5 eV- 0.5 MeV) by a factor of 4 (*Figure 5.1*). Fast neutron spectrum is important for the tritium breeding in the deep zones i.e. low energy neutrons at first wall can't penetrate through materials.

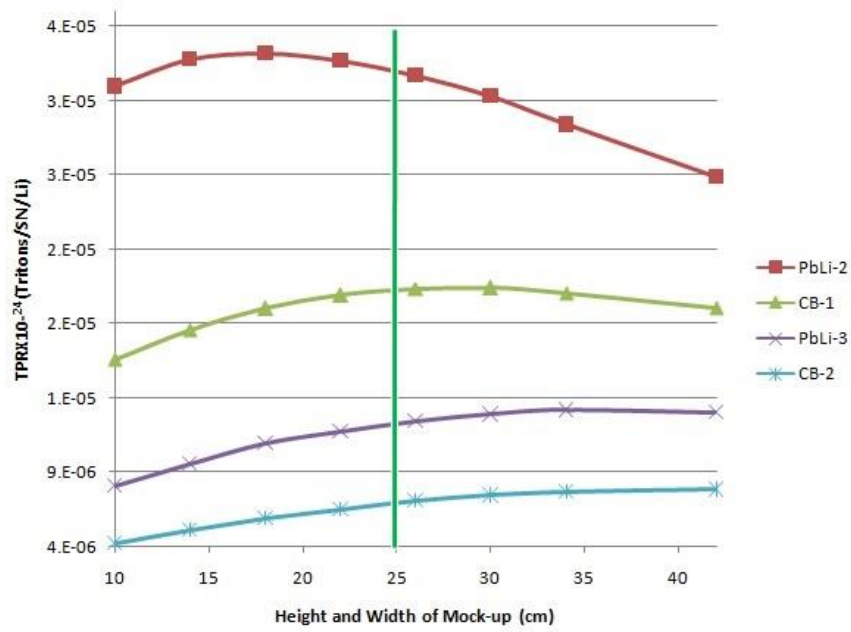


Figure 5.2: Tritium production in mock-up zones as a function of height and width of mock-up

The other two dimensions (other than radial) of the mock-up are optimized to maximize tritium production in mock-up zones with the help of neutron transport calculations. Height and width of the mock-up also has impact on the tritium production rate at the central part due to neutron multiplication and reflection. Tritium production rates in mock-up zones as a function of mock-up height and width is shown in *Figure 5.2*. It can be seen from *Figure 5.2* that the tritium production saturates at a certain height and width for deeper zones of the mock-up. 25 cm height and width of the mock-up assembly gives maximum tritium production in most of the zones. Therefore the optimized height and width of the mock-up is 25 cm. The outer plates covering the mock-up were kept 2 mm thick and the rationale behind this chosen thickness was based on the availability, structural strength and minimum neutron absorption. Circular channels were provided for the diagnostics placement in each mock-up zone.

5.3 Experimental details

This section describes the geometry & materials of the experimental assembly, neutron yield measurement, and details of the diagnostics for nuclear responses measurement.

5.3.1 Geometry of the mock-up assembly

The breeding blanket mock-up assembly consists of three layers of Lead and two layers of lithium titanate pebbles with natural lithium isotopic composition. Lead serves the purpose of the neutron multiplication and lithium titanate as breeder. These layers in the mock-up are separated by 5 mm thick MS plates. The outer walls of the mock-up assembly are also made of MS plates and have following thicknesses: 12 mm thick first wall, 5 mm thick wall opposite to first wall, rest four sides of mock-up assembly are 2 mm thick. Thicknesses of the breeding layers, multiplier, separation walls and first wall materials in mock-up replicate the radial build-up of LLCB TBM in ITER. The optimized height and width of the mock-up assembly (section 5.2) is 25 cm. The overall external dimension of the mock-up is $25\text{cm} \times 25\text{cm} \times 26\text{ cm}$. The mock-up is provided with five penetrations at 5.1, 10.6, 14.7, 18.8 and 22.8 cm from the front surface of the mock-up to facilitate insertion of the pellet detectors and activation foils in each breeding and multiplier layers. Another penetration for the on-line tritium detector was provided in the last zone from backside of the mock-up assembly. The mock-up assembly is surrounded by high density polyethylene (HDPE) neutron reflecting material to simulate reflected neutrons from machine structure to the TBM and to shield the room reflected neutrons at the measurement positions. The

whole assembly is surrounded by 1 mm thick Cd to reduce the room reflected thermal neutrons into experimental assembly through the tiny gaps between HDPE sheets. Photograph of the mock-up assembly ready for irradiation is shown in *Figure 5.3*.

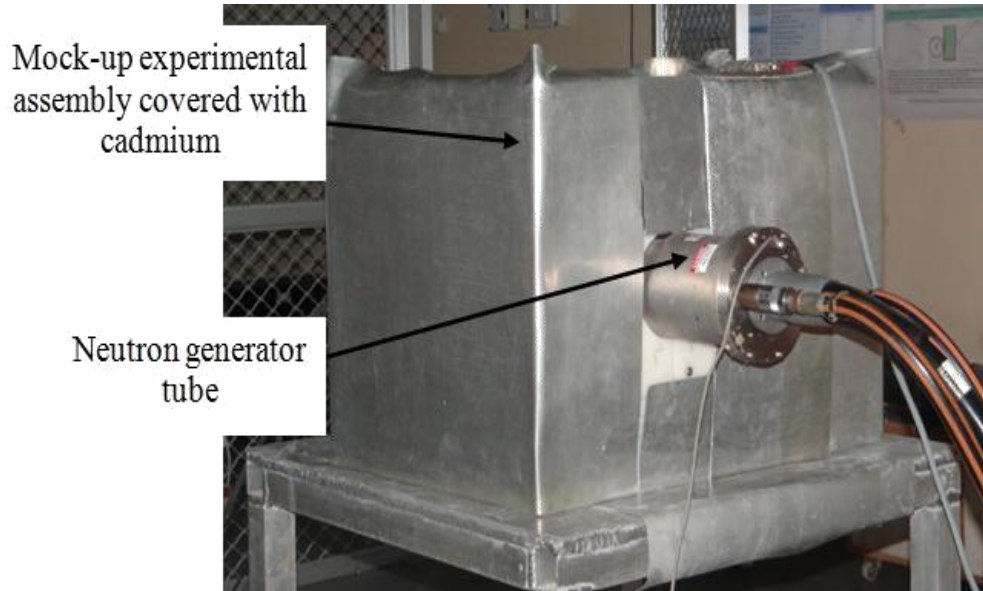


Figure 5.3: Photograph of the breeding blanket mock-up assembly ready for irradiation with 14 MeV neutrons

Figure 5.4 shows the horizontal cross-section through the mid plane of the experimental assembly showing the dimensions of the multiplier and breeding zones, positions of pellet detectors and dimensions of the HDPE etc. The color coding of the material used in the experiment are shown in *Table 5.1*.

Table 5.1: Color coding of the material used in the MCNP model of mock-up assembly

Color	Material
Pink	HDPE
Cyan	Lead
Green	Li_2TiO_3
Yellow	MS
Blue	SS316
Violet	Cooling oil

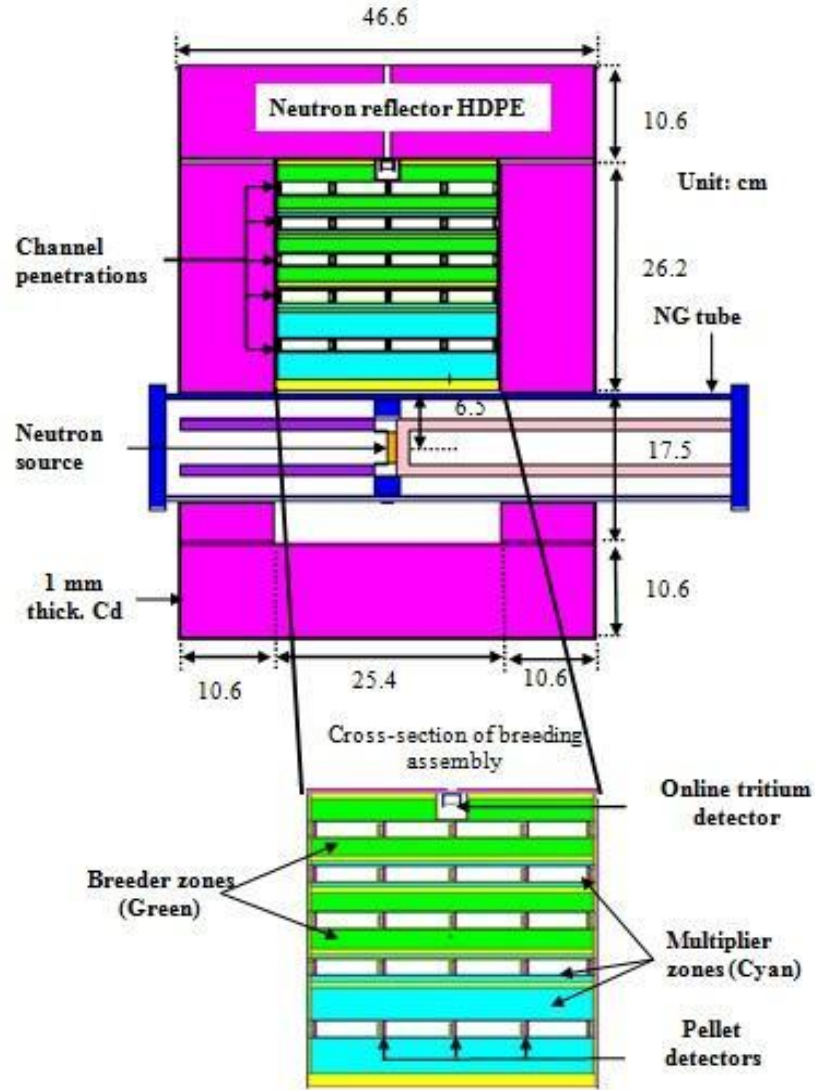


Figure 5.4: Cross-section of the mock-up assembly with HDPE reflector and tritium pellet detectors

Figure 5.5 shows the vertical cross-section through the assembly showing the radial build-up of the assembly (thicknesses of MS plates, Lead and Breeder zones), location of the pellet and on-line tritium detectors from the source. Cadmium sheets are not seen clearly in these pictures due to their relatively smaller thickness. The lithium titanate pebbles were modelled as homogenized material i.e. the pebbles in the calculation model were not represented individually. This is reasonable approximation as the mean free path of the neutrons is less than the size of the pellets.

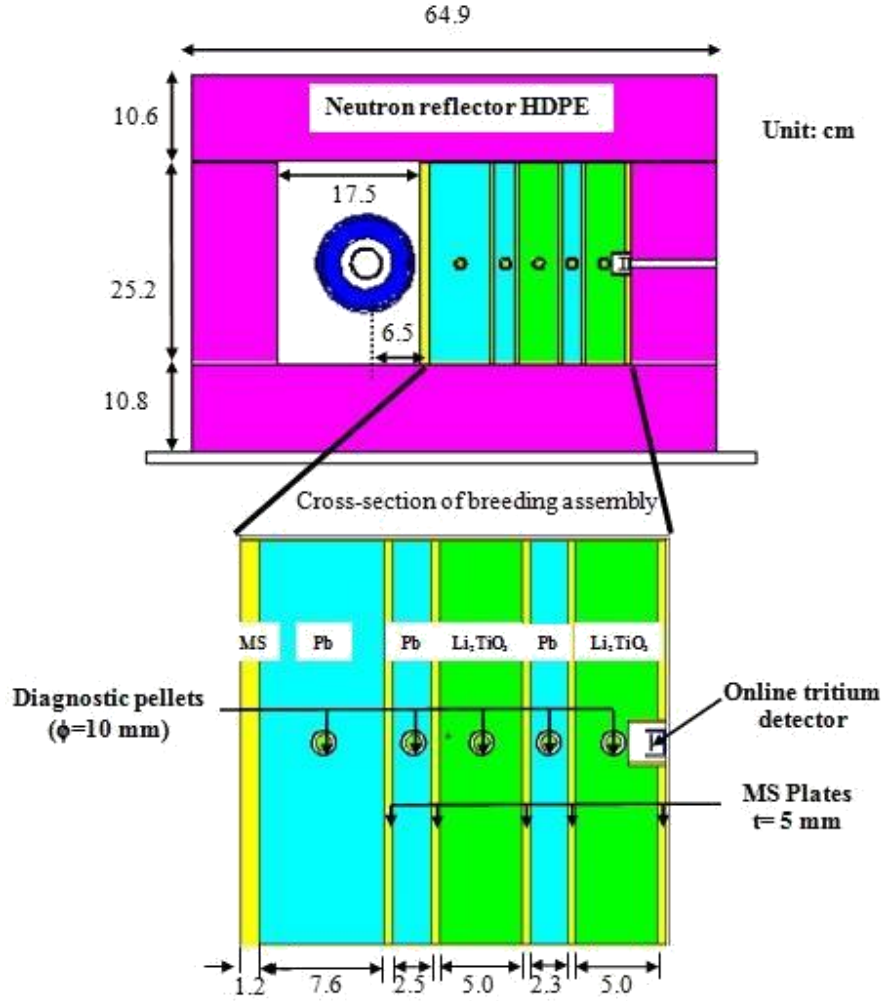


Figure 5.5: Cross-sectional view of the MCNP model of breeding assembly with HDPE

5.3.2 Measurement of the neutron yield

The Mock-up assembly was irradiated with neutrons from SODERN made sealed neutron generator tube which can produce neutron yield up to 10^{10} n/s. The mock-up assembly was irradiated in three shifts accumulating total 15 hours of irradiation. The time profile of the source neutron yield was monitored with a ^3He counter covered with neutron moderator. This monitor was calibrated against the activation measurement done with Al foil using the $^{27}\text{Al}(n, \alpha)^{24}\text{Na}$ reaction. The measured total source neutron emission during 15 hours of irradiation was 4.42×10^{14} neutrons with

uncertainty 4.73%. Time profile of the neutron yield during three shifts is shown in *Figure 5.6*.

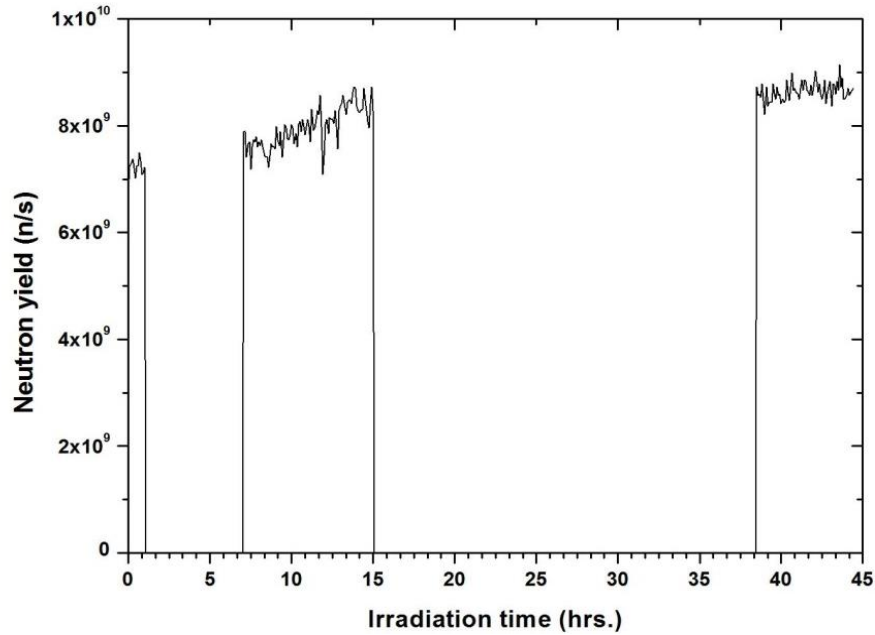


Figure 5.6: Time profile of the 14 MeV neutron source during mock-up irradiation

The time profile of the neutron generator emission shows good stability with 5% difference with average neutron yield. The fluctuations in the second shift were relatively higher due to non-operation of the neutron generator for long time. The operating parameters of neutron generator tube such as beam acceleration voltage, beam current and vacuum were kept similar during all three shifts. The neutron yield shows increasing yield trend due to conditioning of the tube environment with operation. The neutron generator conditioning systems are actuated during the neutron generator operation.

5.3.3 Materials properties

The Li_2TiO_3 ceramic pebbles were synthesized and fabricated by the solid state reaction process developed by Mandal et al. and described in details in references [72,

73]. The impurities, in the materials used in the experiment namely lithium titanate, Lead and MS, were determined by Inductively Coupled Plasma Optical Emission Spectroscopy (ICPOES). The weight percentage of impurities and constituent elements in the materials used in the experiment are listed in *Table 5.2*.

Table 5.2: Elemental composition of materials with impurities used in the experiment

Li₂TiO₃		Lead		MS	
Element	Wt%	Element	Wt%	Element	Wt%
Na	0.018	Bi	0.014	Co	0.002
K	0.084	Fe	0.436	Mn	1.370
Ca	0.041	Sb	0.025	Cr	0.640
Mg	0.007	Pb	99.525	Ni	0.270
Al	0.082			Cu	0.007
Co	0.028			B	0.039
Fe	0.055			Fe	97.711
Li	12.609				
Ti	43.479				
O	43.598				

Size distribution of the pebbles used in the experiment was also determined experimentally. The result of the pebbles size distribution is shown in *Figure 5.7*.

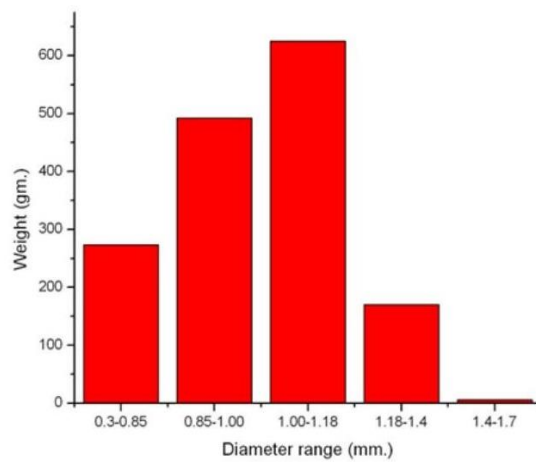


Figure 5.7: Size distribution of the Li₂TiO₃ pebbles used in the experiment

It can be seen from *Figure 5.7* that the most of the pebbles are having diameter in the range of 1-1.18 mm.

Lead in the mock-up assembly was filled from an external tank in inert gas environment to avoid oxidation. Lead was filled in the molten state and it got solidified by natural cooling in the assembly zones. Density of Lead in the zones was determined with the help of measured mass and volume of zones. Measured density was found close to the theoretical density (2% less than the theoretical density). The small difference may be ascribed to the inaccuracy in the volume and mass measurement of Lead.

5.3.4 Diagnostics details

TPR in breeding zones were measured with lithium carbonate pellets having two different enrichment levels of ^6Li , one with enrichment of 60.69% and another with natural lithium composition. The measurement positions of the pellet detectors in assembly zones are shown in *Figure 5.8*.

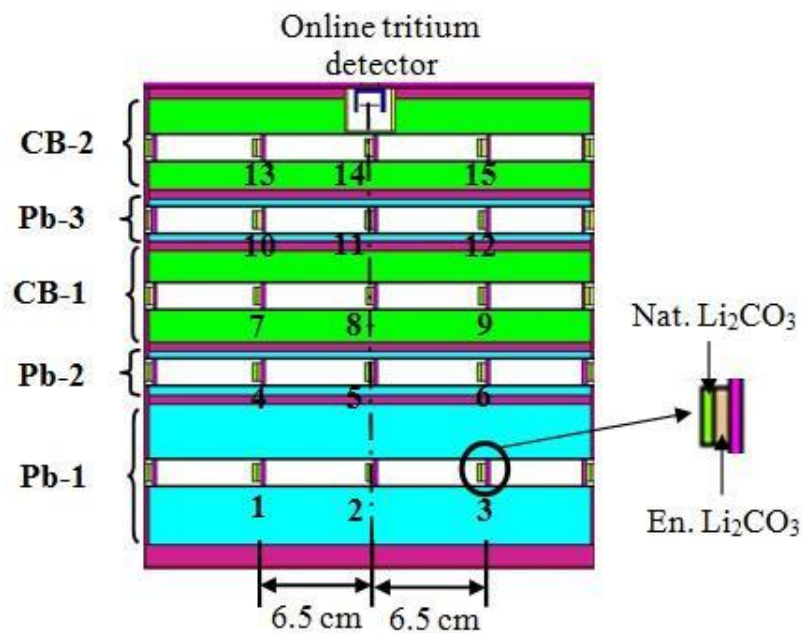
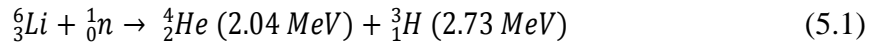


Figure 5.8: Cross-section of the mock-up assembly showing tritium measurement locations

The three multiplier zones of the mock-up are named as Pb-1, Pb-2 and Pb-3. The breeding zones are named as CB-1 (ceramic breeder) and CB-2 (*Figure 5.8*). There were six measurement positions (positions 7, 8, 9, 13, 14 and 15 in *Figure 5.8*) in the breeding zones and two pellets at each position one enriched and another natural lithium isotopic composition. Diameter of the pellets was 10 mm and the masses were in the range 300-400 mg. Tritium production in the multiplier zones were also measured at 9 locations (1, 2, 3, 4, 5, 6, 10, 11 and 12 as shown in *Figure 5.8*) to compare the measured tritium produced in these pellets with the calculated values. As such these measurements don't represent the TPR in these multiplier regions but they can provide comparison with the calculated results. These measurement positions are important for the next experiment which is planned by replacing Lead with Lead-lithium. Diagnostic pellets were fabricated by mixing the Li_2CO_3 with polyvinyl alcohol (PVA) binder and then compressed to 5 tons of pressure. After that, the pellets were slightly heated to remove the binder material PVA. Each pellet was sealed in very thin polyethylene cover to avoid the contamination from adjacent pellet. Tritium activity in irradiated pellets was measured with liquid scintillation spectrometer after wet chemistry treatment procedure. Details of this technique are given in Chapter 3. The pellets were dissolved in the binary acid solvent [61]. The binary acid solvent was prepared with 70% HNO_3 and 100% CH_3COOH . The pellets were kept in this solution for 10 hours to dissolve completely. The pellet solution was mixed with commercially available liquid scintillation cocktail Optiphase HISAFE-3 in HDPE counting vials. The beta counting from tritium activity in the scintillation sample was performed with Ultra Low Level liquid scintillation counter Quantulus 1220

manufactured by M/s Perkin Elmer limited. The minimum detectable activities of this counter for natural and enriched pellets were 0.052Bq and 0.043Bq respectively for a counting time of 250min (50minutes \times 5cycles). The liquid scintillation counter was calibrated for tritium detection efficiency and quenching by acid solvent using calibrated tritiated water from North American Scientific (see Chapter 3 for more details).

TPR- ^6Li in the second breeder zone was also measured with the help of on-line tritium diagnostics (*Figure 5.8*) described in Chapter 3. In this diagnostic, a converter foil of few m thick Li_2CO_3 enriched with ^6Li (60.69%) was placed in front of a silicon surface barrier detector (SBD). 2.73 MeV triton produced from the thermal neutron reaction with ^6Li in the converter foil was directly measured in the silicon surface barrier detector (100 μm thick and 50 mm^2 active area) using standard nuclear instrumentation. The exothermic nuclear reaction of neutron with ^6Li and the energies of emergent particles are shown in nuclear reaction 5.1.



The converter foil used with the SBD detector in the experimental assembly was same as characterized in the section 3.3.2. The number of ^6Li atoms in this converter foil was determined to be 6.3×10^{17} ($\pm 4.17\%$).

The neutron spectra ($E_n > 0.35 \text{ MeV}$) in all five zones were verified by performing $^{115}\text{In}(n, n')^{115\text{m}}\text{In}$ reaction rate measurement. The objective of this measurement was to check the neutron multiplication capability of MCNP with FENDL-2.1 data in Lead. This reaction has threshold of 0.35 MeV therefore it is well suited to measure the secondary neutrons from the (n, 2n) reactions in the Lead isotopes. This experiment was done by removing the pellet detectors from the assembly. The γ -activity ($E_\gamma = 336.2 \text{ keV}$) in the irradiated foils were measured by well calibrated HPGe detector.

5.4 Computational model

The results were analyzed with Monte Carlo code MCNP and FENDL-2.1 transport library. FENDL-3.0 was also used for those isotopes whose cross-section files are unavailable in the FENDL-2.1 library. The mock-up assembly, support structure of the assembly, experimental hall, detectors and their surrounding were modelled in MCNP as close to reality as possible to minimize the systematic errors due to modelling. Modelling of the neutron generator geometry and materials are described in section 2.7. Significant amount of tritium is bred by low energy neutrons of energy below 1 eV. So, it is necessary to calculate the low energy neutron population precisely in the experimental assembly. Hence, the $S(\alpha, \beta)$ thermal neutron tables from the ENDF-VI.5 (poly.60t) library was used to consider thermal motion of hydrogen atom in polyethylene molecule. Cell averaged tallies were used to calculate the TPR in diagnostic pellets since they can model the self-shielding effect adequately. The diagnostic pellets and activation foils were explicitly modelled in the calculation model (*Figure 5.8*). The reaction number 105 for ^6Li and 205 for ^7Li was used to evaluate the TPR from FENDL-2.1 library. The energy spectra and angular distribution of D-T neutron source in MCNP was modelled based on the calculation of reaction kinematics determined by modelling the D^+ beam energy and beam loss in tritium target using SRIM-2008 Monte Carlo code (see sections 2.4 and 2.5 for more details). Two views of MCNP model of mock-up assembly are shown in *Figure 5.4* and *Figure 5.5*. The maximum statistical error (fractional standard deviation) in the MCNP results was less than 1%. The IRDF-2002 dosimetry file was used for the calculation of the $^{115}\text{In}(n, n')^{115\text{m}}\text{In}$ reaction rate [59, 60].

5.5 Results and discussion

5.5.1 TPR from ^6Li and ^7Li in breeder zones

In order to separate tritium contribution from ^6Li and ^7Li isotopes, two Li_2CO_3 pellets having different Li isotopic compositions, one with natural Li composition and another with enriched ^6Li were irradiated adjacently in the mock-up zones. It can be assumed that the TPR remains constant over the area of two adjacent pellets. Let TPR- ^6Li is “ x ” and TPR- ^7Li is “ y ”. Let the ^6Li and ^7Li atom fractions in the diagnostic pellet are “ a ” and “ b ” respectively. Then the total tritium production in the pellet (z) can be written by following linear equation having two variables x and y .

$$z = ax + by \quad (5.2)$$

Tritium production measured with Li_2CO_3 pellet having natural composition of Li isotopes ($a_1=0.0754$, $b_1=0.9246$) can be written as:

$$z_1 = a_1x + b_1y \quad (5.3)$$

Tritium production measured with Li_2CO_3 pellet having enrichment of ^6Li ($a_2=0.6069$, $b_2=0.3931$) can be written as:

$$z_2 = a_2x + b_2y \quad (5.4)$$

The solutions of system of linear equations 5.3 and 5.4 are as follows:

$$\text{TPR-}^6\text{Li} : x = \frac{z_2 - b_2y}{a_2} \quad (5.5)$$

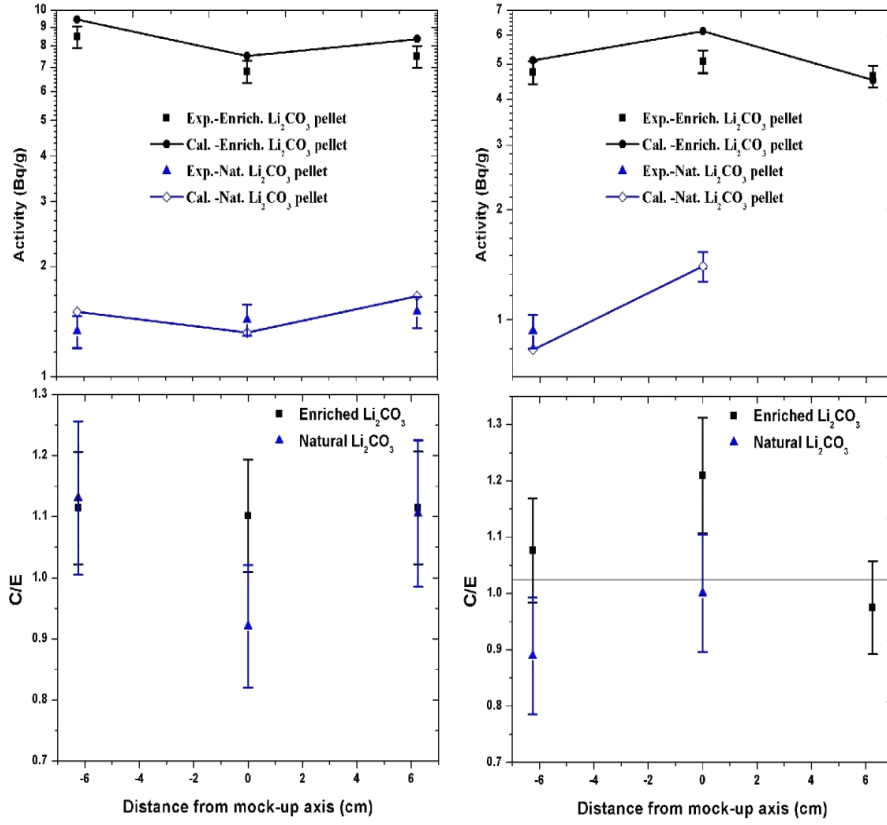
$$\text{TPR-}^7\text{Li} : y = \frac{a_2z_1 - a_1z_2}{a_2b_1 - a_1b_2} \quad (5.6)$$

In the above discussion, it is assumed that the neutron spectrum remains unaltered with the introduction of pellet having enriched ^6Li but in reality it is changed and it results in the lower tritium production. Therefore it is necessary to correct the

measured tritium production with enriched ^6Li pellets (z_2 values). This effect can be estimated with the help of neutron transport calculations by replacing the pellet with enriched ^6Li with natural isotopic composition pellet in the MCNP model.

Six measurement positions for the TPR measurement in two breeder layers are depicted in *Figure 5.8*. The experimental errors at 1σ level on tritium measurement include uncertainty in HTO standard (2.3%), uncertainty in sample weight (0.18%), uncertainty in quench correction (3%), statistical error of tritium counts during efficiency calibration (0.88%), uncertainty on chemical procedure (5%) and statistical error of the beta counting from individual pellet (1-3% for enriched Li_2CO_3 pellets and 1-7% for natural Li_2CO_3 pellets). To estimate the overall error on measured tritium activity all these errors were added using quadratic sum law. The error on C/E ratios includes tritium measurement error, the statistical error on the calculations (< 1%) and the error on neutron yield measurement (4.73%).

The experimental and calculated tritium specific activities and C/E ratios in the first breeder zone (CB-1) for both types of pellets are shown in *Figure 5.9a*. The average value of C/E for tritium production in enriched pellets is 1.11 and 1.05 in natural pellets showing the tendency of overestimation by calculations in first breeder zone (CB-1). Maximum error on C/E is 8.3% and 11.1% at 1σ level for enriched and natural pellets respectively. *Figure 5.9b* shows the measured and calculated specific tritium activities and C/E ratios in the second breeder zone (CB-2) for both types of pellets. The average value of C/E at 3 positions for enriched pellets is 1.09. The maximum error on C/E at 1 level for enriched pellets is 8.6%. The average value of C/E for tritium production in natural Li_2CO_3 pellets is 0.94 with maximum error (1σ level) on C/E 11.6%.

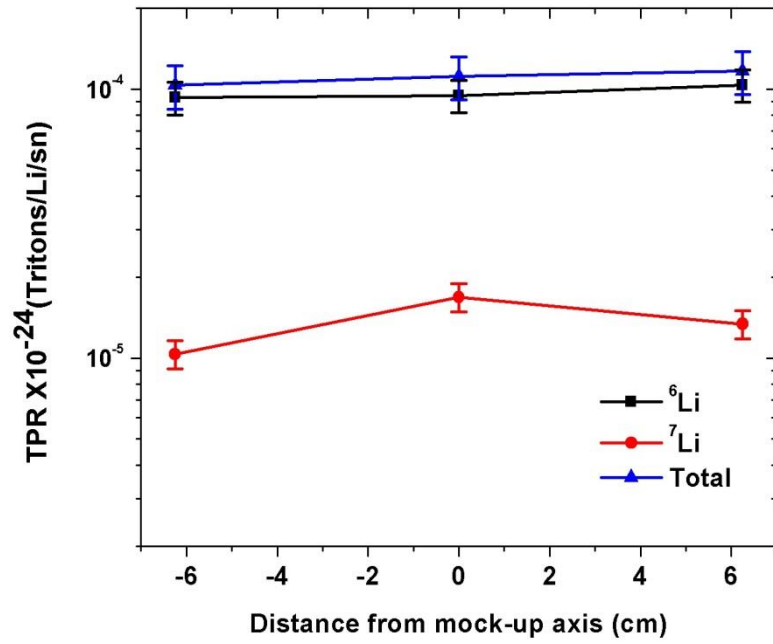


(a) CB-1 (mean distance 14.8 cm from mock-up surface)

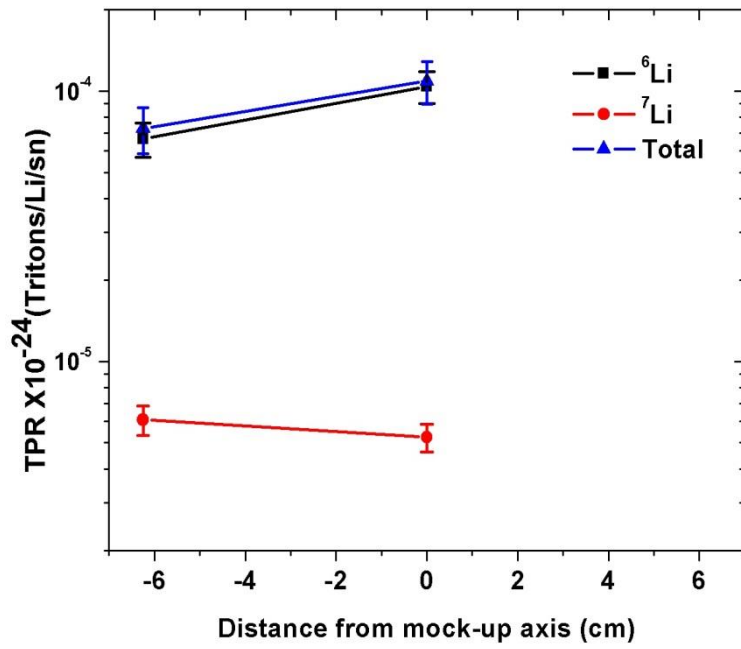
(b) CB-2 (mean distance 23.1 cm)

Figure 5.9: Measured and calculated specific tritium activities and C/E ratios in the natural and enriched Li_2CO_3 pellets in the breeding zones

Using tritium activity results from *Figure 5.9a* and *Figure 5.9b* and the methodology described in the beginning of the section, ^6Li , ^7Li and total TPR results in CB-1 and CB-2 are shown in the *Figure 5.10a* and *Figure 5.10b* respectively. The results show that 90% of tritium is produced from ^6Li at off-axial positions (point 7 and 9) and 85% at axial position (point 8) in breeding zone CB-1. The TPR shows the flat profile along the length (perpendicular to the central axis) of breeding zone. ^6Li contribution increases to 95% in total TPR in second breeder zone CB-2.



(a) CB-1 (mean distance 14.8 cm from mock-up surface)



(b) CB-2 (mean distance 23.1 cm from mock-up surface)

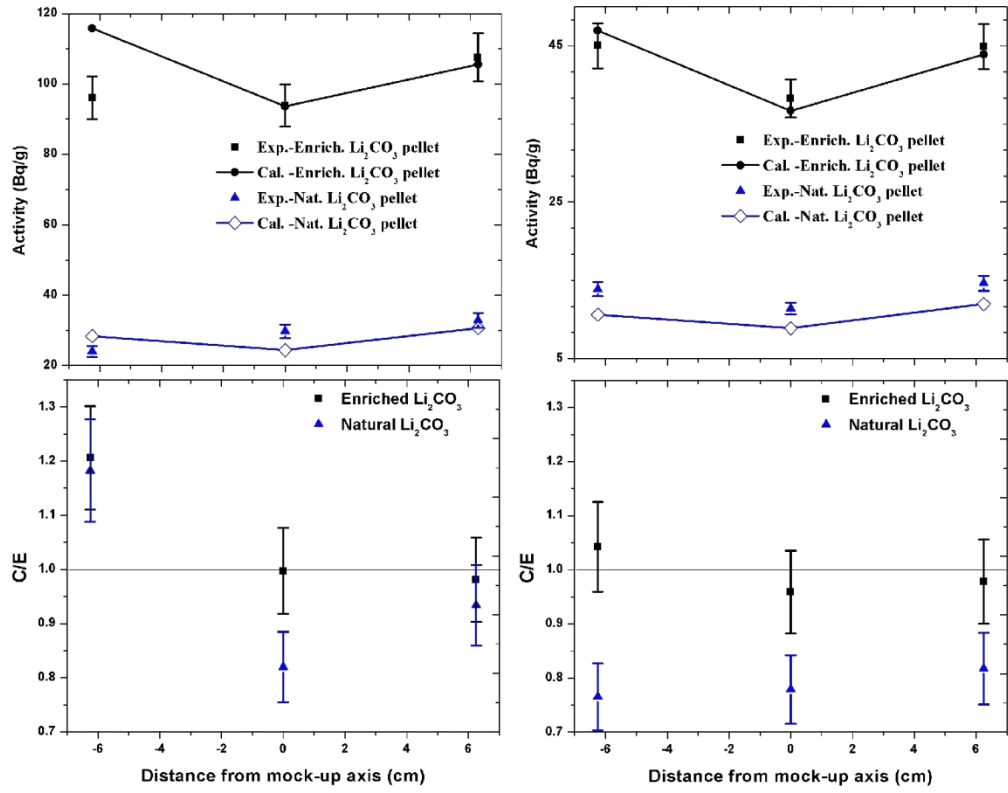
Figure 5.10: Measured ${}^6\text{Li}$, ${}^7\text{Li}$ and total TPR in first and second breeding layers

5.5.2 Tritium measurement in multiplier zones

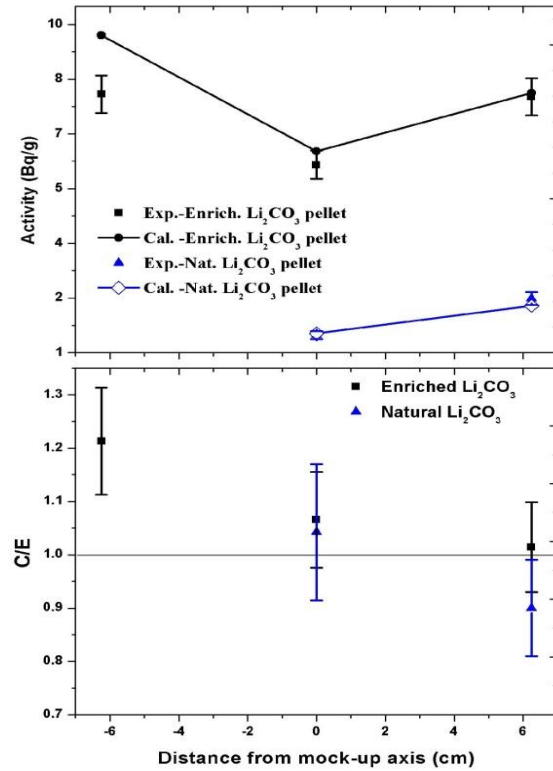
Lead-lithium eutectic is proposed as breeder, multiplier and coolant in LLCB TBM [17]. In the present experiment it was replaced by Lead only which provides the function of neutron multiplication. In order to check the neutron multiplication and moderation prediction properties of the Lead by transport tools, the tritium production in the multiplier zones (Pb-1, Pb-2 and Pb-3) was also measured with the help of two types of Li_2CO_3 pellets described earlier. There were three measurement points in each zone (one at mock-up axis and two at 6.5 cm in both sides of axis). There were two diagnostic pellets at each measurement point, one with ^6Li enriched Li_2CO_3 and another with natural Li composition in Li_2CO_3 .

The measured and calculated tritium activities and their ratios (C/E) in both types of pellets for first multiplier zone (Pb-1) are shown in *Figure 5.11a*. The average value of C/E for enriched pellets (enriched with ^6Li) is 1.06 and for natural lithium pellets 0.98. The measured and calculated tritium activities and C/E ratios in both types of pellets for second multiplier zone (Pb-2) are shown in *Figure 5.11b*. The average value of C/E for tritium production in enriched pellets (enriched with ^6Li) is 0.99 and 0.79 for natural lithium pellets.

The measured and calculated tritium activities and C/E ratios in both types of pellets for third multiplier zone (Pb-3) are shown in *Figure 5.11c*. The average value of C/E for enriched pellets (enriched with ^6Li) is 1.10 and for natural lithium pellets 0.97.



(a) Pb-1 (5 cm from mock-up surface) (b) Pb-2 (10.5 cm from mock-up surface)



(c) Pb-3
(18.95 cm from mock-up surface)

Figure 5.11: Experimental & calculated tritium activity and C/E ratios for two types of diagnostic pellets in multiplier zones

Central pellets are most representative of the nuclear responses in LLCB TBM as they are least affected by the reflections from the HDPE through diagnostic channels. It is clear from *Figure 5.11a* and *Figure 5.11b* that the TPR at the central measurement points are underestimated by calculations (C/E less than unity beyond estimated error bar). The underestimation value is higher in zone-2 than zone-1 due to larger thickness seen by source neutrons i.e. neutron multiplication effect of source neutrons is more dominant in zone-2 than zone-1. Zone-3 is too thin to see any effect of neutron multiplication.

5.5.3 TPR ${}^6\text{Li}$ experimental results with SBD detector

The TPR from ${}^6\text{Li}$ isotope was measured in the second breeding layer CB-2 with the help of SBD detector with ${}^6\text{Li}$ to triton converter. The depth of this measurement point from the mock-up surface is 25 cm. The pulse height spectra (PHS) measured with SBD detector and kept in the second breeder zone of the mock-up is shown in *Figure 5.12*.

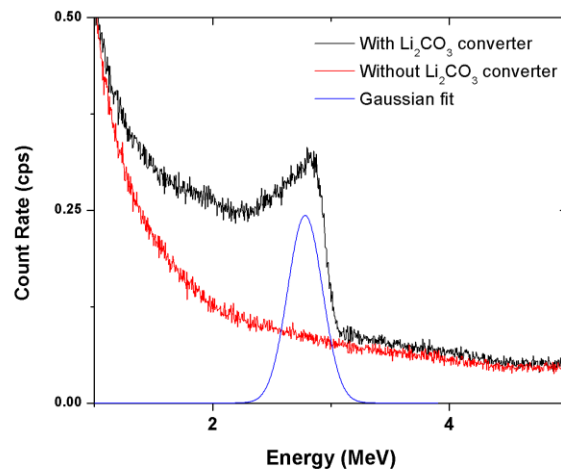


Figure 5.12: Pulse height spectra with and without converter foil measured in breeding layer 2 (CB-2) and the gaussian fit for the triton peak

The PHS shown in *Figure 5.12* is for two cases with and without ^6Li converter foil on the SBD detector and taken in the experimental assembly for 1 hour neutron irradiation at the neutron emission of 7.23×10^9 n/s ($\pm 4.73\%$). The 2.73 MeV triton peak is clearly visible in the spectra with converter foil. PHS without foil was considered to measure the background from the charged particles in the vicinity of the detector and elastic scattering of neutron within detector in the peak region. The gaussian fitting was done to get the net counts in the triton peak.

The calculated and measured TPR results with on-line tritium detector are listed in *Table 5.3*. The calculated TPR agrees with the measured TPR with on-line tritium detector within the error bar on C/E.

Table 5.3: Experimental and calculated TPR- ^6Li in the second breeder zone (CB-2) with on-line tritium diagnostics

Experiment (E)			Calculation (C)	C/E
Parameter	Value	Error (%)	TPR (T/Li-6/s.n.)	
Triton count rate (cps)	20.25	0.37	8.54×10^{-27} ($\pm 0.46\%$)	0.96 ($\pm 6.33\%$)
Neutron yield (n/s)	7.23×10^9	4.73		
^6Li atoms in converter	6.30×10^{17}	4.17		
Solid angle factor	0.5	-		
TPR(T/nuclei/sn)	8.91×10^{-27}	6.32		

5.5.4 Spectral distribution of tritium production

In order to understand the observed differences between measured and calculated tritium production, tritium production profile as a function of neutron energy gives important information. Tritium production in enriched lithium carbonate pellets from both lithium isotopes (^6Li , and ^7Li) were calculated as a function of neutron energy for the mid-points in each zone (Points 2, 5, 8, 11, 14 in *Figure 5.8*). Then the tritium

production from each lithium nuclide was normalized with their atom fractions in the enriched lithium to get the tritium production per lithium atom. Tritium production was calculated in five energy bins **E1**: 1E-11-1E-6 MeV, **E2**: 1 eV-100 keV, **E3**: 100 keV-8 MeV, **E4**: 8-12 MeV, and **E5**: > 12 MeV. The spectral distribution of tritium production in enriched lithium carbonate pellets irradiated at the mid of each zone is shown in *Figure 5.13*.

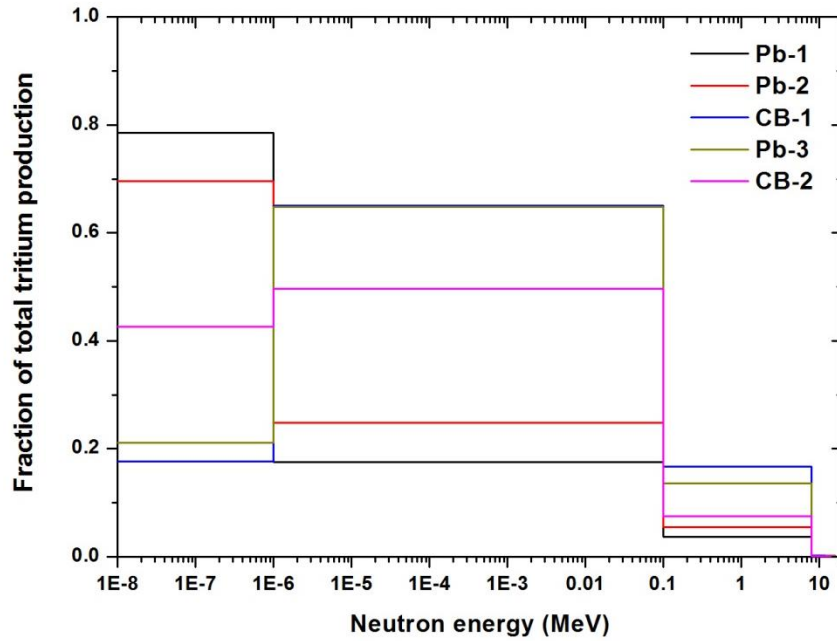


Figure 5.13: Tritium production as a function of neutron energy in the enriched lithium carbonate pellets in the mid of each assembly zone

It is clear from *Figure 5.13* that the tritium production in the first two lead zones (Pb-1 and Pb-2) is dominated by low energy neutrons below 1 eV. The tritium production in the first breeder zone (CB-1) and third multiplier zone (Pb-3) is dominated by neutrons in the energy range 1 eV-100 keV. The tritium production in the second breeder zone (CB-2) is rather flat in the energy range 1E-11 to 0.1 MeV.

Ratios of calculated to experimental tritium production (C/Es) at the mid-point of Pb-1, Pb-2, CB-1, Pb-3 and CB-2 zones are 1.0, 0.96, 1.10, 1.07 and 1.21 respectively. As

shown in section 5.5.5, the evaluated Pb(n, 2n) cross-section is lower in the FENDL-2.1 library than the experimental Lead multiplication. This results into the lower calculated Lead multiplication and higher un-collided neutrons in the lead regions. Lower calculated Lead multiplication will result into the lower calculated tritium production than the measured which is observed in zone Pb-2. The higher number of un-collided neutrons will further slowed down in the first breeder zone and will result into the higher calculated tritium production than the measured. This phenomenon is observed in CB-1. The thickness of the Pb-3 is not such that it can change the multiplier neutrons drastically. Therefore the tendency of overestimation by calculations is observed in all assembly zones after CB-1. In summary it can be said that the LLCB TBM will see the overestimated tritium production in the breeder zones and underestimation in the multiplier zones with FENDL-2.1 library.

5.5.5 Activation foil results

Five indium foils one in each mock-up zone was irradiated to verify the neutron spectra above the threshold of the $^{115}\text{In}(n, n')^{115\text{m}}\text{In}$ reaction. The positions of these foils were at the middle of each zone along the mock-up axis (point 2, 5, 8, 11, and 14 of *Figure 5.8*). The neutron induced reaction investigated was $^{115}\text{In}(n, n')^{115\text{m}}\text{In}$ which has threshold at 0.35 MeV and its response is maximum in the range 0.35-2.5 MeV. Therefore it can give the information of neutron spectra in this energy range which will be mostly dominated by (n, 2n) and (n, n') reaction in Lead isotopes. The irradiation was done for one hour with total neutron emission of 3.03×10^{13} source neutrons with uncertainty 4.73%. The results of measured and calculated reaction rates and C/E ratios in all five zones are shown in *Figure 5.14*.

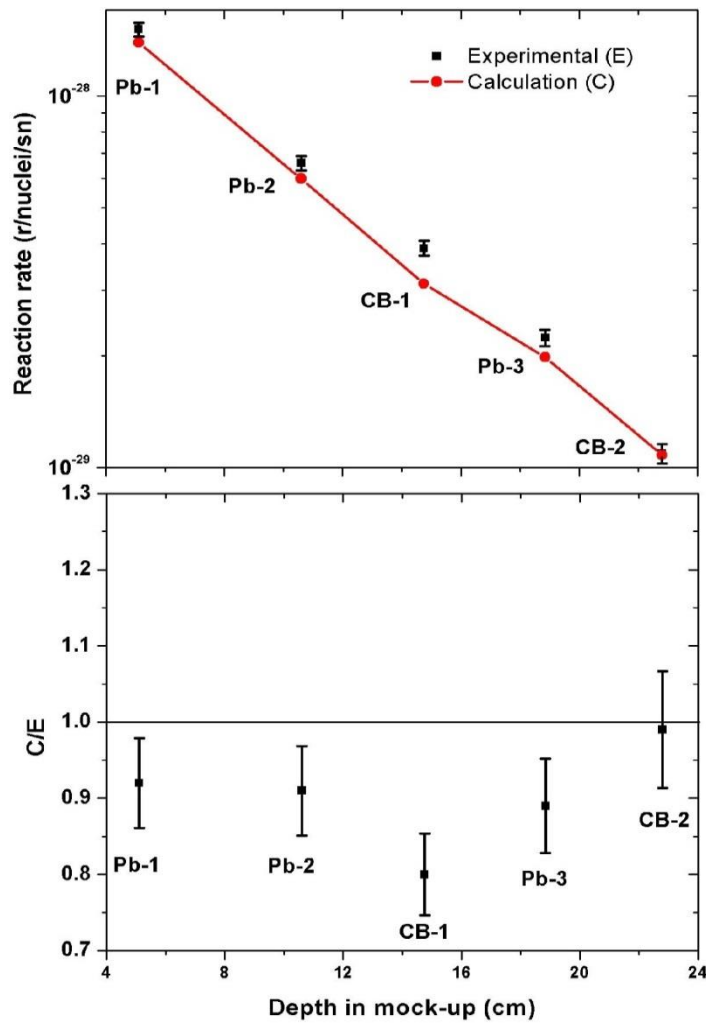


Figure 5.14: $^{115}\text{In}(n, n')^{115m}\text{In}$ reaction rate profile and C/E ratios in the mock-up assembly

The calculated $^{115}\text{In}(n, n')^{115m}\text{In}$ reaction rate using FENDL-2.1 transport library for mock-up materials and IRDF-02 dosimetry file underestimates the measured reaction rates in first four zones. It implies that the neutron spectra in the response range of $^{115}\text{In}(n, n')^{115m}\text{In}$ reaction is underestimated by the calculations. The major reactions responsible for the neutron spectra in this range are (n, 2n) and (n, n') reactions of Lead isotopes.

5.6 Conclusions

The first of the four mock-up experiments to investigate the neutronics performance of the materials used in the LLCB TBM was performed. The tritium production rates in the mock-up zones were measured with Li_2CO_3 pellets and on-line tritium detector. The TPR from both lithium isotopes ^6Li and ^7Li were estimated with the help of Li_2CO_3 pellets having two different compositions of Li isotopes. The activation foil measurement was employed to validate the neutron spectra above $^{115}\text{In}(n, n')^{115\text{m}}\text{In}$ reaction threshold in the mock-zones. The average value of C/E of tritium production in enriched Li_2CO_3 pellet for three positions is 1.11 for CB-1 (first breeder zone) and 1.09 for CB-2 (second breeder zone). The average value of C/E of tritium production in natural Li_2CO_3 pellet is 1.05 for CB-1 and 0.94 for CB-2. The TPR in breeding zones is mostly contributed by tritium production from ^6Li isotope in the breeder material (> 90%). C/E ratio for TPR- ^6Li with on-line tritium detector is close to unity (0.96). The $^{115}\text{In}(n, n')^{115\text{m}}\text{In}$ reaction rate measurement shows the tendency of underestimation by calculations at most of the measurement positions. Sensitivity/uncertainty analyses should be carried out as future work along with the total uncertainty on the C/E ratio.

Chapter 6

Neutron flux spectra investigations in breeding blanket assembly containing lithium titanate and Lead

6.1 Introduction

Neutron flux spectrum is a fundamental quantity which is used to calculate the nuclear responses in the breeding blankets of a D-T fusion reactor. The main nuclear responses of interest are tritium production, gas production (helium and hydrogen), nuclear heating, radiation damage, and activation. In the breeding blanket design, the neutron flux spectrum is calculated with the help of 3D radiation transport codes and nuclear data libraries such as FENDL-2.1 and FENDL-3.0. The uncertainties of design parameters are determined by uncertainties of both cross-section data and calculated neutron flux spectrum obtained with transport codes and cross-section libraries [8]. FISPACT-2007 inventory code with EAF-2007 library is widely used for the radioactive inventory calculations in the fusion reactor environment for rad-waste and occupational exposure calculations [74]. Therefore validation of radiation transport tools and data is an important task for the materials proposed for the breeding blankets.

Lithium titanate (Li_2TiO_3) is chosen as the material for tritium breeding and Lead in eutectic form as neutron multiplier in the breeding blankets of future Indian DEMO reactor [16]. An experimental mock-up assembly was designed using Li_2TiO_3 powder as the tritium breeder, pure Lead as the neutron multiplier, Mild Steel (MS) as the structural material and High Density Polyethylene (HDPE) as neutron reflector and shield. Li_2TiO_3 powder used in the study was synthesized by Solid State Reaction Process (SSRP) developed by Mandal et al. [72-73]. X-Ray Diffraction (XRD) analysis confirmed the single phase formation of the synthesized Li_2TiO_3 powder. MS used in the experiment was of grade 55 as per ASTM (American Society for Testing and Materials) A516 standard. Lead used in the experiment was of purity with 99.525%.

The neutron spectra in assembly zones were obtained from thermal to 14 MeV covering the energy range for tritium production by ^6Li and ^7Li isotopes and neutron multiplication range in the Lead isotopes. Measured saturation activities in irradiated foils along-with the guess spectrum was used as input to unfold the neutron flux spectrum using the code SAND-II-SNL (Spectrum Analysis by Neutron Detectors-II-Sandia National Laboratories) with SNLRML (Sandia National Laboratories Radiation Metrology Library) cross-section library [75]. SAND-II-SNL code uses an iterative perturbation method to obtain a "best-fit" neutron flux spectrum for a given input set of infinitely dilute foil activities.

The experimental results were analyzed with radiation transport code MCNP and transport libraries FENDL-2.1 and FENDL-3.0 [3, 4]. IRDFF-1.05 (International Reactor Dosimetry and Fusion File) activation cross-section library was used for the calculation of neutron induced reaction rates in foils [76]. Measured reaction rates

were also compared with calculated values obtained with European Activation System (EASY-2007) which consists of inventory code FISPACT-2007 and cross-section library EAF-2007 (European Activation File). The present experimental results are also compared with the previous experiment performed with pure Lead at TUD, Dresden, Germany.

6.2 Experimental details

6.2.1 Geometry and irradiation parameters

Experimental assembly described in section 5.3.1 was also used in the current experiment except physical form of Li_2TiO_3 . The physical form of the Li_2TiO_3 in this experiment was powder instead of pebbles in previous experiment. Multiplier and breeding layers in the experimental assembly are separated by 5 mm thick MS plates. The outer walls of the experimental assembly are also made of MS plates and having thicknesses as: 12 mm for first wall, 5 mm for wall opposite to first wall, and 2 mm for the rest four sides of experimental assembly. Thicknesses of the breeding layers, multiplier layers, separation walls and first wall replicate the radial build-up of Lead-Lithium Ceramic Breeder (LLCB) Test Blanket Module (TBM) in ITER. The overall external dimension of the experimental assembly is $25\text{cm} \times 25\text{cm} \times 26\text{cm}$. The experimental assembly is provided with five cylindrical penetrations at 5.1, 10.6, 14.7, 18.8 and 22.8 cm from the front surface to facilitate insertion of the activation foils in each breeding and multiplier layer. The experimental assembly is surrounded by HDPE to simulate the reflected neutrons from ITER machine structure and to shield the room reflected neutrons into assembly. The whole assembly is surrounded by 1

mm thick cadmium sheets to reduce the room reflected low energy neutrons into experimental assembly through tiny gaps between HDPE sheets. This arrangement almost isolates the measurements inside assembly from the room reflected neutrons. *Figure 6.1* shows the horizontal cross-section through the mid plane of the experimental assembly showing the dimensions of the multiplier and breeding zones, and dimensions of the HDPE etc.

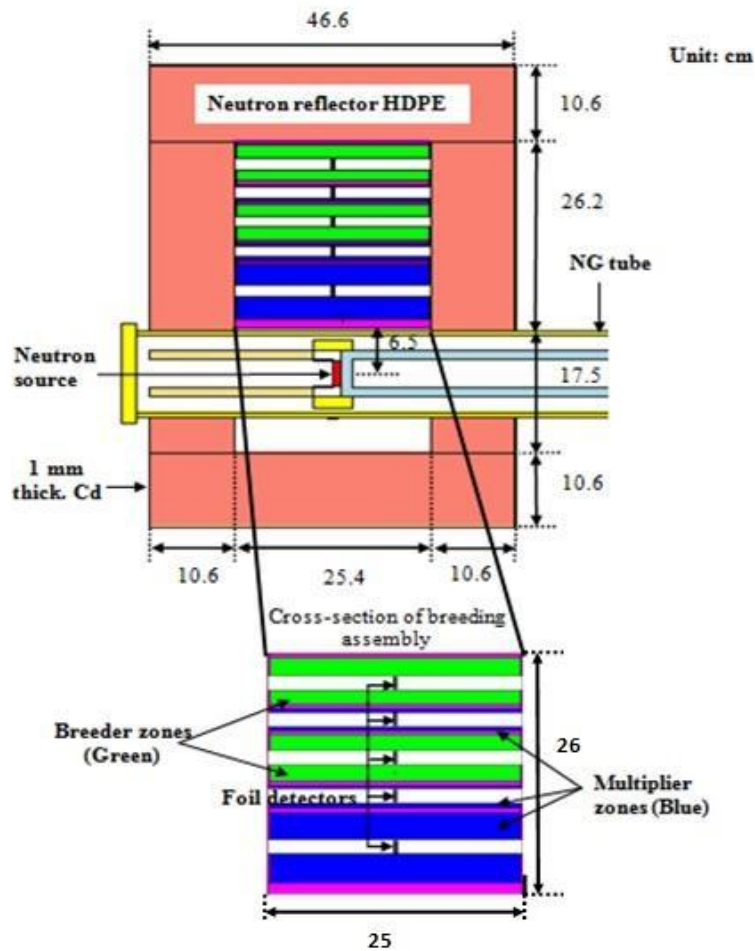


Figure 6.1: Cross-section of the experimental assembly used for measurement of neutron flux spectra

Figure 6.2 shows the vertical cross-section through the assembly showing the distances of the activation foils sets from the source and penetration depth of foil measurement in the assembly.

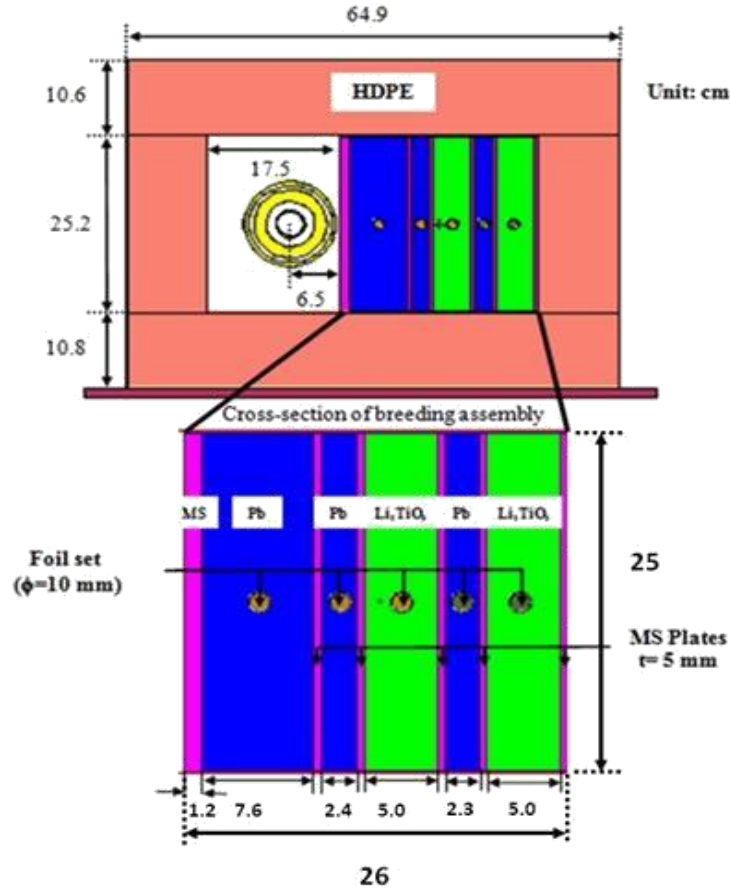


Figure 6.2: Cross-sectional view of the MCNP model of breeding assembly showing dimensions and materials

The experimental assembly was irradiated with neutrons from a sealed neutron generator tube manufactured by M/s Sodern, France [39]. The experimental assembly was continuously irradiated with D-T neutrons for 3 hours in one shift. The time profile of the source neutron yield was monitored with a ^3He counter covered with neutron moderator HDPE. This monitor was absolutely calibrated against the activation measurement by using $^{27}\text{Al}(n, \alpha)^{24}\text{Na}$ reaction at 90° angle with respect to incident deuteron beam. The measured total source neutron emission during 3 hours of irradiation was 7.14×10^{13} neutrons. The experimental uncertainty in the source neutron emission was estimated considering uncertainty in High Purity Germanium (HPGe) detector calibration (4%), gamma peak counting area uncertainty (2%), cross-

section uncertainty (1.04%), statistical error in measured gamma counts (1.15%) and foil mass (0.12%). All these errors being independent to each other were summed by quadratic law to obtain the uncertainty in the neutron yield at 1σ . The uncertainty in the neutron yield measurement was estimated to be 4.73% at 1σ . The uncertainty on the $^{27}\text{Al}(n, \alpha)^{24}\text{Na}$ cross-section is taken at 12.5 MeV neutron energy from reference [57] because the reported uncertainty in the source neutron energy range is maximum at this energy. Time profile of the source neutron emission during the 3 hour irradiation is shown in *Figure 6.3*. The measured time profile of neutron emission shows quite a good stability within 5%.

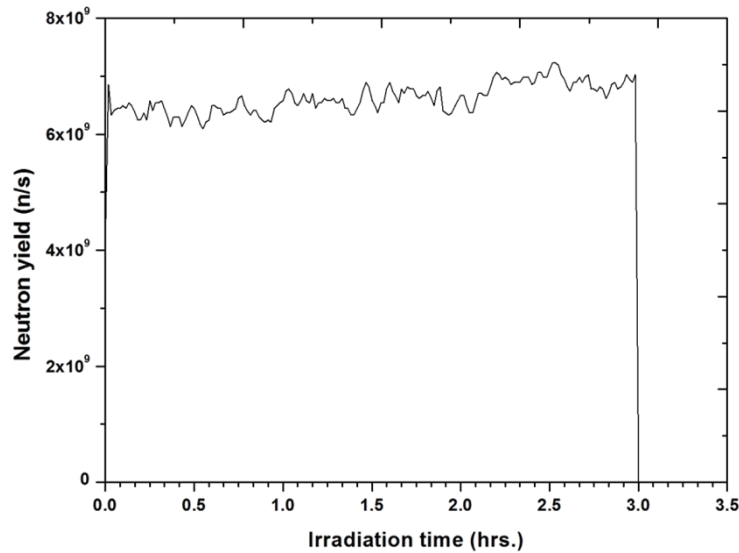


Figure 6.3: Measured time profile of source neutron yield from generator tube during irradiation experiment with ^3He counter

6.2.2 Elemental composition of materials with impurities

The impurities in the materials, namely Li_2TiO_3 , Lead and MS, were determined by inductively coupled plasma optical emission spectroscopy (ICP-OES). The weight percentage of impurities and constituent elements in the materials used in the experiment are listed in *Table 6.1*.

Table 6.1: Elemental composition of materials with impurities used in the experiment

Li₂TiO₃		Lead		MS	
Element	Wt%	Element	Wt%	Element	Wt%
Na	0.005	Bi	0.014	Co	0.002
K	0.180	Fe	0.436	Mn	1.370
Ca	0.017	Sb	0.025	Cr	0.640
Mg	0.004	Pb	99.525	Ni	0.270
Al	0.019			Cu	0.007
Co	0.035			B	0.039
Fe	0.011			Fe	97.711
Li	12.615				
Ti	43.498				
O	43.617				

The composition shown in *Table 6.1* was used as such for modelling in MCNP. All the impurities having high neutron cross-sections were investigated in the materials.

Lead in the experimental assembly zones was filled from an external tank having molten Lead. Lead was allowed to enter in the assembly zones in molten state and finally it got solidified by natural cooling. After filling the Lead, its density in the assembly zones was determined with the help of measured mass and volume of zones. Measured density was found close to the theoretical density (2% less than the theoretical density). The small difference may be ascribed to the inaccuracy in the volume and mass measurement of Lead. For the diagnostic channels in the assembly zones, stainless steel pipes were welded with the outer plates of assembly. This allows separating the diagnostic channels physically from rest of the zone. Lithium titanate powder densities in breeder zones were also determined from the measured mass and volume. The measured densities of Lead and lithium titanate powder were modelled in the calculations instead of the theoretical densities reported in the literature.

6.2.3 Activation foils

Stacked multiple foils were irradiated in all five zones of the mock-up assembly. The stacked foils axis was parallel to the neutron generator tube. The irradiated foils in the assembly were having purity levels up to 99.999%. Purity level is important to avoid the interference in terms of the gamma counts arising from impurity atoms in the foil material. The activation foils in each zone were packed in a very thin polyethylene cover to avoid any contamination from the surrounding materials and to minimize the neutron field perturbation due to cover material. The neutron source was kept at 6.5 cm away from the surface of the experimental assembly. The foils were selected based on their availability and neutron cross-section characteristics in the energy range of interest. For neutron spectrum unfolding, it is important that a variety of different neutron induced reactions are used such that they span a variety of energy ranges to provide adequate details for unfolding. Different thresholds allow the deduction of spectrum information in a broad range of energies. Threshold-less reactions, like radiative capture, are used for slowed (scattered) neutron measurements. Details of the neutron induced reactions and the physical properties of the foils used in the assembly zones are given in *Table 6.2*. The thickness of the foils is typically 250 μm i.e. the perturbation of the neutron field by foil materials is minimal for high energy neutrons and moderate for low energy neutrons. The thickness of the foil is also important for the self-support. Decay data of the neutron induced reactions are based on Nudat 2.6 database [77].

Table 6.2: List of foils irradiated in the breeding assembly zones and neutron induced reactions used in the study for neutron spectra measurement

Reaction	Half-life	Threshold (MeV)	E γ (keV)	Thickness (μm)	Assembly zone
$^{27}\text{Al}(n, \alpha)^{24}\text{Na}$	14.95 h	3.2	1368.6	250	1-5
$^{27}\text{Al}(n, p)^{27}\text{Mg}$	9.46 m	1.9	843.8	250	1
$^{63}\text{Cu}(n, 2n)^{62}\text{Cu}$	9.75 m	11.0	511.0	250	1-2
$^{65}\text{Cu}(n, 2n)^{64}\text{Cu}$	12.7 h	10.1	511.0	250	1-5
$^{63}\text{Cu}(n, \gamma)^{64}\text{Cu}$	12.7 h	-	511.0	250	1-5
$^{115}\text{In}(n, n')^{115\text{m}}\text{In}$	4.49 h	0.5	336.2	250	1-5
$^{19}\text{F}(n, 2n)^{18}\text{F}$	1.83 h	11.0	511.0	1000	1-5
$^{64}\text{Zn}(n, p)^{64}\text{Cu}$	12.7 h	0.6	511.0	250	1-4
$^{58}\text{Ni}(n, 2n)^{57}\text{Ni}$	35.6 h	12.4	1377.6	250	1,3
$^{58}\text{Ni}(n, p)^{58}\text{Co}$	70.86 d	1.6	810.8	250	1-5
$^{90}\text{Zr}(n, 2n)^{89}\text{Zr}$	3.27 d	12.1	909.2	250	1-5
$^{93}\text{Nb}(n, 2n)^{92\text{m}}\text{Nb}$	10.15 d	8.9	934.4	250	1-5
$^{59}\text{Co}(n, 2n)^{58}\text{Co}$	70.86 d	10.6	810.8	250	1-3
$^{59}\text{Co}(n, \gamma)^{60}\text{Co}$	5.27 y	-	1333.0	250	1

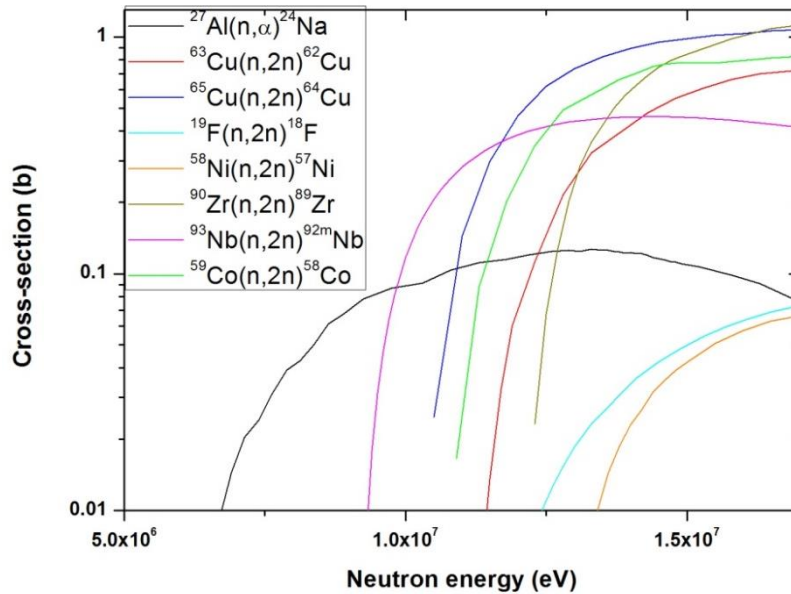


Figure 6.4: Excitation functions of high threshold reactions irradiated in the assembly for unfolding of neutron flux spectra [59].

In order to present the extent of the neutron energy coverage by studied reactions, excitation functions of the neutron induced reactions are given in the *Figure 6.4* and *Figure 6.5*. The excitation functions are taken from dosimetry file IRDF-2002 [59]. It can be seen from the excitation functions that the selected reactions span the whole range from thermal to D-T source neutron energy. The thresholds of the selected reactions for neutron spectra unfolding are also evenly distributed in the fast neutron energy range.

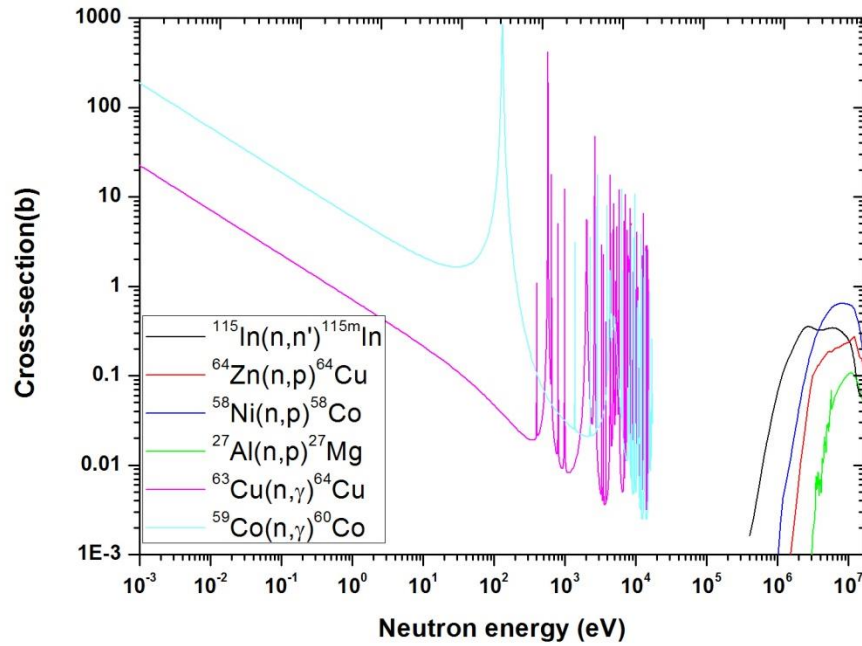


Figure 6.5: Excitation functions of low threshold and radiative capture reactions irradiated in the assembly for unfolding of neutron flux spectra [59]

Experimental reaction rate results for three reactions in copper foil namely $^{65}\text{Cu}(n, 2n)^{64}\text{Cu}$, $^{63}\text{Cu}(n, 2n)^{62}\text{Cu}$, and $^{63}\text{Cu}(n, \gamma)^{64}\text{Cu}$ are reported with measurement of 511 keV peak energy. In order to obtain the experimental reaction rates of three reactions in copper, MCNP calculated reaction rates of these three reactions were converted into 511 keV gamma counts at the time of measurement considering cooling time, counting time, irradiation time, decay properties etc. From these calculated gamma counts, fraction of each reaction in total gamma counts at the time of measurement was

estimated. The measured total gamma counts were distributed in proportion to their fractional contribution calculated from MCNP reaction rates.

Gamma rays in the irradiated foils were measured by absolutely calibrated HPGe detector using 16k multi-channel analyzer and GENIE-2000 acquisition software [78]. Saturation activities of the various nuclear reactions as input to SAND-II unfolding code were derived from measured photo-peak counts by applying corrections due to counting, cooling, and irradiation times, detector absolute efficiency, branching ratio, neutron yield, foil mass etc.

6.3 Computational model

Geometry and support structure of the experimental assembly, activation foils, neutron generator tube and experimental hall were accurately described in the calculation model. Source neutrons are affected by the neutron generator geometry and its materials therefore the details of the neutron generator components such as copper backed Ti-T target, cooling-circuit, high-voltage insulation, and structural materials were included in the calculation model. The dimensions and materials of these internal components were provided by manufacturer. All the activation foils were explicitly modelled to consider the self-shielding effect and scattering by nearby foils for reaction rate calculations. Two views of the calculation model are shown in *Figure 6.1* and *Figure 6.2*. Radiation transport code MCNP with FENDL-2.1 cross-section library was employed to calculate the neutron spectra in the assembly zones and neutron induced reaction rates. For spectra calculation in zones, cross-section data for ^{13}C , ^{204}Pb , $^{\text{nat}}\text{Zn}$, $^{\text{nat}}\text{Ar}$, $^{\text{nat}}\text{Sb}$ and $^{\text{nat}}\text{Sn}$ isotopes were taken from FENDL-3.0 library. Reaction rates in the assembly zones were calculated with two libraries FENDL-2.1

and FENDL-3.0. IRDFF-1.05 reactor dosimetry and fusion file was used to calculate the reaction rates using tally multiplier cards in MCNP. $S(\alpha, \beta)$ thermal neutron tables from the ENDF-VI.5 (poly.60t) library was used to calculate the thermal neutron population precisely. The neutron spectra were calculated in 640 energy groups for SAND-II unfolding and in 175 energy groups (VITAMIN-J) for FISPACT-2007 reaction rate calculation.

The energy-angle distributions of the source neutrons were determined using the target model, deuteron beam loss in Ti-T target and relativistic reaction kinematics. Deuteron beam loss and straggling in the target was calculated by SRIM-2008 Monte Carlo code. The calculated neutron spectra were modelled in calculation model with angular resolution of 1° . The source neutron spectra modelled in MCNP were validated with measurement of reaction rates in various high threshold reactions irradiated on the neutron generator surface (90° location).

6.4 Results and discussions

6.4.1 Reaction rates

The neutron spectral indices in the experimental assembly zones were studied by measuring different neutron induced reactions which cover the energy range from thermal to D-T source neutron energy. The experimental errors in reaction rate measurements include statistics of the photo-peak counts, error in photo-peak area determination, error in the calibration of HPGe detector (mainly due to uncertainty of calibration source), error in neutron yield measurement, error in foil mass measurements, error in the reaction products half-lives, errors in counting, and cooling

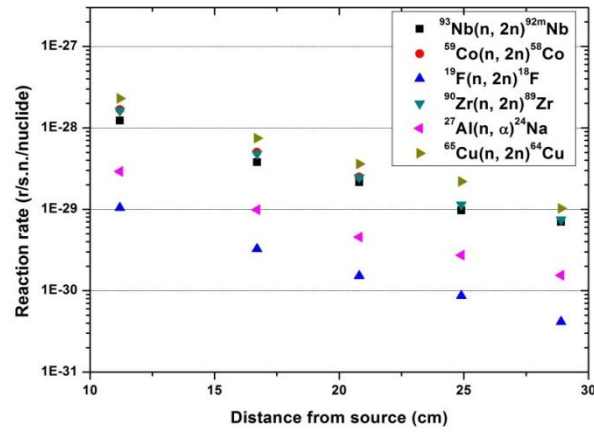
times measurement. Typical ranges of these experimental uncertainties are given in *Table 6.3*.

Table 6.3: Uncertainties on measured neutron induced reaction rates in foils

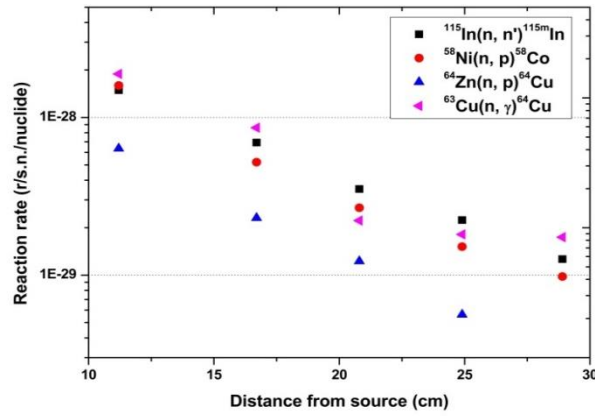
Type of uncertainty	Relative error range (%)
Statistics on photo-peak counts	0.70-8.98
Photo-peak area determination	2.00
Efficiency of HPGe detector	4.00
Neutron yield	4.73
Foil mass	0.5-1.2
Half-life of reaction products	0.02-0.84
Counting time	0.01-0.25
Cooling time	0.01-0.14
Total uncertainty at 1σ	6.6-12.09

The experimental uncertainty on each measured reaction rate at 1σ was determined with quadratic sum of the above mentioned errors. The uncertainty in the ratio of calculation to experimental reaction rates (C/E) were determined by combining uncertainty on experiment and statistical error on calculation.

The reaction rate results presented hereafter are divided into two groups for the sake of clarity in the interpretation of results: high threshold reactions ($E_n > 1$ MeV) and low threshold plus radiative capture reactions. The absolute experimental reaction rates for high threshold reactions in all five assembly zones are shown in *Figure 6.6a*. The absolute experimental reaction rates for low threshold and radiative capture reactions are shown in *Figure 6.6b*. Five assembly zones in *Figure 6.6a* and *Figure 6.6b* are represented in terms of the mean distance between foils and source location. Reaction rate is represented as the number of reactions per target nuclei and per source neutron (reaction/nuclide/source neutron).



(a) High threshold reactions



(b) Low threshold and radiative capture reactions

Figure 6.6: Experimental reaction rate results in assembly zones

The neutron induced reaction rates were also calculated to compare them with the measurements shown in *Figure 6.6a* and *Figure 6.6b*. Calculation details are described in section 6.3. Measured (E) and calculated (C) reactions rates and C/E ratios in five experimental assembly zones are given in Tables 6.4-6.8 respectively. C/E ratios are given for two cross-section libraries, dosimetry cross-section file IRDFF-1.05 and European Activation File (EAF-2007). IRDFF-1.05 was used with Monte Carlo Code MCNP and EAF-2007 was used with code FISPACT-2007. The neutron spectra required for FISPACT-2007 were also obtained with MCNP. Experimental and calculated reaction rate results are given zone wise.

Table 6.4: Measured (E) and calculated (C) reaction rates and C/E ratios in zone-1

Reaction	Reaction rate (r/nuclide/s.n./)			C/E	
	Experiment (E)	IRDFF-1.05 (C)	EAF-2007 (C)	IRDFF-1.05	EAF-2007
$^{93}\text{Nb}(n, 2n)^{92\text{m}}\text{Nb}$	1.23E-28	1.36E-28	1.35E-28	1.11	1.10
$^{59}\text{Co}(n, 2n)^{58}\text{Co}$	1.68E-28	1.97E-28	1.81E-28	1.17	1.08
$^{19}\text{F}(n, 2n)^{18}\text{F}$	1.04E-29	1.02E-29	1.09E-29	0.98	1.04
$^{90}\text{Zr}(n, 2n)^{89}\text{Zr}$	1.62E-28	1.73E-28	1.51E-28	1.07	0.93
$^{27}\text{Al}(n, \alpha)^{24}\text{Na}$	2.91E-29	3.39E-29	3.67E-29	1.16	1.26
$^{65}\text{Cu}(n, 2n)^{64}\text{Cu}$	2.30E-28	2.27E-28	2.41E-28	0.99	1.05
$^{63}\text{Cu}(n, 2n)^{62}\text{Cu}$	1.15E-28	1.13E-28	1.27E-28	0.99	1.11
$^{58}\text{Ni}(n, 2n)^{57}\text{Ni}$	5.39E-30	6.30E-30	6.29E-30	1.17	1.17
$^{27}\text{Al}(n, p)^{27}\text{Mg}$	2.01E-29	2.38E-29	2.54E-29	1.18	1.26
$^{115}\text{In}(n, n')^{115\text{m}}\text{In}$	1.49E-28	1.43E-28	1.43E-28	0.96	0.96
$^{58}\text{Ni}(n, p)^{58}\text{Co}$	1.60E-28	1.71E-28	1.78E-28	1.07	1.12
$^{64}\text{Zn}(n, p)^{64}\text{Cu}$	6.36E-29	7.06E-29	7.07E-29	1.11	1.11
$^{63}\text{Cu}(n, \gamma)^{64}\text{Cu}$	1.89E-28	2.11E-28	-	1.12	-
$^{59}\text{Co}(n, \gamma)^{60}\text{Co}$	1.52E-27	1.50E-27	1.80E-27	0.99	1.19

Table 6.5: Measured (E) and calculated (C) reaction rates and C/E ratios in zone-2

Reaction	Reaction rate (r/nuclide/s.n./)			C/E	
	Experiment (E)	IRDFF-1.05 (C)	EAF-2007 (C)	IRDFF-1.05	EAF-2007
$^{93}\text{Nb}(n, 2n)^{92\text{m}}\text{Nb}$	3.80E-29	3.91E-29	3.84E-29	1.03	1.01
$^{59}\text{Co}(n, 2n)^{58}\text{Co}$	5.02E-29	5.30E-29	5.05E-29	1.06	1.01
$^{19}\text{F}(n, 2n)^{18}\text{F}$	3.26E-30	2.85E-30	3.01E-30	0.87	0.92
$^{90}\text{Zr}(n, 2n)^{89}\text{Zr}$	4.83E-29	4.75E-29	4.21E-29	0.98	0.87
$^{27}\text{Al}(n, \alpha)^{24}\text{Na}$	9.88E-30	1.02E-29	1.05E-29	1.03	1.07
$^{65}\text{Cu}(n, 2n)^{64}\text{Cu}$	7.46E-29	6.66E-29	-	0.89	-
$^{63}\text{Cu}(n, 2n)^{62}\text{Cu}$	3.69E-29	3.30E-29	3.53E-29	0.89	0.96
$^{115}\text{In}(n, n')^{115\text{m}}\text{In}$	6.93E-29	6.07E-29	6.05E-29	0.88	0.87
$^{58}\text{Ni}(n, p)^{58}\text{Co}$	5.21E-29	5.50E-29	5.88E-29	1.06	1.13
$^{64}\text{Zn}(n, p)^{64}\text{Cu}$	2.31E-29	2.33E-29	2.25E-29	1.01	0.97
$^{63}\text{Cu}(n, \gamma)^{64}\text{Cu}$	8.60E-29	8.64E-29	-	1.00	-

Table 6.6: Measured (E) and calculated (C) reaction rates and C/E ratios in zone-3

Reaction	Reaction rate (r/nuclide/s.n./)			C/E	
	Experiment (E)	IRDFF-1.05 (C)	EAF-2007 (C)	IRDFF-1.05	EAF-2007
$^{93}\text{Nb}(n, 2n)^{92\text{m}}\text{Nb}$	2.16E-29	1.86E-29	1.89E-29	0.86	0.88
$^{59}\text{Co}(n, 2n)^{58}\text{Co}$	2.50E-29	2.56E-29	2.44E-29	1.02	0.97
$^{19}\text{F}(n, 2n)^{18}\text{F}$	1.52E-30	1.37E-30	1.43E-30	0.90	0.94
$^{90}\text{Zr}(n, 2n)^{89}\text{Zr}$	2.47E-29	2.14E-29	1.98E-29	0.87	0.80
$^{27}\text{Al}(n, \alpha)^{24}\text{Na}$	4.56E-30	5.27E-30	5.29E-30	1.16	1.16
$^{65}\text{Cu}(n, 2n)^{64}\text{Cu}$	3.60E-29	3.34E-29	-	0.93	-
$^{58}\text{Ni}(n, 2n)^{57}\text{Ni}$	7.79E-31	8.17E-31	8.18E-31	1.05	1.05
$^{115}\text{In}(n, n')^{115\text{m}}\text{In}$	3.52E-29	3.16E-29	3.13E-29	0.90	0.89
$^{58}\text{Ni}(n, p)^{58}\text{Co}$	2.67E-29	3.00E-29	3.09E-29	1.12	1.15
$^{64}\text{Zn}(n, p)^{64}\text{Cu}$	1.23E-29	1.25E-29	1.17E-29	1.02	0.96
$^{63}\text{Cu}(n, \gamma)^{64}\text{Cu}$	2.22E-29	2.23E-29	-	1.01	-

Table 6.7: Measured (E) and calculated (C) reaction rates and C/E ratios in zone-4

Reaction	Reaction rate (r/nuclide/s.n./)			C/E	
	Experiment (E)	IRDFF-1.05 (C)	EAF-2007 (C)	IRDFF-1.05	EAF-2007
$^{93}\text{Nb}(n, 2n)^{92\text{m}}\text{Nb}$	9.67E-30	1.03E-29	1.05E-29	1.06	1.08
$^{19}\text{F}(n, 2n)^{18}\text{F}$	8.66E-31	7.38E-31	7.77E-31	0.85	0.90
$^{90}\text{Zr}(n, 2n)^{89}\text{Zr}$	1.14E-29	1.19E-29	1.07E-29	1.05	0.94
$^{27}\text{Al}(n, \alpha)^{24}\text{Na}$	2.73E-30	2.99E-30	2.95E-30	1.09	1.08
$^{65}\text{Cu}(n, 2n)^{64}\text{Cu}$	2.20E-29	1.86E-29	-	0.85	-
$^{115}\text{In}(n, n')^{115\text{m}}\text{In}$	2.23E-29	2.00E-29	2.00E-29	0.90	0.89
$^{58}\text{Ni}(n, p)^{58}\text{Co}$	1.52E-29	1.71E-29	1.82E-29	1.13	1.20
$^{64}\text{Zn}(n, p)^{64}\text{Cu}$	5.62E-30	7.40E-30	6.85E-30	1.32	1.22
$^{63}\text{Cu}(n, \gamma)^{64}\text{Cu}$	1.81E-29	1.71E-29	-	0.94	-

Table 6.8: Measured (E) and calculated (C) reaction rates and C/E ratios in zone-5

Reaction	Reaction rate (r/nuclide/s.n./)			C/E	
	Experiment (E)	IRDFF-1.05 (C)	EAF-2007 (C)	IRDFF-1.05	EAF-2007
$^{93}\text{Nb}(n, 2n)^{92\text{m}}\text{Nb}$	7.00E-30	6.14E-30	6.17E-30	0.88	0.88
$^{19}\text{F}(n, 2n)^{18}\text{F}$	4.17E-31	4.19E-31	4.47E-31	1.00	1.07
$^{90}\text{Zr}(n, 2n)^{89}\text{Zr}$	7.48E-30	6.55E-30	6.15E-30	0.88	0.82
$^{27}\text{Al}(n, \alpha)^{24}\text{Na}$	1.55E-30	1.76E-30	1.75E-30	1.14	1.13
$^{65}\text{Cu}(n, 2n)^{64}\text{Cu}$	1.02E-29	1.06E-29	-	1.04	-
$^{115}\text{In}(n, n')^{115\text{m}}\text{In}$	1.26E-29	1.09E-29	1.08E-29	0.86	0.86
$^{58}\text{Ni}(n, p)^{58}\text{Co}$	9.79E-30	1.02E-29	1.08E-29	1.04	1.10
$^{63}\text{Cu}(n, \gamma)^{64}\text{Cu}$	1.74E-29	1.78E-29	-	1.02	-

C/E ratios of high threshold reactions namely $^{93}\text{Nb}(n, 2n)^{92\text{m}}\text{Nb}$, $^{59}\text{Co}(n, 2n)^{58}\text{Co}$, $^{19}\text{F}(n, 2n)^{18}\text{F}$, $^{90}\text{Zr}(n, 2n)^{89}\text{Zr}$, $^{27}\text{Al}(n, \alpha)^{24}\text{Na}$ and $^{65}\text{Cu}(n, 2n)^{64}\text{Cu}$ are shown in *Figure 6.7a-f* respectively. The error bars on MCNP-IRDFF-1.05 plots shown in *Figure 6.7a-f* include the uncertainties in the reaction rate measurements (*Table 6.3*) and statistical errors in MCNP calculation. The error bars on FISPACT-EAF2007 plots shown in *Figures 6.7a - 6.7f* include the uncertainties in the reaction rate measurements (*Table 6.3*) only. The average C/E values obtained with MCNP-IRDFF-1.05 for high threshold reactions in zones-1, 2, 3, 4 and 5 are 1.09, 0.97, 0.97, 1.00 and 0.98 respectively showing good agreement between experimental and calculated values. In zone-1, four reactions $^{93}\text{Nb}(n, 2n)^{92\text{m}}\text{Nb}$, $^{59}\text{Co}(n, 2n)^{58}\text{Co}$, $^{27}\text{Al}(n, \alpha)^{24}\text{Na}$ and $^{58}\text{Ni}(n, 2n)^{57}\text{Ni}$ show C/E ratios (MCNP-IRDFF-1.05) more than unity beyond the estimated error bar. C/E (MCNP-IRDFF-1.05) ratios are close to unity for all reactions in zone-2 with the exceptions of $^{19}\text{F}(n, 2n)^{18}\text{F}$ and $^{65}\text{Cu}(n, 2n)^{64}\text{Cu}$ reactions which show C/E values less than unity beyond the estimated error bar. The exceptions in zone-3 are $^{93}\text{Nb}(n, 2n)^{92\text{m}}\text{Nb}$, $^{19}\text{F}(n, 2n)^{18}\text{F}$ and $^{90}\text{Zr}(n, 2n)^{89}\text{Zr}$ where calculations underestimate

the experimental values beyond the error bar. In zone-4, $^{19}\text{F}(n, 2n)^{18}\text{F}$ and $^{65}\text{Cu}(n, 2n)^{64}\text{Cu}$ calculated reaction rates are underestimated with respect to experimental values. In zone-5, $^{93}\text{Nb}(n, 2n)^{92m}\text{Nb}$ and $^{90}\text{Zr}(n, 2n)^{89}\text{Zr}$ calculated reaction rates are underestimated beyond estimated error bar.

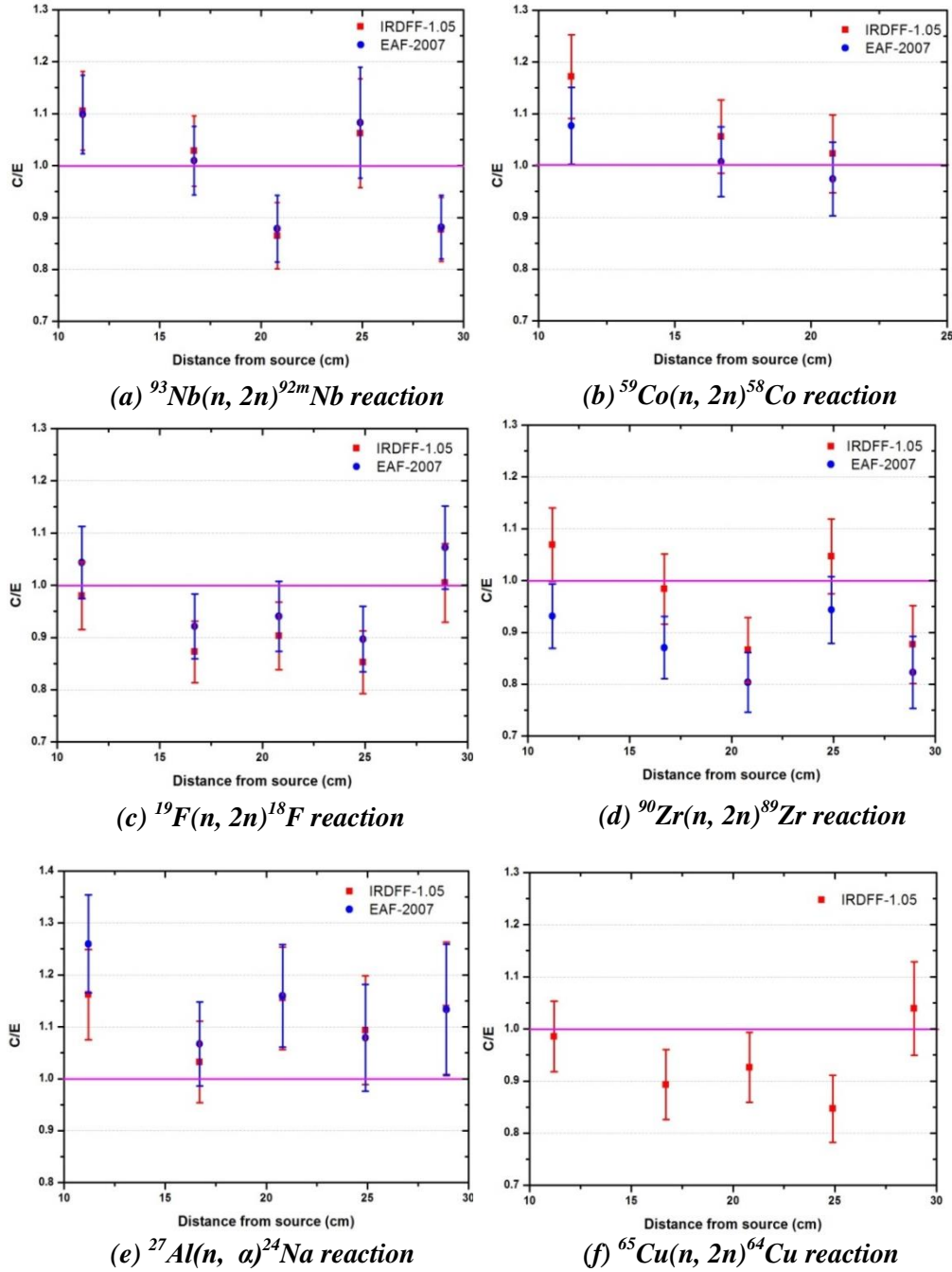


Figure 6.7: C/E ratios of high threshold reactions with MCNP-IRDFF-1.05 and FISPACT-EAF2007

C/E ratios for the intermediate energy range reactions are shown in Figs. 6.8a - 6.8c.

The C/E ratios for the $^{63}\text{Cu}(n, \gamma)^{64}\text{Cu}$ reaction in experimental assembly zones are plotted in *Figure 6.8d*.

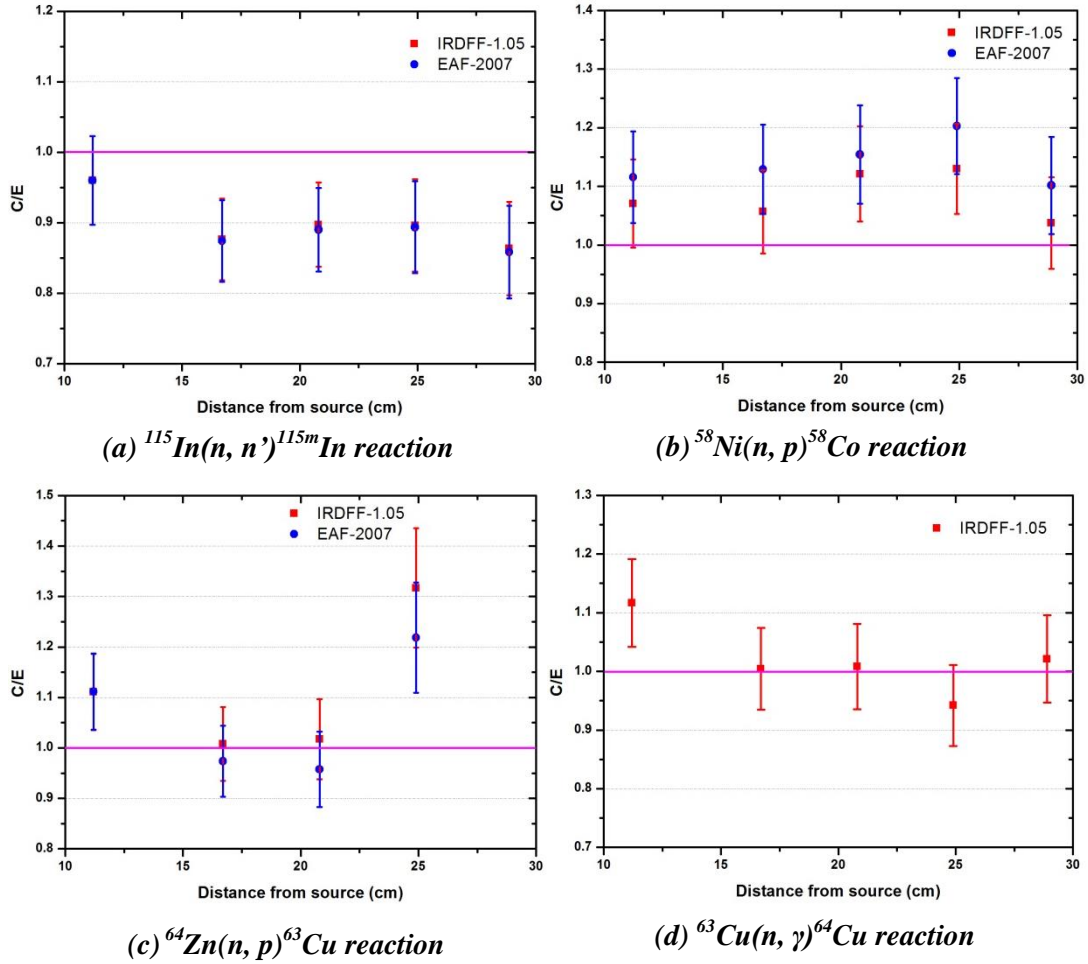


Figure 6.8: C/E ratios of low threshold and radiative capture reactions with MCNP-IRDF-1.05 and FISPACT-EAF2007

Average C/E ratios obtained with MCNP and IRDF-1.05 library for the intermediate energy range reactions in zones-1, 2, 3, 4 and 5 are 1.05, 0.98, 1.01, 1.11 and 0.95 respectively showing good agreement between experimental and calculated values. It can be seen from *Figure 6.8a* that both libraries underestimate the measured reaction rate of $^{115}\text{In}(n, n')^{115m}\text{In}$ in zones-2, 3 4 and 5 beyond the estimated error bar.

It can be seen from *Figure 6.9* that more than 85% response of the $^{115}\text{In}(n, n')^{115\text{m}}\text{In}$ reaction in these zones comes from the secondary neutron emission range of $\text{Pb}(n, xn)$ reactions (0.1-8 MeV). Therefore this result indicates that the calculations underestimate the measured Lead multiplication.

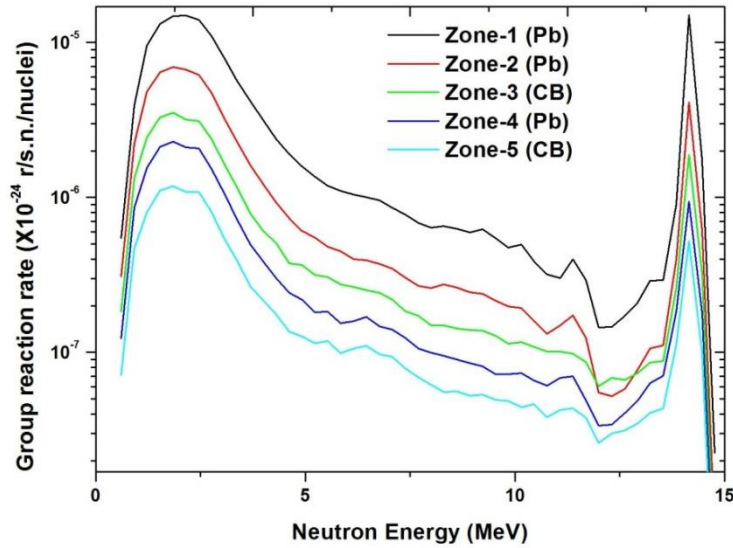


Figure 6.9: Spectral response of $^{115}\text{In}(n, n')^{115\text{m}}\text{In}$ reaction in experimental assembly zones

6.4.2 Comparison of reaction rates with FENDL-2.1 and FENDL-3.0

FENDL-3.0 library has been recently released as substitute of FENDL-2.1. FENDL-2.1 library was used for the nuclear analyses of fusion systems till the release of FENDL-3.0. Therefore it is important to see the difference due to transition from FENDL-2.1 to FENDL-3.0. Reaction rates in assembly zones were calculated purely with FENDL-3.0 library and comparison of reaction rates for both libraries is given in Tables 6.9 - 6.13. The changes in the reaction rates are represented with plus and minus signs. The plus (minus) sign indicate the increase (decrease) in the reaction rate value with respect to FENDL-2.1. The reaction rate results for both neutron transport

libraries were obtained with dosimetry file IRDFF-1.05. It can be seen from Table 6.9 that difference in zone-1 reaction rates with both libraries is less than 0.55% which is of the order of statistical error in the Monte Carlo calculations. As seen from Table 6.10, difference in zone-2 reaction rates is within statistical error except $^{115}\text{In}(n, n')^{115\text{m}}\text{In}$ and $^{64}\text{Zn}(n, p)^{64}\text{Cu}$ reactions. $^{115}\text{In}(n, n')^{115\text{m}}\text{In}$ and $^{64}\text{Zn}(n, p)^{64}\text{Cu}$ reaction rates with FENDL-3.0 are increased with respect to FENDL-2.1 by 1.7 and 0.9% respectively. Increase in $^{115}\text{In}(n, n')^{115\text{m}}\text{In}$ reaction rate shows improvement in the Lead multiplication towards measured value. It can be observed from Table 6.11 that four reactions in zone-3 show differences more than 1% [$^{58}\text{Ni}(n, 2n)^{57}\text{Ni}$ (-1.4%), $^{115}\text{In}(n, n')^{115\text{m}}\text{In}$ (1.4%), $^{64}\text{Zn}(n, p)^{64}\text{Cu}$ (1.2%) and $^{63}\text{Cu}(n, \gamma)^{64}\text{Cu}$ (1.0%)]. Most of the zone-3 calculated reaction rates with FENDL-3.0 show tendency to make C/E ratio towards unity. Table 6.12 lists the difference in calculated reaction rates in zone-4 from FENDL-2.1 to FENDL-3.0. Three reactions show differences more than 1% in zone-4 between two libraries [$^{115}\text{In}(n, n')^{115\text{m}}\text{In}$ (1.9%), $^{58}\text{Ni}(n, p)^{58}\text{Co}$ (1.5%), and $^{63}\text{Cu}(n, \gamma)^{64}\text{Cu}$ (2.7%)]. Zone-5 differences between two libraries are listed in Table 6.13. In zone-5, four reactions show differences between two libraries by more than 1% [$^{65}\text{Cu}(n, 2n)^{64}\text{Cu}$ (1.2%), $^{115}\text{In}(n, n')^{115\text{m}}\text{In}$ (2.3%), $^{58}\text{Ni}(n, p)^{58}\text{Co}$ (1.7%), and $^{63}\text{Cu}(n, \gamma)^{64}\text{Cu}$ (5.1%)]. As shown in Figure 6.9 that the $^{115}\text{In}(n, n')^{115\text{m}}\text{In}$ is most suitable for the measurement of Lead multiplication. The calculated response of this reaction with FENDL-3.0 in comparison to FENDL-2.1 is improved towards making C/E ratio unity in most of the assembly zones. The magnitude of Lead multiplication improvement is typically 2% from FENDL-2.1 to FENDL-3.0. In conclusion it can be said that Lead multiplication is improved in FENDL-3.0 with respect to FENDL-2.1 but still the C/E ratios fall below unity in the range of 5-10%.

Table 6.9: Comparison of neutron induced reaction rates in assembly zone-1 with FENDL-2.1 and FENDL-3.0 libraries

Reaction N	Reaction rate (r/s.n./nuclide)		Difference (%)
	FENDL-2.1	FENDL-3.0	
$^{93}\text{Nb}(n, 2n)^{92\text{m}}\text{Nb}$	1.3587E-28	1.3596E-28	0.07
$^{59}\text{Co}(n, 2n)^{58}\text{Co}$	1.9701E-28	1.9592E-28	-0.55
$^{19}\text{F}(n, 2n)^{18}\text{F}$	1.0238E-29	1.0244E-29	0.06
$^{90}\text{Zr}(n, 2n)^{89}\text{Zr}$	1.7332E-28	1.7361E-28	0.17
$^{27}\text{Al}(n, \alpha)^{24}\text{Na}$	3.3865E-29	3.3797E-29	-0.20
$^{65}\text{Cu}(n, 2n)^{64}\text{Cu}$	2.2679E-28	2.2700E-28	0.09
$^{63}\text{Cu}(n, 2n)^{62}\text{Cu}$	1.1307E-28	1.1316E-28	0.08
$^{58}\text{Ni}(n, 2n)^{57}\text{Ni}$	6.2960E-30	6.3017E-30	0.09
$^{27}\text{Al}(n, p)^{27}\text{Mg}$	2.3816E-29	2.3710E-29	-0.45
$^{115}\text{In}(n, n')^{115\text{m}}\text{In}$	1.4301E-28	1.4360E-28	0.41
$^{58}\text{Ni}(n, p)^{58}\text{Co}$	1.7086E-28	1.7041E-28	-0.26
$^{64}\text{Zn}(n, p)^{64}\text{Cu}$	7.0626E-29	7.0599E-29	-0.04
$^{63}\text{Cu}(n, \gamma)^{64}\text{Cu}$	2.1088E-28	2.1094E-28	0.03
$^{59}\text{Co}(n, \gamma)^{60}\text{Co}$	1.5001E-27	1.4980E-27	-0.14

Table 6.10: Comparison of neutron induced reaction rates in assembly zone-2 with FENDL-2.1 and FENDL-3.0 libraries

Reaction	Reaction rate (r/s.n./nuclide)		Difference (%)
	FENDL-2.1	FENDL-3.0	
$^{93}\text{Nb}(n, 2n)^{92\text{m}}\text{Nb}$	3.9105E-29	3.9156E-29	0.13
$^{59}\text{Co}(n, 2n)^{58}\text{Co}$	5.2981E-29	5.2908E-29	-0.14
$^{19}\text{F}(n, 2n)^{18}\text{F}$	2.8486E-30	2.8464E-30	-0.08
$^{90}\text{Zr}(n, 2n)^{89}\text{Zr}$	4.7521E-29	4.7687E-29	0.35
$^{27}\text{Al}(n, \alpha)^{24}\text{Na}$	1.0200E-29	1.0154E-29	-0.45
$^{65}\text{Cu}(n, 2n)^{64}\text{Cu}$	6.6618E-29	6.6655E-29	0.06
$^{63}\text{Cu}(n, 2n)^{62}\text{Cu}$	3.2968E-29	3.2991E-29	0.07
$^{115}\text{In}(n, n')^{115\text{m}}\text{In}$	6.0689E-29	6.1742E-29	1.73

$^{58}\text{Ni}(\text{n}, \text{p})^{58}\text{Co}$	5.5015E-29	5.5118E-29	0.19
$^{64}\text{Zn}(\text{n}, \text{p})^{64}\text{Cu}$	2.3253E-29	2.3466E-29	0.92
$^{63}\text{Cu}(\text{n}, \gamma)^{64}\text{Cu}$	8.6397E-29	8.5856E-29	-0.63

Table 6.11: Comparison of neutron induced reaction rates in assembly zone-3 with FENDL-2.1 and FENDL-3.0 libraries

Reaction	Reaction rate (r/s.n./nuclide)		Difference (%)
	FENDL-2.1	FENDL-3.0	
$^{93}\text{Nb}(\text{n}, 2\text{n})^{92\text{m}}\text{Nb}$	1.8644E-29	1.8681E-29	0.20
$^{59}\text{Co}(\text{n}, 2\text{n})^{58}\text{Co}$	2.5601E-29	2.5660E-29	0.23
$^{19}\text{F}(\text{n}, 2\text{n})^{18}\text{F}$	1.3725E-30	1.3762E-30	0.27
$^{90}\text{Zr}(\text{n}, 2\text{n})^{89}\text{Zr}$	2.1367E-29	2.1464E-29	0.45
$^{27}\text{Al}(\text{n}, \alpha)^{24}\text{Na}$	5.2663E-30	5.2651E-30	-0.02
$^{65}\text{Cu}(\text{n}, 2\text{n})^{64}\text{Cu}$	3.3366E-29	3.3621E-29	0.76
$^{58}\text{Ni}(\text{n}, 2\text{n})^{57}\text{Ni}$	8.1712E-31	8.0572E-31	-1.40
$^{115}\text{In}(\text{n}, \text{n}')^{115\text{m}}\text{In}$	3.1571E-29	3.2028E-29	1.45
$^{58}\text{Ni}(\text{n}, \text{p})^{58}\text{Co}$	2.9973E-29	2.9995E-29	0.07
$^{64}\text{Zn}(\text{n}, \text{p})^{64}\text{Cu}$	1.2473E-29	1.2627E-29	1.23
$^{63}\text{Cu}(\text{n}, \gamma)^{64}\text{Cu}$	2.2343E-29	2.2562E-29	0.98

Table 6.12: Comparison of neutron induced reaction rates in assembly zone-4 with FENDL-2.1 and FENDL-3.0 libraries

Reaction	Reaction rate (r/s.n./nuclide)		Difference (%)
	FENDL-2.1	FENDL-3.0	
$^{93}\text{Nb}(\text{n}, 2\text{n})^{92\text{m}}\text{Nb}$	1.0272E-29	1.0306E-29	0.33
$^{19}\text{F}(\text{n}, 2\text{n})^{18}\text{F}$	7.3832E-31	7.3752E-31	-0.11
$^{90}\text{Zr}(\text{n}, 2\text{n})^{89}\text{Zr}$	1.1917E-29	1.1839E-29	-0.66
$^{27}\text{Al}(\text{n}, \alpha)^{24}\text{Na}$	2.9894E-30	2.9973E-30	0.26
$^{65}\text{Cu}(\text{n}, 2\text{n})^{64}\text{Cu}$	1.8622E-29	1.8765E-29	0.77
$^{115}\text{In}(\text{n}, \text{n}')^{115\text{m}}\text{In}$	2.0017E-29	2.0403E-29	1.93
$^{58}\text{Ni}(\text{n}, \text{p})^{58}\text{Co}$	1.7127E-29	1.7391E-29	1.54

$^{64}\text{Zn}(n, p)^{64}\text{Cu}$	7.4020E-30	7.4095E-30	0.10
$^{63}\text{Cu}(n, \gamma)^{64}\text{Cu}$	1.7056E-29	1.7508E-29	2.65

Table 6.13: Comparison of neutron induced reaction rates in assembly zone-5 with FENDL-2.1 and FENDL-3.0 libraries

Reaction	Reaction rate (r/s.n./nuclide)		Difference (%)
	FENDL-2.1	FENDL-3.0	
$^{93}\text{Nb}(n, 2n)^{92\text{m}}\text{Nb}$	6.1408E-30	6.1790E-30	0.62
$^{19}\text{F}(n, 2n)^{18}\text{F}$	4.1906E-31	4.2180E-31	0.65
$^{90}\text{Zr}(n, 2n)^{89}\text{Zr}$	6.5548E-30	6.5692E-30	0.22
$^{27}\text{Al}(n, \alpha)^{24}\text{Na}$	1.7589E-30	1.7665E-30	0.43
$^{65}\text{Cu}(n, 2n)^{64}\text{Cu}$	1.0646E-29	1.0769E-29	1.16
$^{115}\text{In}(n, n')^{115\text{m}}\text{In}$	1.0914E-29	1.1164E-29	2.28
$^{58}\text{Ni}(n, p)^{58}\text{Co}$	1.0159E-29	1.0327E-29	1.65
$^{63}\text{Cu}(n, \gamma)^{64}\text{Cu}$	1.7782E-29	1.8686E-29	5.08

6.4.3 Neutron spectra

Neutron spectrum unfolding code SAND-II-SNL (Spectrum Analysis by Neutron detectors-II-Sandia National Laboratory) utilizes an initial guess spectrum and compares the expected activity in materials, calculated using neutron cross-section tables, with the measured saturated activity from neutron activation analysis. Comparing these two pieces of information, the program calculates correction factors, perturbs the guess spectrum, and repeats the process until a solution criterion is met [75]. In the current work, the iteration process was stopped when the difference of the average standard deviation of saturation activities between two consecutive iterations became less than 2%.

Guess spectra in assembly zones were calculated with MCNP and FENDL-2.1 library as input to SAND-II unfolding code. Comparison of the guess and solution spectra

obtained with SAND-II-SNL code in all five zones of the experimental assembly is given in *Figure 6.10*.

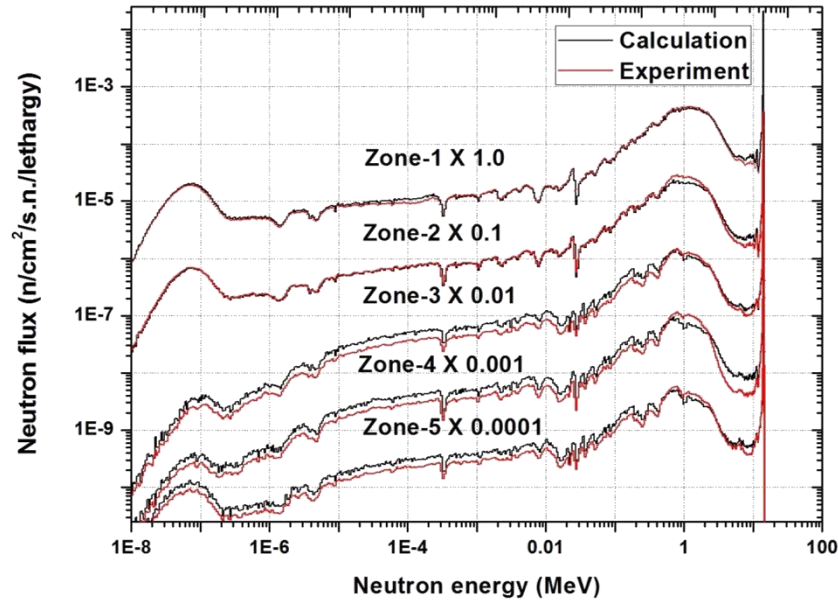


Figure 6.10: Unfolded neutron spectra with SAND-II and calculated spectrum with MCNP and FENDL-2.1 in breeding assembly zones

In order to compare calculated and solution spectra, the finer spectra in *Figure 6.10* was integrated into five course energy bins: (1) thermal and epithermal neutrons (< 1 eV) (2) slow and resonance neutrons (1 eV - 100 keV) (3) secondary neutrons from Pb(n, xn) reactions (100 keV - 8 MeV) (4) inelastic scattering range (8 - 12 MeV) (5) source neutrons (> 12 MeV) and (6) total neutron flux. High energy bins are chosen based on the importance of spectrum for the breeding blankets based on the Lead as multiplier material. Low energy bins are important for the tritium breeding by the lithium isotope ${}^6\text{Li}$. Comparison of calculated (MCNP with FENDL-2.1) and solution spectra (unfolded with code SAND-II-SNL) in assembly zones for these course energy bins is shown in *Figure 6.11*.

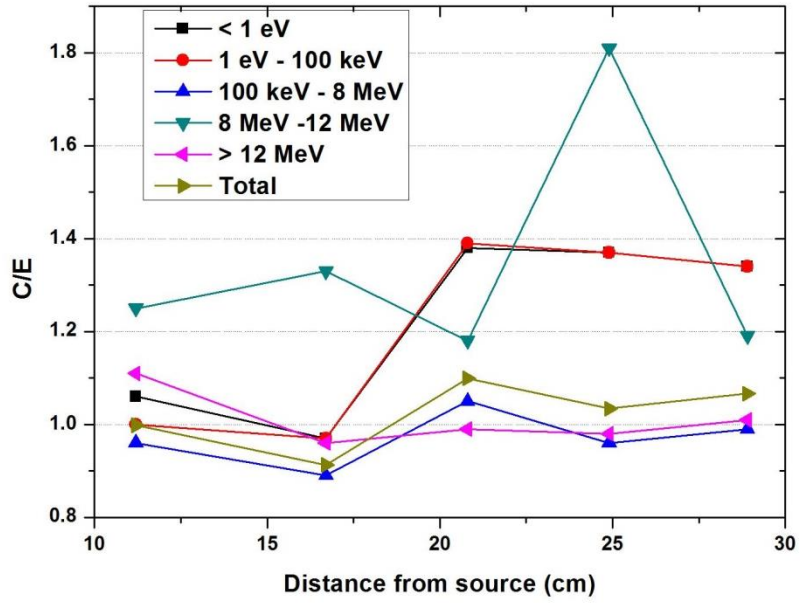


Figure 6.11: Ratio of calculated and experimental neutron spectra integrated in five energy bins shown as a function of assembly zone

Calculated neutron fluxes show good agreement with the experimental fluxes in thermal, slow and resonance region for zone-1 and zone-2. Calculations overestimate the measured thermal fluxes in zones 3-5. In the thermal energy range, only one reaction is measured and calculated flux shown in *Figure 6.10* is calculated over the volume of all foils of each zone. Therefore thermal flux guess spectra are not so precise. The secondary neutron emission range from Pb(n, xn) reactions is well covered with different reactions. It is worth to note that in the secondary neutron emission range of Pb(n, xn) reactions, the calculations underestimates the measured neutron flux in all the zones having Lead (zones 1-2, 4). The magnitude of underestimation is up to 10% of experimental value. This observation confirms the underestimation by calculations observed with $^{115}\text{In}(n, n')^{115\text{m}}\text{In}$ reaction and described in section 6.4.1 and 6.4.2. This result shows that there is a need to improve (n, 2n) reaction cross-sections of Lead isotopes in FENDL-2.1 library. The observed

underestimation by calculations in the Lead multiplication puts the LLCB TBM and others with Lead multiplier tritium production calculations on the conservative side. The inelastic scattering range of Lead isotopes is overestimated in all zones. The overestimation is as large as 80% of the measured flux in zone-4. The inelastic scattering cross-sections of Lead isotopes also need improvement in the FENDL-2.1 nuclear data library. The source neutron flux is very well predicted by calculations. There is slight overestimation observed in zone-1.

6.4.4 Comparison with previous experiment / analyses

A clean benchmark experiment with Lead sphere is reported in the IAEA FENDL-2.0 benchmark database [79]. This benchmark experiment was performed at Technische Universitat Dresden (TUD), Germany using isotropic point source of $^3\text{H}(d, n)^4\text{He}$ neutrons in the center of the spherical lead assembly [80]. The inner and outer radii of the Pb sphere were 2.5 and 25 cm respectively i.e. Pb thickness used in the experiment was 22.5 cm. The leakage neutron spectrum was measured at 431 cm from the source with NE-213 liquid scintillation spectrometer.

In the current work, this experiment was modelled in the MCNP with two libraries FENDL-2.1 and FENDL-3.0. Comparison of the measured and calculated leakage spectrum with two libraries is given in *Figure 6.12*. Calculated and measured total and partial neutron multiplication in the Pb sphere is given in *Table 6.14*. It can be seen from *Table 6.14* that the total measured neutron multiplication is underestimated by both libraries and the major contribution of this underestimation comes from the neutrons in the energy range 0.05 to 1 MeV. FENDL-3.0 data is improved with respect to FENDL-2.1 in the energy range 1-14.9 MeV. Neutron multiplication in the energy

range 0.05-1.00 MeV is similar in both libraries and contribution of this range is 58% of total multiplication. Due to this reason the total neutron multiplication is improved only 1% in the FENDL-3.0 library. The magnitude of Lead multiplication underestimation of TUD Pb sphere experiment is comparable to the present experiment (5-10%).

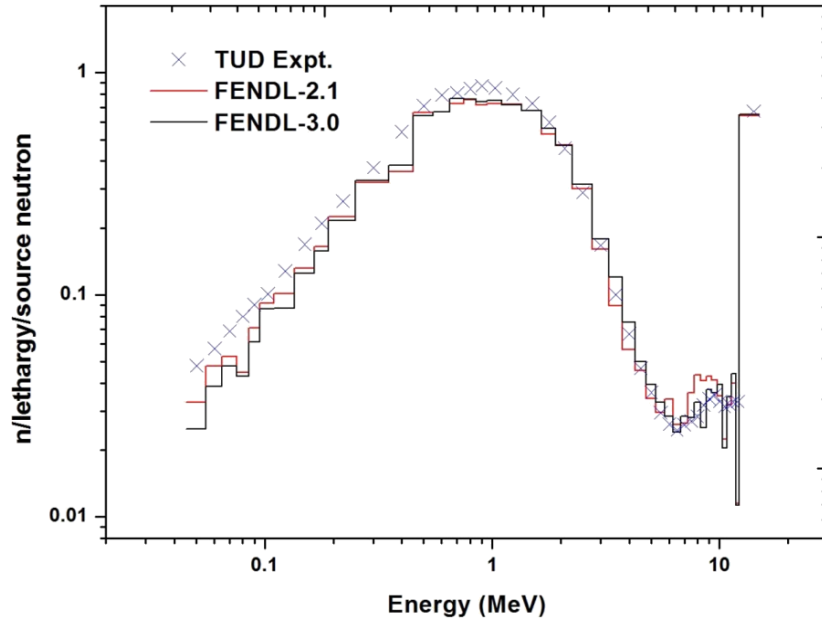


Figure 6.12: Comparison of calculated leakage neutron spectrum from Lead sphere (FENDL-2.1 and FENDL-3.0) with measurement performed at TUD, Germany

Table 6.14: Measured and calculated neutron multiplication (partial and total) in TUD Lead sphere experiment

Neutron energy range	Experiment	Calculation		Ratio	
		FENDL-2.1	FENDL-3.0		
MeV	E	C1	C2	C1/E	C2/E
0.05-1.00	1.126	0.935	0.937	0.83	0.83
1.00-5.00	0.668	0.626	0.641	0.94	0.96
5.00-10.00	0.020	0.024	0.022	1.17	1.06
10.00-14.90	0.140	0.134	0.136	0.96	0.97
0.05-14.90	1.954	1.719	1.735	0.88	0.89

Comparison of the TUD Pb sphere leakage spectrum with the neutron spectrum in zone-2 of present experiment is shown in *Figure 6.13*. The shape of the neutron spectra in both cases is similar but the ratio of the source neutrons to the secondary neutrons is larger in present experiment due to lesser thickness of lead (7 cm in present experiment while 22.5 cm in TUD Lead sphere).

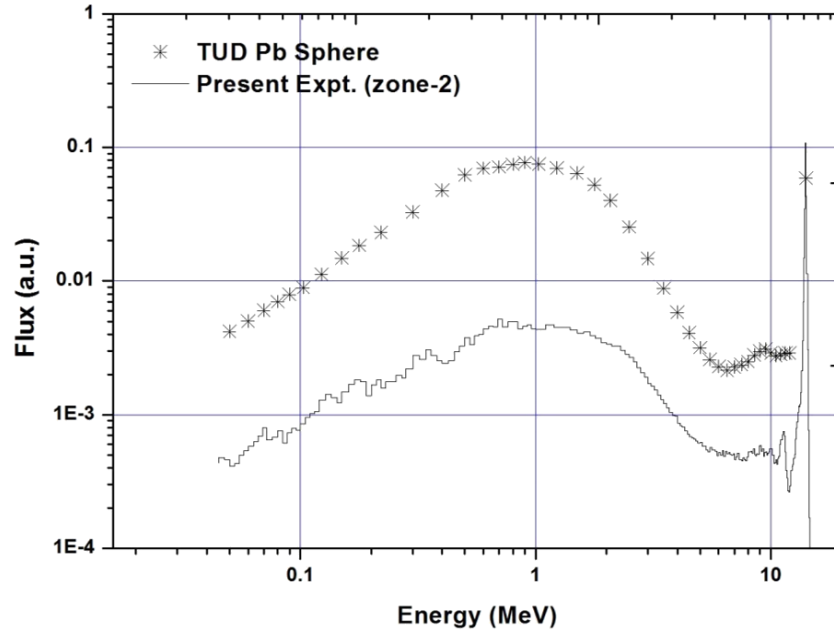


Figure 6.13: Leakage neutron spectrum from TUD Pb sphere experiment and neutron spectrum in zone-2 of present experiment

Another experiment with Lead spheres with thicknesses 3, 6, 9 and 12 cms was performed at OSAKA University, Japan. The original paper publishing the results was not available. However sufficient details of this experiment are given in reference [81] which can be used for the comparison between measured and calculated neutron leakage. In this experiment the inner radius was kept fixed at 10 cm and the outer radius was varied from 13 to 22 cm. The thickness of the Lead shell thus varied from 3 to 12 cm. Experiment in the same geometry was performed twice 1982 and 1985 following doubts regarding the existence of the systematic errors in the 1982

experiment. The difference between two measurements was less than 5% which is less than the reported overall uncertainty in the experimental responses. Comparison of the calculated and measured Lead multiplication for OSAKA experiment is given in *Table 6.15* and *Table 6.16*.

Table 6.15: Neutron leakage multiplication in OSAKA experiment (0.017-15 MeV)

Pb thickness (cm)	Experiment (E)	Calculation (C)		C/E	
		FENDL-2.1	FENDL-3.0	FENDL-2.1	FENDL-3.0
3	1.34	1.20	1.22	0.89	0.91
6	1.54	1.37	1.39	0.89	0.90
9	1.69	1.50	1.51	0.89	0.90
12	1.80	1.61	1.64	0.90	0.91

Table 6.16: Neutron leakage multiplication in OSAKA experiment (0.3-15 MeV)

Pb thickness (cm)	Experiment (E)	Calculation (C)		C/E	
		FENDL-2.1	FENDL-3.0	FENDL-2.1	FENDL-3.0
3	1.27	1.17	1.19	0.92	0.94
6	1.41	1.31	1.33	0.93	0.94
9	1.50	1.41	1.42	0.94	0.95
12	1.58	1.48	1.51	0.94	0.95

It can be seen from *Table 6.15* and *Table 6.16* that the both FENDL-2.1 and FENDL-3.0 underestimates the Lead multiplication up to 10% in the energy range 0.017-15 MeV and up to 5% in the energy range 0.3-15 MeV. This result is in line with the TUD experimental results.

The similar behavior of $^{115}\text{In}(n, n')^{115\text{m}}\text{In}$ reaction rate has been observed with the measured Lead multiplication in the work reported in the reference [82] at JAEA.

In 2009, another experiment with Lead and LiAl was performed at TUD, Germany by measuring the neutron spectra with NE-213 detector [83]. This experiment highlights

the problems in the JENDL-3.3 data library in the energy range 0.5-15 MeV. It also reports the problem in the nuclear data library JEFF-3.1 in the energy range 5-10 MeV. However enough geometrical details of the experiment are not given to further analyses it with FENDL libraries. The numerical data for the measured values are also not given. In absence of these data, the analysis of this experiment is not possible.

6.5 Conclusions

A benchmark experiment, having three layers of neutron multiplying material Lead and two layers of breeder material Li_2TiO_3 , was performed in the geometry of LLCB TBM by measuring the reaction rates in activation foils and subsequently unfolding of the neutron spectra. The measured reaction rates were compared with the calculations performed with FENDL-2.1 transport library and dosimetry IRDFF-1.05 and activation library EAF-2007. The calculated reaction rates in the foils are in agreement with the measured reaction rates within combined uncertainty of experiment and calculations with few exceptions. Calculations of reaction rates in assembly zones were also performed with newly released FENDL-3.0 library and results were compared with FENDL-2.1 values. The comparison reveals that the Lead multiplication is improved typically 2% with FENDL-3.0 but still the C/E ratios are less than unity beyond the estimated error bar. The comparison of measured and calculated neutron spectra in Lead zones show that measured neutron spectra in the $\text{Pb}(n, xn)$ secondary neutron emission range is slightly underestimated by calculations. Therefore there is a need to improve the $(n, 2n)$ cross-sections of the Lead isotopes in FENDL-2.1 and FENDL-3.0 libraries. The observed underestimation by calculations in the Lead multiplication puts the tritium production calculation of TBM designs using Lead as multiplier on

conservative side. The measured neutron flux in inelastic scattering range in one of the zone is overestimated by calculations as large as up to 80%. So inelastic scattering cross-sections of Lead isotopes also need to be improved in the FENDL-2.1 and FENDL-3.0 libraries.

Chapter 7

Summary, conclusions and future

outlook

Integral benchmark experiments play a key role in knowing accuracy of neutron transport computational tools i.e. codes and data used in the nuclear design of the breeding blankets. This is essential when testing nuclear data evaluations and assessing uncertainty margins for design calculations. To this end, appropriate material assemblies were irradiated with 14 MeV neutrons from D-T generator tube. The resulting neutron flux spectra as well as specific nuclear responses of interest were measured by applying various experimental techniques such as activation foils measurements and tritium production rate with lithium carbonate pellets and on-line detector. Measured nuclear responses were compared with the calculated values obtained with neutronics code MCNP and nuclear data library FENDL-2.1 and FENDL-3.0.

In the first part of the thesis, development and performance characterization of the diagnostics for source neutrons and tritium production are described. Second part of the thesis is focused to analyze the measured nuclear responses in the three experiments with breeding blanket materials highlighting the deficiencies in the neutron induced cross-sections for the isotopes used in the experiments and their

impact on the LLCB TBM design calculations. Summary, conclusions and future outlook is discussed in the following sections.

7.1 Summary and conclusions

Characterization of the source neutron emission from the 14 MeV neutron generator, used for the irradiation experiments, is an essential component for the benchmark experiments. In the present thesis, a methodology was developed to measure the time integrated source neutron yield using foil activation technique. Time profile of the source neutron emission was measured with ^3He counter cross-calibrated with activation measurement. Anisotropy of the source neutrons from D-T reaction was calculated using relativistic kinematics and energy loss of incident D^+ beam in the Ti-T target. Angular source neutron spectra was estimated with the help of code NeuSDesc considering energy distribution of incident deuterons in the Ti-T target. A Monte Carlo calculation model was developed using the calculated anisotropy, angle dependent neutron spectra and physical model of the neutron generator tube. Validation of the calculated anisotropy, neutron spectra and neutron generator tube materials was done by comparing the calculated reaction rates with measured rates in the various foils covering the energy range from thermal to source neutrons. The comparison shows a very good agreement between measured and calculated reaction rates with this model within 2% demonstrating that the developed model can be used for the analyses of the benchmark experiments.

The other requirement for the benchmark experiments is development of the appropriate diagnostics to measure the tritium production rate in the experimental assemblies with good spatial resolution. Two independent tritium measurement

diagnostics were developed. The first diagnostic was based on the irradiation of lithium carbonate pellets in the experimental assemblies and the counting of tritium in these pellets off-line using liquid scintillation counting technique. This technique was further extended to measure tritium production separately from ^6Li and ^7Li isotopes. The second tritium diagnostics developed was based on the on-line measurement of tritons in the silicon surface barrier detector (SBD) having a layer of ^6Li on its window. The tritons produced from $^6\text{Li}(n, t)^4\text{He}$ reaction in the lithium layer were directly measured in the SBD detector. The measured triton count rate was converted into tritium production rate from ^6Li in the breeding blanket mock-up by characterizing the lithium converter layer for ^6Li atoms and source neutron yield. The other application of this diagnostic was shown to determine the ratio of lithium isotopes in the enriched lithium samples.

Having developed all the required diagnostics, the first experiment was performed with lithium aluminate (LiAlO_2) breeding material with objective to test the developed diagnostics and comparison with the calculations. The experiment was performed with LiAlO_2 due to its availability at the time of experiment. The experimental tritium production rates in the LiAlO_2 assembly were compared with the calculated values using MCNP and FENDL-2.1 data library. Both results were in agreement within the estimated error bar except one point.

A mock-up experiment was designed for the LLCB TBM in ITER by measuring tritium production rate and neutron induced reaction rate of $^{115}\text{In}(n, n')^{115\text{m}}\text{In}$ reaction. The first of the four mock-up experiments to investigate the neutronics performance of the materials used in the LLCB TBM was performed. The tritium production rates in the mock-up zones were measured with Li_2CO_3 pellets and on-line tritium detector.

The TPR from both lithium isotopes ^6Li and ^7Li were estimated with the help of Li_2CO_3 pellets having two different compositions of Li isotopes. The activation foil measurement was employed to validate the neutron spectra above 0.5 MeV using $^{115}\text{In}(n, n')^{115\text{m}}\text{In}$ reaction rates in the mock-zones. The average value of C/E of tritium production in enriched Li_2CO_3 pellet for three positions is 1.11 for CB-1 (first breeder zone) and 1.09 for CB-2 (second breeder zone). The average value of C/E of tritium production in natural Li_2CO_3 pellet is 1.05 for CB-1 and 0.94 for CB-2. The measurement of TPR from ^6Li and ^7Li reveals that the TPR in breeding zones is mostly contributed by tritium production from ^6Li isotope (> 90%). C/E ratio for TPR- ^6Li with on-line tritium detector is close to unity (0.96). The $^{115}\text{In}(n, n')^{115\text{m}}\text{In}$ reaction rate measurement shows the tendency of underestimation by calculations at most of the measurement positions indicating deficiency in the $\text{Pb}(n, xn)$ cross-sections. This was further investigated by irradiating more foils in the experimental assembly and subsequently unfolding the spectra in each zone.

A benchmark experiment, having three layers of neutron multiplying material Lead and two layers of breeder material Li_2TiO_3 , was performed in the geometry of LLCB TBM by measuring the reaction rates in activation foils and subsequently unfolding of the neutron spectra. The measurements were compared with the calculations obtained with two different cross-section libraries, dosimetry library IRDFF-1.05 and activation library EAF-02. The calculated reaction rates in the foils are in agreement with the measured reaction rates within combined uncertainty of experiment and calculations with few exceptions. The comparison of measured and calculated neutron spectra in Lead zones show that measured neutron spectra in the $\text{Pb}(n, xn)$ secondary neutron emission range is slightly underestimated by calculations (5-10%). This implies that

the calculated tritium production rate in Lead zones of LLCB TBM with FENDL-2.1 library is on the conservative side. TPR is overestimated by the calculations with FENDL-2.1 library in the breeding zones of LLCB TBM. This trend is confirmed with the TPR experiment performed in this thesis. The recently released version 3.0 of FENDL library improves the Lead multiplication by typically 2% with respect to FENDL-2.1. But still the underestimation is not fully resolved and that demands further improvement in the FENDL-3.0 evaluation. The measured neutron flux in inelastic scattering range is overestimated by calculations as large as up to 80%. So inelastic scattering cross-sections of Lead isotopes also need to be improved in the FENDL-2.1 and FENDL-3.0 libraries.

7.2 Future outlook

Table 7.1 : Summary of the future experiments in support of the LLCB TBM nuclear design

	Materials		
	Experiment-1	Experiment-2	Experiment-3
Zone-1	Pb-Li (Nat. Li)	Pb-Li (Enri.)	Liq. Pb-Li (Enri.)
Zone-2	Pb-Li (Nat. Li)	Pb-Li (Enri.)	Liq. Pb-Li (Enri.)
	Li ₂ TiO ₃ pebbles	Li ₂ TiO ₃ pebbles	Li ₂ TiO ₃ pebbles
Zone-3	(Nat. Li)	(Enri. Li)	(Enri. Li)
Zone-4	Pb-Li (Nat. Li)	Pb-Li (Enri.)	Liq. Pb-Li (Enri.)
	Li ₂ TiO ₃ pebbles	Li ₂ TiO ₃ pebbles	Li ₂ TiO ₃ pebbles
Zone-5	(Nat. Li)	(Enri. Li)	(Enri. Li)
Structural material	P91	P91	P91
Neutron reflector	HDPE	HDPE	HDPE

The first experiment in support of LLCB TBM nuclear design was completed in the thesis work. Next three experiments as described in section 5.1 should be performed

to give the complete picture of the tritium breeding performance of LLCB TBM. The summary of all the three future experiments is given in *Table 7.1*.

In order to understand the role of individual isotope in tritium breeding and other nuclear parameters, sensitivity analysis of the reported experiments should be performed as future work. The sensitivity analysis helps to figure out the contribution of each nuclear reaction in the tritium production rate and hence the reactions whose evaluated cross-sections need to be improved can be identified. Uncertainty analysis investigates the uncertainty of cross-sections into analysis and finally gives the uncertainty in the calculated tritium production rate. It can also combine measurement uncertainty and finally gives the overall uncertainty in the prediction of tritium production rate. Therefore uncertainty analysis of the reported experiments should be performed. Both sensitivity and uncertainty analyses allow estimating the sensitivities and uncertainties of computational predictions for the tritium production rates and neutron flux. The importance and results of sensitivity and uncertainty analyses performed for other blanket concepts can be found in the references [84–88].

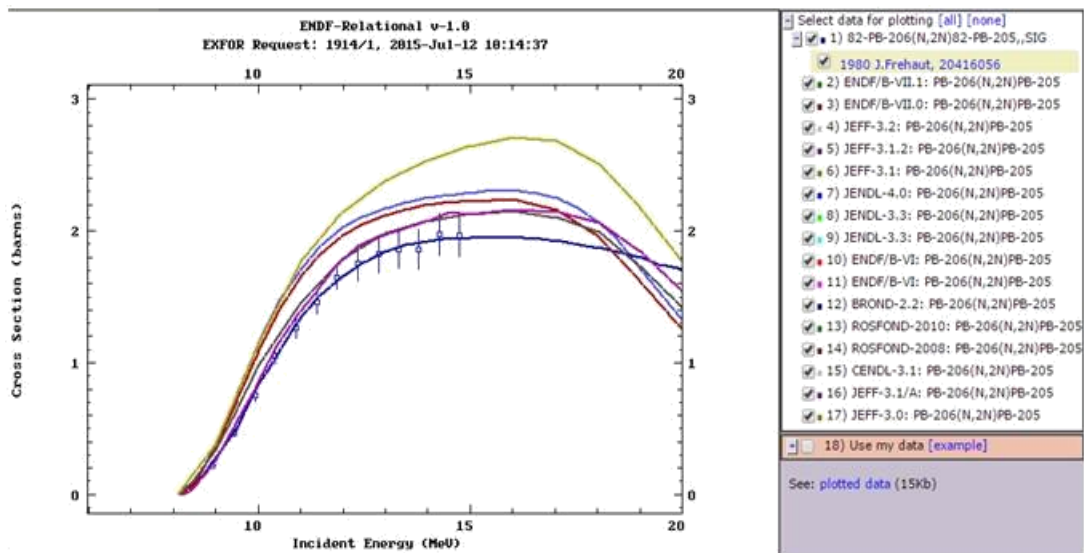


Figure 7.1: Measured and evaluated excitation function of $^{206}\text{Pb}(n, 2n)^{205}\text{Pb}$ reaction [22, 54, 89–98]

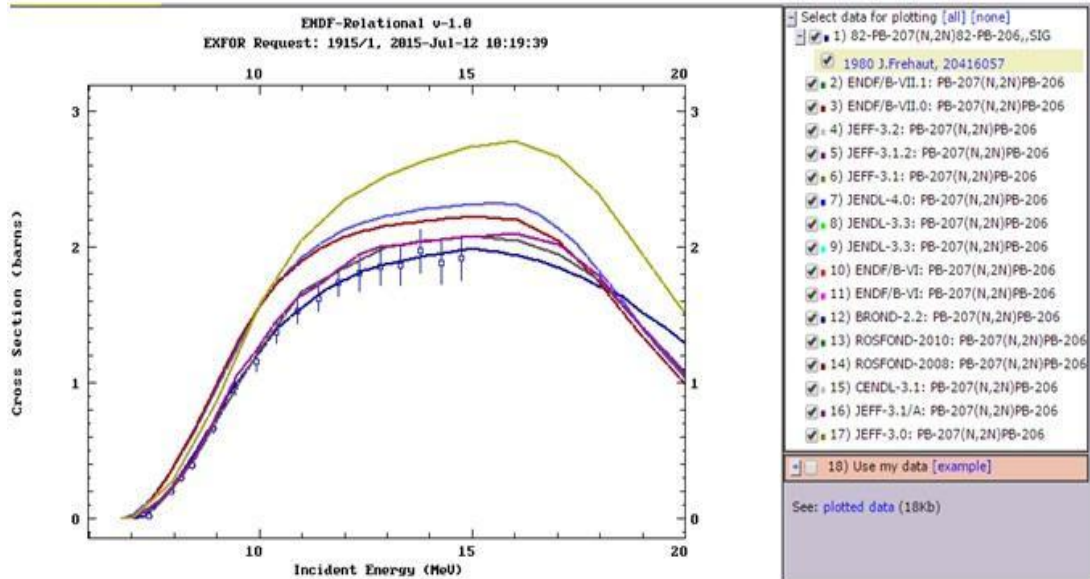


Figure 7.2: Measured and evaluated excitation function of $^{207}\text{Pb}(n, 2n)^{206}\text{Pb}$ reaction [22, 54, 89–98]

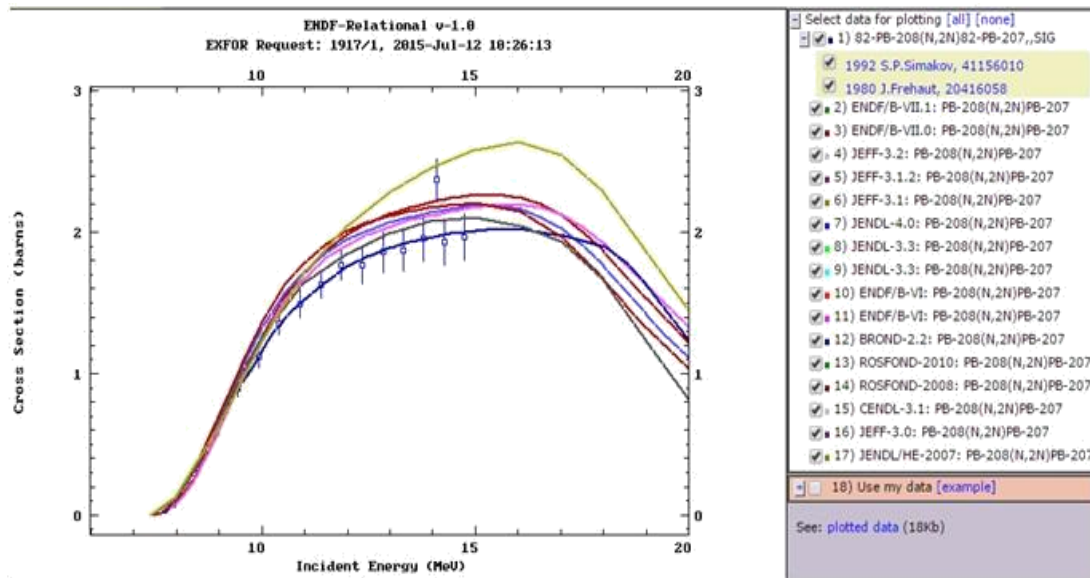


Figure 7.3: Measured and evaluated excitation function of $^{208}\text{Pb}(n, 2n)^{207}\text{Pb}$ reaction [22, 54, 89–98]

Lead (Pb) is an important material for the breeding blanket technology of D-T fusion reactor as a neutron multiplier. It has three major isotopes in its natural form: ^{206}Pb (24.1%), ^{207}Pb (22.1%) and ^{208}Pb (52.4%) [55]. Measured and evaluated excitation functions for (n, 2n) reaction in Lead isotopes are shown in Figure 7.1, Figure 7.2 and

Figure 7.3. (n, 2n) reaction in the Lead isotopes is predominantly responsible for the neutron multiplication. It can be seen from these figures that experimental measurement of (n, 2n) reaction cross-sections on Pb isotopes are few. Only one measurement exists for ^{206}Pb & ^{207}Pb isotopes and two measurements for ^{208}Pb . These measurements are quite old (1980 & 1992). Difference between measured $^{208}\text{Pb}(\text{n}, 2\text{n})^{207}\text{Pb}$ cross-section at 14.1 MeV by two independent measurements is approximately 20%. Evaluated (n, 2n) cross-sections of Lead isotopes show big discrepancy in the fusion neutron energy range of interest (Figs. 7.1, 7.2 and 7.3). Typical difference between maximum and minimum (n, 2n) evaluated cross-section at 14.1 MeV is 25%. Therefore it is of utmost important to measure the cross-section of Pb isotopes, perform benchmark experiments by measuring leakage neutrons and improve the evaluated cross-section libraries based on these measurements.

Bibliography

- [1] M. E. Sawan, M. A. Abdou, "Physics and technology conditions for attaining tritium self-sufficiency for the DT fuel cycle", Fusion Eng. Des. 81 (2006) 1131-1144.
- [2] Laila A El-Guebaly, S Malang, "Toward the ultimate goal of tritium self-sufficiency: Technical issues and requirements imposed on ARIES advanced power plants", Fusion Eng. Des., 84, (2009), 2072-2083.
- [3] <http://www-nds.iaea.org/fendl21/> FENDL-2.1 library.
- [4] <https://www-nds.iaea.org/fendl3/>: Fusion Evaluated Nuclear Data Library FENDL-3.0.
- [5] P. Batistoni et al., "Neutronics experiments for uncertainty assessment of tritium breeding in HCPB and HCLL blanket mock-ups irradiated with 14 MeV neutrons", Nuclear Fusion 52, (2012), 08314.
- [6] Batistoni P. et al, "Neutronics experiment on a HCPB breeder blanket mock-up", Fusion Eng. Des., 82, (Oct.2007), 2095-2104.
- [7] P. Batistoni, M. Angelone, P. Carconi, U. Fischer, K. Fleischer, et al, "Neutronics experiments on HCPB and HCLL TBM mock-ups in preparation of nuclear measurements in ITER", Fusion Eng. Des., 85(7-9), (Dec. 2010), 1675-1680.
- [8] K. Seidel, P. Batistoni, U. Fischer, H. Freiesleben, A. Klix, D. Leichtle, E. Poenitz, S. Unholzer, R. Villari, "Measurement and analysis of neutron and gamma-ray flux spectra in a neutronics mock-up of the HCPB Test Blanket Module", Fusion Eng. Des., 82, (2007), 2212-2216.
- [9] Klix A., Batistoni P., B'ottger R., Lebrun-Grandie D., Fischer U., Henniger J., Leichtle D. and Villari R., "Measurement and analysis of neutron flux spectra in a neutronics mock-up of the HCLL test blanket module", Fusion Eng. Des., 85, (Dec. 2010), 1803-1806.
- [10] P. Batistoni, M. Angelone, U. Fischer, D. Leichtle, A. Klix, I. Kodeli, L. Petrizzi, W. Pohorecki, A. Trkov, R. Villari, "Design optimisation and measuring techniques for the neutronics experiment on a HCLL-TBM mock-up", Fusion Eng. Des. 84 (2009) 430-434.

- [11] S. Sato, K. Ochiai, Y. Verzilov, M. Wada, N. Kubota, K. Kondo, M. Yamanchi, T. Nishitani, and C. Konno, "Measurement of tritium production rate in water cooled pebble bed multi-layered blanket mockup by DT neutron irradiation experiment", *Nuclear Fusion* 47, (2007), 517-521.
- [12] S Sato et al, "Progress in the blanket neutronics experiments at JAERI/FNS", *Fusion Eng. Des.*, 81, (2006), 1183-1193.
- [13] A. Klix, K. Ochiai, Yu. Verzilov, A. Takahasi, "Tritium breeding experiments with blanket mock-ups containing ^6Li -enriched lithium titanate and beryllium irradiated with DT neutrons", *Fusion Eng. Des.*, 75-79, (November 2005), 881-884.
- [14] A. Klix, K. Ochiai, T. Nishitani, A. Takahasi, "Direct tritium measurement in lithium titanate for breeding blanket mock-up experiments with D-T neutrons", *Fusion Eng. Des.*, 70(4), (Oct. 2004), 279-287.
- [15] A Klix et al, "Heterogeneous breeding blanket experiment with lithium titanate and beryllium", *Fusion Eng. Des.*, 72, (2005), 327-337.
- [16] E. Rajendra Kumar, C. Danani, I. Sandeep, Ch. Chakrapani, N. Ravi Pragash, V. Chaudhari, C. Rotti, P.M. Raole, J. Alphonsa, S.P. Deshpande, "Preliminary design of Indian Test Blanket Module for ITER", *Fusion Eng. Des.*, 83(7-9), (2008), 1169-1172.
- [17] Paritosh Chaudhuri et al, "Status and progress of Indian LLCB test blanket systems for ITER", *Fusion Eng. Des.*, 87(7-8), (2012), 1009-1013.
- [18] Shrichand Jakhar, M. Abhangi, S. Tiwari, R. Makwana, V. Chaudhari, H. L. Swami, C. Danani, C. V. S. Rao, T. K. Basu, D. Mandal, Sonali Bhade, R. V. Kolekar, P. J. Reddy, R. Bhattacharyay, P. Chaudhuri, "Tritium breeding mock-up experiments containing lithium titanate ceramic pebbles and Lead irradiated with DT neutrons", *Fusion Eng. Des.*, 95, (June 2015), 50-58.
- [19] Shrichand Jakhar, S. Tiwari, M. Abhangi, V. Chaudhari, R. Makwana, C. V. S. Rao, T. K. Basu, D. Mandal, "Neutron flux spectrum investigations in breeding blanket assembly containing lithium titanate and Lead irradiated with DT neutrons", *Fusion Eng. Des.*, 100, (2015), 619-628.
- [20] Shrichand Jakhar, M. Abhangi, C. V. S. Rao, T. K. Basu, Sonali P. D. Bhade, Priyanka J. Reddy, "Measurement of tritium production rate distribution in

- natural LiAlO₂ /HDPE assembly irradiated by D-T neutrons", *Fusion Eng. Des.*, 87(2), (2012), 184-187.
- [21] Keishiro Niu, "Nuclear fusion", Cambridge University Press, Cambridge, 1989, ISBN 0 521 32994 9.
- [22] M.B. Chadwick, M. Herman, P. Obložinský, et al., "ENDF/B-VII.1 Nuclear Data for Science and Technology: Cross Sections, Covariances, Fission Product Yields and Decay Data", *Nuclear Data Sheets*, 112, (2011), 2887-2996.
- [23] Thomas James Dolan, "Fusion Research: Principles, Experiments and Technology", 2000, ISBN 0-08-0255855.
- [24] Edited by: Mitsuru Kikuchi, Karl Lackner, Minh Quang Tran, "Fusion Physics", International Atomic Energy Agency, Vienna, 2012.
- [25] Web-site: www.iter.org.
- [26] Garry McCracken and Peter Stott, "Fusion: The Energy of the Universe", Elsevier Academic Press, Burlington, MA01803, USA, 2005, ISBN 0-12-481851-X.
- [27] K. Shibata, O. Iwamoto, T. Nakagawa, N. Iwamoto, A. Ichihara, S. Kunieda, S. Chiba, K. Furutaka, N. Otuka, T. Ohsawa, T. Murata, H. Matsunobu, A. Zukeran, S. Kamada, J. Katakura, "JENDL-4.0: A new library for nuclear science and engineering", *Journal of Nuclear Science and Technology*, 48, (2011).
- [28] Weston M. Stacey, "Fusion: An Introduction to the Physics and Technology of Magnetic Confinement Fusion", ©2010 WILEY-VCH Verlag GmbH & Co. KGaA, Weinheim1.
- [29] L.M. Giancarli et al, "Overview of the ITER TBM Program", *Fusion Eng. Des.*, 87, (2012), 395-402.
- [30] K. M. Feng et al, "Progress on design and R& D for helium-cooled ceramic breeder TBM in China", *Fusion Eng. Des.*, 87(7-8), (August 2012), 1138-1145.
- [31] Mikio Enoeda et al, "Development of the Water Cooled Ceramic Breeder Test Blanket Module in Japan", *Fusion Eng. Des.*, 87(7-8), (August 2012), 1363-1369.
- [32] L. V. Boccaccini et al, "Present status of the conceptual design of the EU test blanket systems", *Fusion Eng. Des.*, 86, (October 2011), 478-483.

- [33] C. P. C. Wong et al, "An overview of the US DCLL ITER-TBM program", *Fusion Eng. Des.*, 85, (2010), 1129-1132.
- [34] V. Chuyanov et al, "TBM Program implementation in ITER", *Fusion Eng. Des.*, 85(10-12), (December 2010), 2005-2011.
- [35] Tetsuo Tanabe, "Tritium handling issues in fusion reactor materials", *Journal of Nuclear Materials*, 417, (2011), 545-550.
- [36] N. B. Morley et al, "Thermofluid magnetohydrodynamic issue for liquid breeders", *Fusion Science and Technology*, 47, (April 2005), 488-501.
- [37] A K Suri et al, "Materials issues in fusion reactors", *Journal of Physics: Conference Series* 208 (2010) 012001.
- [38] B Bornschein et al, "Tritium management and safety issues in ITER and DEMO breeding blankets", *Fusion Eng. Des.*, 88, (2013), 466-471.
- [39] "GENIE 35 Neutron generator user manual", SODERN, France.
- [40] Shrichand Jakhar, M. Abhangi, C. V. S. Rao, T. K. Basu, "Measurement of absolute neutron yield of D-T neutron generator using foil activation", *Proceedings of 25th National Symposium on Plasma Science and Technology at IASST, Guwahati, India during 8-12 Dec 2010*.
- [41] Saheb Hussain Md, Shrichand Jakhar, Mitul Abhangi, Rajnikant Makwana, Sudhirsinh Vala, C V S Rao, T K Basu, A Gopala Krishna, "Absolute measurement of neutron yield for D-T neutron generator using water activation technique", *International Symposium on Accelerator and Radiation Physics, Saha Institute of Nuclear Physics, Kolkata, India; 02/2011*.
- [42] Mitul Abhangi, Nupur Jain, Rajnikant Makwana, Sudhirsinh Vala, Shrichand Jakhar, T. K. Basu, C. V. S. Rao, "Experimental Studies on the Self-Shielding Effect in Fissile Fuel Breeding Measurement in Thorium Oxide Pellets Irradiated with 14 MeV Neutrons", *Plasma Science and Technology* 02/2013; 15(2):166.
- [43] Shrichand Jakhar, C V S Rao, A Shyam and B Das, "Measurement of neutron flux from 14 MeV D-T neutron generator using activation analysis", *Proceedings of IEEE Nuclear science Symposium, Dresden (Germany), 19-25 Oct. 2008*, pp 2335-2338.
- [44] SRIM-2008 code: <http://www.srim.org/SRIM/SRIM-2008.e>.
- [45] <http://publications.jrc.ec.europa.eu/repository/handle/JRC51437>.

- [46] S. Tiwari, S. Jakhar, M. Abhangi, R. Makwana, V. Chaudhari, C.V.S. Rao, T.K. Basu, "Experimental and Monte Carlo absolute efficiency calibration of HPGe γ -ray spectrometer for application in neutron activation analysis", Proceedings of 28th National Symposium on Plasma Science and Technology at KIIT, Bhubneshwar, Odhisha, India during 3-6 Dec 2013.
- [47] M. Angelone et al, "Absolute experimental and numerical calibration of the 14 MeV neutron source at the Frascati neutron generator", Review of Scientific Instruments, 67(6), (1996), 2189-2196.
- [48] M. Pillon, M. Angelone, M. Martone, V. Rado, "Characterization of the source neutrons produced by the Frascati Neutron Generator", Fusion Eng. Des., 28, (1995) 683-688.
- [49] "IEEE Standard Test Procedures for Germanium Gamma-Ray Detectors", ANSI/IEEE Standard 325-1996.
- [50] A. Elanique, O. Marzocchi, D. Leone, L. Hegenbart, B. Breustedt, L. Oufni, "Dead layer thickness characterization of an HPGe detector by measurements and Monte Carlo simulations", Applied Radiation and Isotopes, 70(3), (March 2012), 538-542.
- [51] A. Milocco and A. Trkov, "Modelling of the Production of Source Neutrons from Low-Voltage Accelerated Deuterons on Titanium-Tritium Targets", Science and Technology of Nuclear Installations, 2008, Article ID 340282.
- [52] S. Yamaguchi et al, "Calculation of anisotropy correction factor for determination of DT neutron yield by associated particle method", JAERI Report, JAERI-M 84-109, 1984.
- [53] DROSG2000: <https://www.nds.iaea.org/public/libraries/drosg2000/>.
- [54] N. Otuka, E. Dupont, V. Semkova et al, "Towards a More Complete and Accurate Experimental Nuclear Reaction Data Library (EXFOR): International Collaboration Between Nuclear Reaction Data Centres (NRDC)", Nucl. Data Sheets 120 (2014) 272.
- [55] <http://physics.nist.gov/cuu/index.html>
- [56] <http://www.nndc.bnl.gov/nudat2/chartNuc.jsp>
- [57] K. I. Zolotarev, "Evaluation of cross-section data from threshold to 40-60 MeV for specific neutron reactions important for neutron dosimetry applications",

- IAEA NDS report, INDC (NDS) - 0546, April 2009.
- [58] A. A. Filatenkov, S.V. Chuvaev, V.N. Aksenov and V.A. Jakovlev, "Systematic measurement of activation cross-sections at neutron energies from 13.4-14.9 MeV", IAEA INDC report no. INDC (CCP)-402.
 - [59] International reactor dosimetry file: IRDF-02, <https://www-nds.iaea.org/irdf2002/index.htmlx>.
 - [60] I. Kodeli, A. Trkov, "Validation of the IRDF-2002 dosimetry library", Nuclear Instruments and Methods in Physics Research A, 577, (2007), 664-681.
 - [61] Y. Verzilov et al, "A novel method for solving lithium carbonate pellet by Binary acid for tritium production rate measurement by liquid scintillation counting technique", Journal of nuclear science and technology, 33(5), (1996), 390-395.
 - [62] User Manual of 1220 QUANTULUS Ultra Low Level Liquid Scintillation Spectrometer, Perkin Elmer Life and Analytical Sciences, USA.
 - [63] R. B. M. Sogbadji et al., "Determination of Neutron Fluxes and Spectrum Shaping Factors in Irradiation Sites of Ghana's Miniature Neutron Source Reactor by Activation Method after Compensation of Loss of Excess Reactivity" World Journal of nuclear science and technology, 1, (2011), 50-56.
 - [64] I. A. Alnour et al., "Determination of neutron flux parameters in PUSPATI TRIGA Mark II Research Reactor, Malaysia" Journal of Radioanalytical and Nuclear Chemistry, 296(3), (2013), 1231-1237.
 - [65] P. Batistoni, M. Angelone, P. Carconi, K. Ochiai, I. Schafer, K. Seidel, Y. Verzilov, G. Zappa, M. Pillon, "International comparison of measuring techniques of tritium production for fusion neutronics experiments: Status and preliminary results", Fusion Eng. Des., 75-79, (Nov. 2005), 911-915.
 - [66] U. Fischer, P. Batistoni, Y. Ikeda, M.Z. Youssef, "Neutronics and nuclear data: achievements in computational simulations and experiments in support of fusion reactor design", Fusion Eng. Des., 51-52, (2000), 663-680.
 - [67] C Konno et al, "Analyses of fusion integral benchmark experiments at JAEA/FNS with FENDL-2.1 and other nuclear data libraries", Fusion Eng. Des., 83, (2008), 1774-1781.
 - [68] Y M Verzilov et al, "Integral experiments for verification of tritium production on the beryllium/lithium titanate blanket mockup with one breeding layer",

JAERI Research Report, 2004-015.

- [69] N. Roux et al, "Low-temperature tritium release ceramics as potential materials for the ITER breeding blanket", Journal of Nuclear Materials Volumes 233-237, Part 2, October 1996, Pages 1431-1435.
- [70] R. F. Mattas et al, "Materials for breeding blankets", Journal of Nuclear Materials, Volumes 233-237, Part 1, October 1996, Pages 72-81.
- [71] N. Roux et al, "Properties and performance of tritium breeding ceramics", Journal of Nuclear Materials, Volumes 191-194, Part 1, September 1992, Pages 15-22.
- [72] D. Mandal, D. Sathiyamoorthy, M. R. K. Sheno, S. K. Ghosh, "Synthesis and fabrication of lithium-titanate pebbles for ITER breeding blanket by solid state reaction and spherodization", Fusion Eng. Des., 85, (2010), 819-823.
- [73] D. Mandal, D. Sathiyamoorthy, V. G. Rao, "Preparation and characterization of lithium-titanate pebbles by solid-state reaction extrusion and spherodization techniques for fusion reactor", Fusion Eng. Des., 87, (2012), 7-12.
- [74] R. A. Forrest, "FISPACT-2007: User Manual", Report UKAEA FUS 534, Culham 2007.
- [75] Patrick J. Griffin, J. G. Kelly, Jason W. VanDenburg, "User's Manual for SNL-SAND-II Code" SAND93-3957, April 1994.
- [76] International reactor dosimetry and fusion file: IRDFF-1.05, <https://www-nds.iaea.org/IRDFF/>.
- [77] National Nuclear Data Center, information extracted from the NuDat 2 database, <http://www.nndc.bnl.gov/nudat2/>
- [78] Genie 2000, Gamma Analysis Software, Canberra Industries, USA.
- [79] www-nds.iaea.org/fendl2/validation/benchmarks/dresden/pb/report.txt.
- [80] T. Elfruth, D. Seeliger, K. Seidel, G. Streubel, S. Unholzer, D. Albert, W. Hansen, K. Noack, C. Reiche, W. Vogel, D.V. Markovskij and G.E. Shatalov, "The neutron multiplication of lead at 14 MeV neutron incidence energy", Atomkernenergie-Kerntechnik 49, (1987), 121-125.
- [81] Amit Raj Sharma, Debasis Chandra, Shashank Chaturvedi, S. Ganesan, H. Wienke, "Reinvestigations of integral neutron multiplication experiments with 14 MeV neutrons in lead", Fusion Eng. Des., 55, (2001), 501-512.

- [82] Kentaro Ochiai, Keitaro Kondo, Seiki Ohnishi, Kosuke Takakura, Satoshi Sato, Yuichi Abe and Chikara Konno, "DT Neutronics Benchmark Experiment on Lead at JAEA-FNS", Journal of the Korean Physical Society, Vol. 59, No. 2, August 2011, pp. 1953-1956.
- [83] Keitaro Kondo, Isao Murata, Axel Klix, Klaus Seidel, Hartwig Freiesleben, "Problems of lead nuclear data in fusion blanket design", Fusion Eng. Des., 84, 2009, 1076-1080.
- [84] Dieter Leichtle, Ulrich Fischer, Reuven L. Perel, Arkady Serikov, "Sensitivity and uncertainty analysis of nuclear responses in the EU HCLL TBM of ITER", Fusion Eng. Des., 86, (2011), 2156-2159.
- [85] I. Kodeli, A. Trkov, P. Batistoni, S. Villari, M. Pillon, M. Angelone, U. Fischer, "Sensitivity and uncertainty analysis of the HCLL breeder blanket experiment in the frame of the EU fusion technology programme", Nuclear Engineering and Design, 241, (2011), 1243-1247.
- [86] D. Leichtle, U. Fischer, I. Kodeli, R.L. Perel, M. Angelone, P. Batistoni, P. Carconi, M. Pillon, I. Schafer, K. Seidel, R. Villari, G. Zappa, "Sensitivity and uncertainty analyses of the tritium production in the HCPB breeder blanket mock-up experiment", Fusion Eng. Des., 82, (2007), 2406-2412.
- [87] U. Fischer, D. Leichtle, R.L. Perel, "Monte Carlo based sensitivity and uncertainty analysis of the HCPB Test Blanket Module in ITER", Fusion Eng. Des., 83, (2008), 1222-1226.
- [88] I. Kodeli, K. Kondo, R. L. Perel, U. Fischer, "Cross-section sensitivity and uncertainty analysis of the FNG copper benchmark experiment", Fusion Eng. Des., (2015), doi: [10.1016/j.fusengdes.2015.11.058](https://doi.org/10.1016/j.fusengdes.2015.11.058).
- [89] OECD/NEA Data Bank, "The JEFF-3.1.1 Nuclear Data Library", JEFF Report 22, OECD/NEA Data Bank (2009).
- [90] OECD/NEA Data Bank, "The JEFF-3.1 Nuclear Data Library", JEFF Report 21, OECD/NEA Data Bank (2006).
- [91] OECD/NEA Data Bank, "The JEFF-3.0 Nuclear Data Library", JEFF Report 19, OECD/NEA Data Bank (2005).
- [92] OECD/NEA Data Bank, "The JEF-2.2 Nuclear Data Library", JEFF Report 17, OECD/NEA Data Bank (2000).

- [93] K. Shibata et al, "JENDL-4.0: A new library for nuclear science and engineering", J. Nucl. Sci. Technol. 48, (2011), 1.
- [94] K. Shibata et al, "Japanese Evaluated Nuclear Data Library Version 3 Revision-3: JENDL-3.3", J. Nucl. Sci. Technol. 39, (2002), 1125.
- [95] T. Nakagawa et al, "Japanese Evaluated Nuclear Data Library Version 3 Revision-2: JENDL-3.2", J. Nucl. Sci. Technol. 32, (1995), 1259.
- [96] Z. G. Ge, Y.X. Zhuang, T.J. Liu, J.S. Zhang, H.C. Wu, Z.X. Zhao, H.H. Xia, "The Updated Version of Chinese Evaluated Nuclear Data Library (CENDL-3.1)", J. Kor. Phys. Soc. 59(2011)1052.
- [97] China Nuclear Data Center, "A brief description of the second version of Chinese Evaluated Nuclear Data Library CENDL-2", Communication of Nuclear Data Progress No.6, [same as report INDC (CPR)-25], China Nuclear Information Centre (1991).
- [98] A.I. Blokhin, B.I. Fursov, A.V. Ignatyuk, V.N. Koshcheev, E.V. Kulikov, B.D. Kuzminov, V.N. Manokhin, M.N. Nikolaev, "Current Status of Russian Evaluated Neutron Data Libraries", Proc. International Conference on Nuclear Data for Science and Technology, Gatlinburg, Tennessee, USA, May 9-13, 1994, Vol. 2, (1994), p.695.